COMBINED EXPERIMENTAL AND COMPUTATIONAL STUDIES OF THE INTERACTIONS BETWEEN SMALL MOLECULE LIGANDS AND EUKARYOTIC TRANSLATION INITIATION FACTORS eIF5B AND eIF4E

PRAKASH AMRUTH RAJ CHUKKA
Master of Science, VIT University, 2018

A thesis submitted
in partial fulfilment of the requirements for the degree of

MASTER OF SCIENCE

in

BIOCHEMISTRY

Department of Chemistry and Biochemistry
University of Lethbridge
LETHBRIDGE, ALBERTA, CANADA

COMBINED EXPERIMENTAL AND COMPUTATIONAL STUDIES OF THE INTERACTIONS BETWEEN SMALL MOLECULE LIGANDS AND EUKARYOTIC TRANSLATION INITIATION FACTORS eIF5B AND eIF4E

PRAKASH AMRUTH RAJ CHUKKA

Date of Defence: January 24, 2022

Dr. N. Thakor	Associate Professor	Ph.D.
Dr. S. Wetmore	Professor	Ph.D.
Thesis Co-supervisors		
Dr. R. Golsteyn	Associate Professor	Ph.D.
Thesis Examination Committee Member		
Dr. S. Mosimann	Associate Professor	Ph.D.
Thesis Examination Committee Member		
Dr. M. Roussel	Professor	Ph.D.
Chair, Thesis Examination Committee		

ABSTRACT

eIF5B and eIF4E are aberrantly expressed in several cancers, and there is a growing body of literature that recognises their importance in cancer survival. This thesis attempts to study the interactions of small molecule inhibitors with eIF5B and eIF4E by combining cell, molecular, and computational biology techniques. Through western blotting, we identified that ribavirin does not affect the function of eIF5B in BT48 and U343 cells. These results were corroborated by MD simulations, which suggested that the charge on nucleobase of RTP prevents interaction with eIF5B. Using homology modeling and protein validation, the first human eIF5B structure was generated that facilitated the identification of the LWW31 binding site. In addition, MD simulations provided insights into the stability of m^7GTP and the binding mode of RBV. Overall, this thesis provides insight into small molecule interactions with eIF5B and eIF4E, which might be beneficial for the future drug design of antineoplastic drugs.

ACKNOWLEDGMENTS

First and foremost, I would like to thank my supervisors, Dr. Nehal Thakor and Dr. Stacey Wetmore, who have provided constant support over the past two years. I am thankful for taking time out of their busy schedule to discuss the scientific problems, for mentoring, and making me a better person. I would like to thank my committee members Dr. Roy Golsteyn and Dr. Steven Mosimann, for their valuable feedback throughout my masters. I would also like to thank Dr. Marc R. Roussel for chairing my thesis defense.

I have had a unique opportunity to work closely with members from both Thakor and Wetmore labs. I consider myself very fortunate to have been a part of both research groups. I would like to thank Ryan Kung, Makay Taylor Murray, Kush Patel, and Taylor Katrina for patiently training me in computational and wet lab experiments. I would also like to thank Dr. Preethi Seelam Prabhakar, Rajwinder Kaur, and Briana Boychuk for helping me get through tough times during the COVID-19 pandemic. Thanks to Keiran Vanden Dungen, Bimaldeep Singh, Pavan Lakshmi Narasimha, and Veda Hegde for their constant support and friendship. Thanks to past and present postdocs and graduate students, Dr. Nilakshi Kulathunga, Dr. James McFarlane, Jinay Patel, Dianevys Gonzalez-Pena Fundora, Nathania Takyi, Rebecca Jeong, Dylan Nikkel, Cynthia Fonderson, and Rachana Mulay for making my masters enjoyable.

A special thanks to my friends and family for their support. Finally, I would like to thank my girlfriend, Laura-Ève, for her patience and unconditional support.

TABLE OF CONTENTS

LIST OF TABLES

LIST OF FIGURES

LIST OF ABBREVIATIONS

43S PIC	43S Preinitiation Complex
4E-BP1	Eukaryotic Translation Initiation Factor 4E Binding Protein 1
AF	AlphaFold
AML	Acute Myeloid Leukemia
ATF4	Activating Transcription Factor 4
BBB	Blood–Brain Barrier
Bcl-xL	B-Cell Lymphoma-Extra Large
cFLIP	FLICE-Inhibitory Protein
cIAP1	Cellular Inhibitor of Apoptosis Protein 1
DMEM	Dulbecco's Modified Eagle's Medium
EGF	Epidermal Growth Factor
EGFR	Epidermal Growth Factor Receptor
eIF2	Eukaryotic Initiation Factor 2
eIF2A	Eukaryotic Initiation Factor 2A
eIF5	Eukaryotic Initiation Factor 5
EZH2	Enhancer of Zeste Homolog 2
FGF-2	Fibroblast Growth Factor 2
GAFF	General AMBER Force Field
GAPDH	Glyceraldehyde 3-Phosphate Dehydrogenase
GBM	Glioblastoma
GCN4	General Control Nondepressible
GTP	Guanosine-5'-Triphosphate
HBA	Hydrogen Bond Analysis
HCC	Hepatocellular Carcinoma
IC50	Half Maximal Inhibitory Concentration
IMPDH	Inosine-5′-Monophosphate Dehydrogenase
LUAD	Lung Adenocarcinoma
M^7G	7-Methylguanosine
M^7GTP	7-Methylguanosine-5'-Triphosphate
MAP	Kinase-Interacting Serine/Threonine-Protein Kinase (Mnk)
MD	Molecular Dynamics
MMGBSA	Molecular Mechanics Generalized Born Surface Area
mRNA	Messenger Ribonucleic Acid
mTOR	Mammalian Target of Rapamycin
NRF2	Nuclear Factor-Erythroid Factor 2-Related Factor 2
ODC	Ornithine Decarboxylase
PBS	Phosphate-Buffered Saline
PDB	Protein Data Bank
PLIP	Protein–Ligand Interaction Profiler

RBV	Ribavirin
RESP	Restrained Electrostatic Potential
RIPA	Radioimmunoprecipitation Assay Buffer
RMSD	Root Mean Squared Deviation
RMSF	Root Mean Square Fluctuation
RTP	Ribavirin-5'-Triphosphate
SASA	Solvent Accessible Surface Area
TRAIL	Tumor Necrosis Factor-Related Apoptosis-Inducing Ligand
uORF	Upstream Open Reading Frame
VEGF	Vascular Endothelial Growth Factor
XIAP	X-Linked Inhibitor of Apoptosis Protein
zDOPE	Normalized Discrete Optimized Protein Energy

Chapter 1: Introduction[a,b]

1.1. Overview

Cap-dependent or canonical translation initiation is an intricate process and highly regulated in eukaryotes.[1] It involves multiple eukaryotic initiation factors (eIFs) ranging from small to complex multidomain proteins (Figure 1.1). Translation can be deregulated when the expression levels of certain eIFs are abnormal.[2, 3] For example, overexpression of eIF5B and eIF4E can alter the translation of a sub-set of mRNAs, which promote cancer cell survival.[2, 4-10] Therefore, eIF5B and eIF4E have the potential for being oncogenes, which makes them ideal therapeutic targets for certain cancers. However, to identify the inhibitor binding site and accelerate the structure based drug design in silico, structural information is necessary.[11] Although the X-ray crystal structure of eIF4E is available, eIF5B lacks such information. Intriguingly, techniques like homology modeling, docking, and molecular dynamics (MD) simulations have been successfully combined to predict the protein structure and the ligand binding sites for other systems.[12, 13] Therefore, the objective of this thesis is to predict the structure of human eIF5B, and study the interactions

[a]Adapted from Chukka, P. A. R.; Wetmore, S. D.; Thakor, N., Established and Emerging Regulatory Roles of Eukaryotic Translation Initiation Factor 5B (eIF5B). *Frontiers in Genetics* **2021**, *12*, 737433.
[b]C.P.A.R wrote the manuscript. N.T proposed the idea for minireview. N.T and S.D.W edited the manuscript and assisted with the figure concepts.

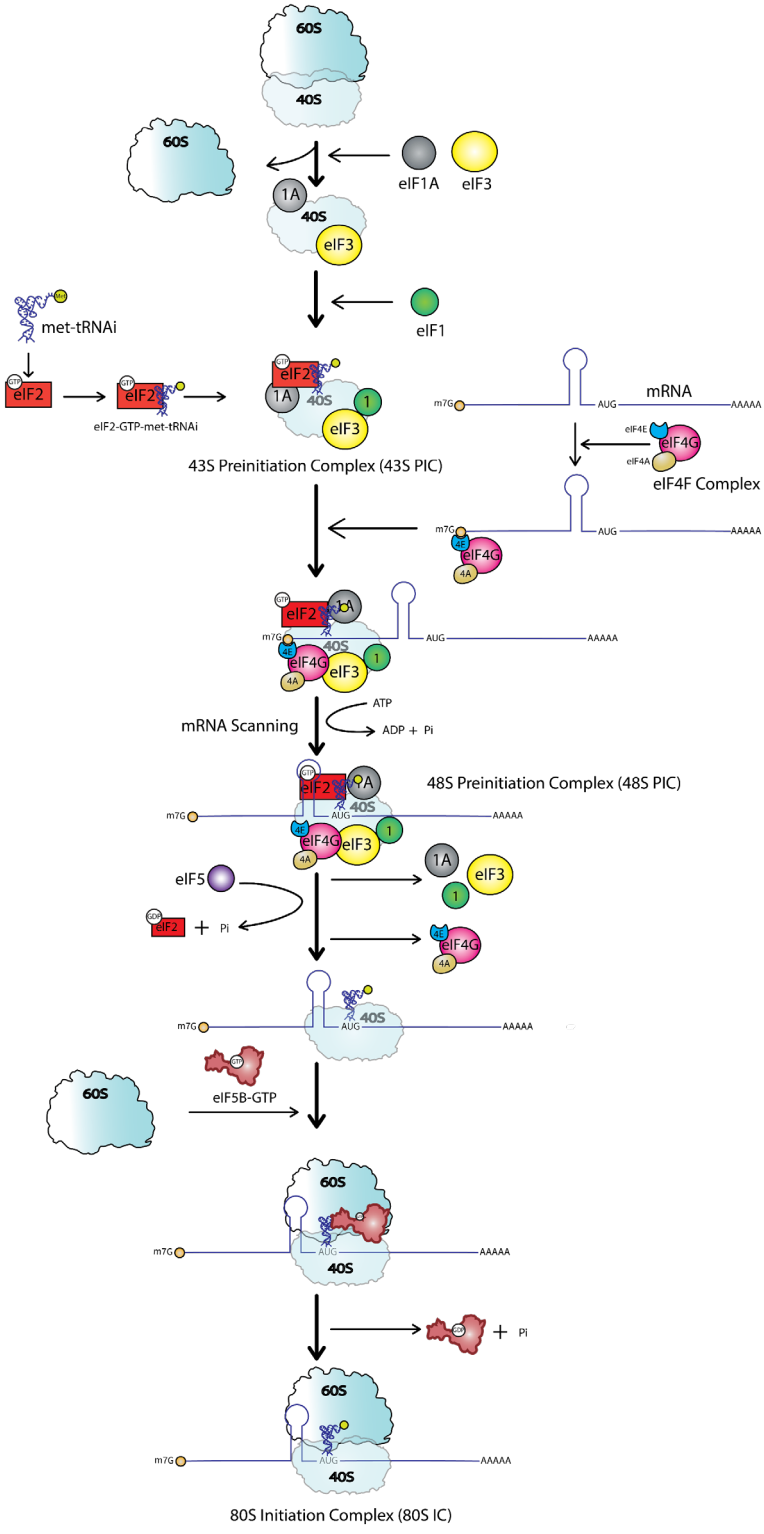

Figure 1.1 During cap-dependent translation, the interaction between eIF4E of the eIF4F complex and 5′-terminal 7-methyl guanosine (m^7G) cap of mRNA helps recruit the eIF4F complex onto the mRNA. Simultaneously, ternary complex (eIF2-GTP-met-tRNAi), eIF1

and eIF3 are recruited to the 40S subunit giving rise to 43S preinitiation complex (43S PIC). The ribosome is recruited onto the mRNA due to interactions between eIF4G (scaffold protein) and eIF3. Once recruited, mRNA is scanned by the ribosome with the help of eIF4A (RNA helicase and ATP-dependent protein) until the AUG start codon is encountered. After start codon selection, eIF2 delivers Met-tRNA$_i^{Met}$ to the P-site of the 40S subunit and a GTPase accelerating protein (GAP), eIF5, induces hydrolysis of GTP on eIF2. This leads to structural changes in the ribosome, releasing most initiation factors. In the absence of eIF2, eIF5B stabilizes the Met-tRNA$_i^{Met}$ and simultaneously mediates 60S subunit association with 48S PIC leading to the formation of the 80S initiation complex (80S IC). In the final step, GTP of eIF5B is hydrolyzed, releasing the remaining factors and the 80S IC transitions into the elongation phase.

between eIF5B or eIF4E and a variety of small molecules using both experimental and computer modeling techniques, which will pave the way to design novel effective compounds for the better management of hard-to-treat and high-fatality cancers. Overall, this chapter provides essential background information on eIF5B and eIF4E that highlights their importance in translation and cancer survival, which is necessary to understand the scope of this thesis.

1.2. Eukaryotic translation initiation factor 5B (eIF5B)

eIF5B, also known as IF-M2A/hIF2, is a GTPase protein discovered in 1975. It is universally conserved among all eukaryotes and encoded by the *EIF5B* gene.[14, 15] eIF5B mediates the association of the 40S and 60S ribosomal subunits during eukaryotic translation initiation.[16, 17] Although eIF5B is highly conserved, its depletion does not have a substantial effect on cell viability under normal conditions.[2, 8, 18, 19] Conversely, reduced levels of eIF5B under stress conditions significantly affects cell viability.[8, 18]

eIF5B consists of a highly conserved functional C-terminal region (human 587-1220, yeast 397-1002 residues) and a less conserved N-terminal region (human 1-586, yeast 1-396 residues).[20, 21] Deleting the N-terminal region does not affect cell viability and

many *in vitro* studies have shown that N-terminally truncated eIF5B is active (human 587-1220, yeast 397-1002 residues).[14, 16, 22-24] On the other hand, the functional C-terminal consists of four domains: G domain (human 629-850, yeast 401-625 residues), domain II (human 856-948, yeast 630-745 residues), domain III (human 951-1082, 755-855 residues), and domain IV (human 1076-1220, yeast 859-1002 residues).[25-27] Additionally, domains III and IV are connected by a helix h12 whose deletion in yeast yields non-functional eIF5B similar to the defects observed in Δdomain IV yeast cells.[23, 28]

Studies have shown that during stress conditions eIF5B demonstrated a non-canonical function that parallels the role of eIF2, a Met-tRNA$_i^{Met}$ delivering eukaryotic initiation factor.[1, 29, 30] The mechanism is activated when an α-subunit of eIF2 is phosphorylated and sequestered by eIF2B. Under these conditions, eIF5B promotes translation of specific proteins by delivering Met-tRNA$_i^{Met}$ to the eukaryotic ribosomes due to its homology to IF-2, which delivers met-tRNAf^{Met} to the bacterial ribosomes.[2] Additionally, recent studies have unveiled a mechanistic role of eIF5B during canonical and non-canonical eukaryotic translation initiation.[2]

The following sections cover the established roles of eIF5B in 40S ribosome maturation, the formation of 48S PIC, the stabilization of Met-tRNA$_i^{Met}$, 60S ribosomal recruitment, and 80S complex formation. Furthermore, the emerging roles of eIF5B during Met-tRNA$_i^{Met}$ delivery, uORF-mediated translation initiation, and IRES-mediated translation initiation are highlighted. Finally, insight is provided on how eIF5B acts as a nexus between non-canonical translation and the survival of cancer cells.

1.2.1. Role of eIF5B in pre-40S ribosome subunit maturation

During ribosome biogenesis, the large and small subunits undergo a translation-like cycle where eIF5B mediates the association of the pre-40S and 60S ribosomal subunits, which acts as a quality control step.[31] The resulting complex is not a true 80S initiation-complex (80S IC) as it lacks initiator tRNA and mRNA. As a result, the 60S ribosomal subunit is displaced by the termination factor Rli-1 during 40S subunit maturation.[32, 33] The 80S-like complex ensures the proper functioning of pre-ribosomes before translation.[33] A study on the YKK392 yeast strain devoid of eIF5B has shown a negative effect on the ribosomal subunit association, resulting in the accumulation of pre-40S subunits.[33] In general, this accumulation is not detrimental, but delays the formation of the 80S-like ribosomal complex and slows down cell growth.[33] Deleting the eIF5B coding gene *FUN12* in yeast also results in the accumulation of pre-18S rRNA, and decreased levels of 27S pre-rRNA and 40S ribosomes.[31, 33] Thus, eIF5B is essential for catalyzing the ribosome maturation process in yeast.

1.2.2. eIF5B interacts with eIF5 to stimulate the formation of 48S initiation complex

Human eIF5B and eIF5 synergistically mediate the efficient formation of the 48S initiation complex (48S IC).[24] The interaction between domain IV of eIF5B and the C-terminus of eIF5 could be crucial for efficient 48S IC formation.[34] Affinity studies inferred a higher affinity of eIF5B for eIF5 compared with eIF1A.[34] It has been hypothesized that human eIF5 and eIF5B together stimulate 43S preinitiation complex (PIC) rearrangement to increase the yield of functional 48S IC.[24] Additionally, eIF5B deletion results in the destabilization of 48S IC, which was suggested to be induced by eIF5.[24] This phenomenon was observed in both optimal and non-optimal AUG context, suggesting the role of eIF5B

in 48S IC stabilization.[24] eIF5 has additional roles as a GTPase-activating protein (GAP) and a GDP-dissociation inhibitor (GDI).[35] While eIF5 induces eIF2-GTP hydrolysis, eIF5B promotes the release of eIF2 from 48S IC.[36, 37] Furthermore, eIF5B assists in establishing 48S IC on a bona fide AUG and prevents leaky scanning along with eIF5.[24, 34] Since codon scanning and selection during translation initiation are essential for generating functional proteins, these studies collectively provide compelling evidence that eIF5B coordinates with eIF5 to aid the establishment of an efficient 48S IC on a bona fide start codon.

1.2.3. Met-tRNA$_i^{Met}$ stabilization by eIF5B

After eIF2-GTP delivers Met-tRNA$_i^{Met}$ to the P-site of the 40S ribosomal subunit, GAP eIF5 induces eIF2-GTP hydrolysis.[35, 38] eIF2B disrupts the eIF5/eIF2-GDP interaction and facilitates eIF2-GDP release.[39, 40] In the absence of eIF2, domains III and IV of eIF5B extend into the inter-subunit space and stabilize initiator tRNA.[26] Conformational changes in domains III and IV facilitate interactions between basic amino acids in domain IV and $_{73}$ACCA$_{76}$-Met of initiator tRNA.[41] This creates a kink in the tRNA stem structure that is not seen in elongation tRNA, which helps initiator tRNA simultaneously interact with both mRNA and eIF5B.[42] Additionally, methionine of tRNA positions itself in the hydrophobic pocket formed by eIF5B and the uL16 loop of the 60S subunit, and single-molecule experiments suggested that the hydrophobic pocket acts as a residue selectivity filter.[42] Ultimately, the eIF5B-initiator tRNA complex places the initiator tRNA aminoacyl end out of the peptidyl transfer center, awaiting GTP hydrolysis. Thus, these eIF5B interactions help in stabilization and correct positioning of initiator

tRNA in the initiation complex after eIF2 is displaced from the ribosome, suggesting the absence of eIF5B could delay the transition into elongation.

1.2.4. Interaction of eIF5B with eIF1A for ribosome recruitment

eIF1A is one of the earliest discovered interacting partners of eIF5B.[43] Similar to eIF5B, eIF1A is considered to be a universal translational factor.[44] The interaction between these two initiation factors is thought to be important for eIF5B recruitment and mediating the joining of the large and small ribosomal subunits.[23] In contrast, another study proposed that eIF5 recruits eIF5B and eIF1A disrupts their interaction after eIF2-GTP hydrolysis.[34] In the absence of the ribosome, interactions between eIF5B and eIF1A are disrupted due to intramolecular interactions within each initiation factor.[27] Interactions between eIF1A and eIF5B are only established after codon recognition when C-terminal tail (CTT) of eIF1A is displaced from the P-site to interact with the adjacent eIF5B.[45] Domains III and IV of eIF5B interact with the oligonucleotide/oligosaccharide-binding (OB) domain and CTT of eIF1A.[27] These interactions are critical for the recruitment of the 60S subunit and formation of the 80S complex.[46, 47] Thus, these studies suggest that interactions between the two universally conserved eIF5B and eIF1A initiation factors are necessary to mediate the association of the 40S and 60S subunits by eIF5B, which forms a viable 80S IC.

1.2.5. Ribosomal subunit association is expedited by eIF5B

One primary role of eIF5B is to promote the ribosomal association of the 40S and 60S subunits (Figure 1.2a).[16, 22] The long retention time (30 to 60 sec) of eIF5B on ribosomes indirectly prevents their collision on mRNA before 80S IC transitions into the elongation step.[48] Apart from ribosomal subunit joining, *in vivo* studies have shown the

stabilization of the halfmer polysome (43S PIC + 80S on an mRNA) by eIF5B.[16] To participate in ribosomal subunit association, eIF5B must be in an active form, which has been proposed to be achieved through a domain release mechanism.[27] According to the proposed mechanism, inherently rigid domains III and IV of eIF5B become flexible upon GTP binding due to the disruption of interactions between domain I and domain III.[27, 49]

Each domain of eIF5B has a specific function during ribosome association: 1) the G-domain interacts with the 60S subunit and is involved in GTP hydrolysis, 2) domain II is anchored to the 40S subunit, 3) domain III also anchors to the 40S subunit, and promotes GTP hydrolysis when Met-tRNA$_i^{Met}$ is delivered, and 4) domain IV interacts with tRNA, eIF1A, and eIF5.[26, 27, 34, 41] GTP hydrolysis is not required for ribosomal subunit association but is required for the release of eIF5B and 80S IC transition into the elongation step.[22, 26] If domain III does not recognize a proper Met-tRNA$_i^{Met}$ delivery or ribosomal association, eIF5B could be trapped in the P/A site, which hampers the recruitment of a new aminoacyl-tRNA, delays the transition to elongation, and obstructs new ribosome recruitment. Although ribosome recruitment occurs even in the absence of eIF5B, 80S IC formation is inefficient and the transition time into the elongation step is longer, resulting in a slow growth phenotype.[23, 50] Overall, once eIF5B induces the 60S and 40S subunit association, eIF5B-GDP is released, making the 80S initiation complex elongation competent.[23]

1.2.6. eIF5B interaction with eIF2A in non-canonical translation initiation

When availability of ternary complex (eIF2-GTP-Met-tRNA$_i^{Met}$) is low under stress conditions, initiation factor eIF2A has been shown to deliver the Met-tRNA$_i^{Met}$ to the 40S ribosome by coordinating with eIF5B.[51] However, eIF5B alone plays a major role in Met-tRNA$_i^{Met}$ delivery during translation initiation in certain viruses.[52, 53] In vitro studies

involving pull down assays suggest that domain IV of eIF5B modestly interacts with the M domain of eIF2A (462-502 residues), but all eIF5B domains are required for a high affinity interaction.[51] A predicted model suggested that eIF5B domain IV might also be responsible for interacting and delivering Met-tRNA$_i^{Met}$.[51] Unlike eIF2, eIF2A does not depend on GTP to deliver Met-tRNA$_i^{Met}$, but may rely on GTP hydrolysis by eIF5B for its release from the ribosome.[51, 54, 55] Studies in *S. cerevisiae* and *Caenorhabditis elegans* showed slow growth phenotype when eIF5B/*iffb-1* was depleted, and the growth deteriorated even more when both eIF5B and eIF2A were depleted.[51, 55] However, under conditions like hypoxia, the initiation process could be solely eIF5B dependent as depletion of eIF2A has no effect on protein synthesis.[8] These studies clearly imply that eIF2A augments eIF5B function during Met-tRNA$_i^{Met}$ delivery, and domain IV of eIF5B that helps stabilize Met-tRNA$_i^{Met}$ during normal conditions could be indispensable for Met-tRNA$_i^{Met}$ delivery under stress conditions.

1.2.7. Role of eIF5B in internal ribosome entry site (IRES)-mediated translation

IRES is a secondary structure present on the mRNA of both viral and cellular origins.[1, 30, 52] These IRES elements can recruit ribosomes directly without a requirement for the 5'-terminal m^{7}G cap during certain stress conditions.[1, 30, 56] Several viral mRNA contain IRES elements, including but not limited to HCV, CSFV, poliovirus (PV), and coxsackie B virus (CBV).[52, 53, 57, 58] In particular, CSFV and HCV IRES depend on eIF5B for translation in the absence of eIF2 (Figure 1.2b).[52, 53, 57] X-linked inhibitor of apoptosis (XIAP, a caspase inhibitor in eukaryotes) mRNA also contains IRES and its translation is eIF5B dependent upon eIF2 sequestration.[30, 59, 60] In general, XIAP is an important anti-apoptotic protein that plays a substantial role in preventing programmed cell death.[61, 62]

Nevertheless, IRES elements of viruses such as cricket paralysis virus (CrPV) do not depend on eIF5B for translation.[63, 64] Thus, although there is strong evidence that eIF5B is involved in IRES mediated translation of several viral and anti-apoptotic mRNAs, not all IRES-containing mRNAs require eIF5B for translation initiation.

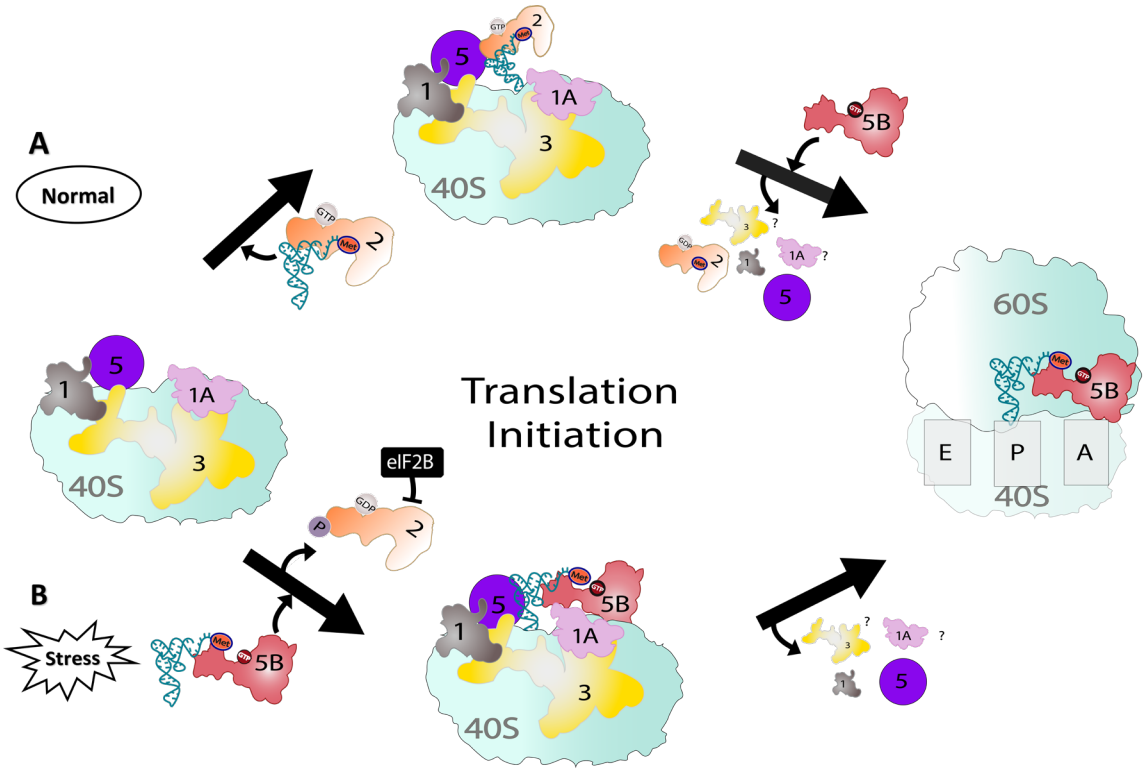

Figure 1.2 Two pathways showing eIF2-dependent (normal) and eIF5B-dependent translation (stress). a) Under normal conditions, eIF2 delivers Met-tRNA$_i$Met to the ribosome and, upon release of eIF2, eIF5B stabilizes Met-tRNA$_i$Met. Once 48S PIC forms, eIF5B assists in large and small ribosomal subunit joining. b) Under stress conditions, eIF2 is phosphorylated and sequestered by eIF2B. However, eIF5B parallels the role of eIF2 and delivers Met-tRNA$_i^{Met}$ to the P-site of the 40S ribosome in addition to its usual function during translation.

1.2.8. Regulation of uORF-mediated translation by eIF5B

Upstream open reading frame (uORF) elements are present in the 5′ untranslated regions (UTR) of mRNA across different species.[65] These elements inhibit mRNA translation under normal conditions and promote their translation during stress conditions that induce eIF2 phosphorylation (Figure 1.3a,b).[66-70] For example, *activating transcriptional factor 4* (*ATF4*) has two uORF regions that keep protein levels low until phosphorylation of α-subunit of eIF2 (Figure 1.3a).[1, 29] During *ATF4* mRNA translation under normal conditions, eIF5B prevents leaky mRNA scanning and ribosomes are recruited onto uORFs, which represses the translation of *ATF4* ORF.[68] In contrast, under stress or eIF5B depleted conditions, ribosomal recruitment occurs on the main ORF AUG sequence, causing de-repression of *ATF4* mRNA translation (Figure 1.3b,c).[68] This in turn leads to the upregulation of other proteins like C/EBP homologous protein (CHOP) and growth arrest and DNA damage-inducible protein (GADD34).[67] This was further corroborated by our recent study on human embryonic kidney 293T (HEK-293T) cells, where depleting eIF5B induced ER stress upregulating mRNA and protein levels of CHOP and GADD34.[71] eIF5B requires cooperativity with initiation factors eIF5 and eIF1A to repress ATF4 expression, and the mechanism of repression is predominantly dependent on uORF2.[68] Apart from ATF4, general control non-depressible 4 (GCN4), a transcription factor containing 4 uORFs, is repressed both in starved and non-starved yeast cells in the absence of eIF5B.[22, 72] Similarly, depletion of eIF5B decreased the levels of programmed death-ligand 1 (PD-L1) in heme starved non-small cell lung cancer (NSLC) and lewis lung carcinoma (LLC) cells.[5] In contrast, eIF5B negatively regulates p21 and p27 in serum starved THP1 cells, which have been linked to cell cycle progression, and anti-apoptosis.[18]

Numerous uORF-dependent proteins have been identified of which expression is regulated by eIF5B, and many of these proteins have implications in resistance of cancer cells to chemotherapy and cell cycle regulation. Thus, regulating eIF5B could impact such pathways necessary for cancer cell survival.

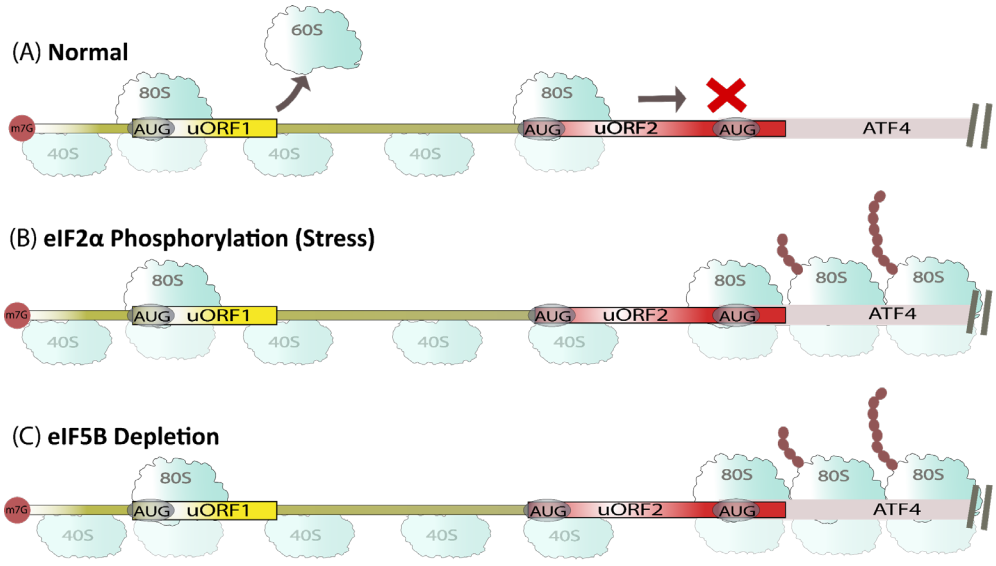

Figure 1.3 Summary of uORF-mediated ATF4 translation. a) Under normal conditions, ribosomes are recruited on uORF regions, repressing ATF4 expression in the presence of eIF5B. b) Under aberrant stress conditions, ribosomes scan past uORF2, resulting in the synthesis of ATF4 in the presence of eIF5B. c) eIF5B depletion in normal cells also promotes ATF4 synthesis.

1.2.9. eIF5B promotes cancer cell survival

Previous studies suggest eIF5B mediates the IRES containing subset of mRNA translation to resist apoptosis in cancer cells.[2] Translation of IRES-containing mRNAs, which encode anti-apoptotic proteins such as XIAP, Bcl-xL, and cellular inhibitor of apoptosis protein 1 (cIAP1) as well as nuclear factor erythroid 2-related factor 2 (NRF2), are regulated by eIF5B in glioblastoma multiforme (GBM) cells.[2, 19] There is also growing evidence of high eIF5B expression levels in various malignancies like GBM, lung

adenocarcinoma (LUAD) and hepatocellular carcinoma (HCC), signifying the importance of eIF5B as the stress-related tumorigenic eIF.[2, 4, 5] In fact, high eIF5B levels were associated with poor prognosis for HCC patients, while low eIF5B levels resulted in smaller tumor sizes, lower vascular invasions, and better patient survival rates.[4] Studies on GBM cells show eIF5B depletion leads to blunting of pro-growth pathways and sensitization to temozolomide (TMZ)-mediated apoptosis.[2, 19] Further, eIF5B aids the survival of GBM cells under hypoxic conditions by acting as one of the essential translational factors for the synthesis of hypoxia-response proteins and regulates carbon metabolism.[8] In HCC, eIF5B indirectly promotes metastasis and proliferation by upregulating ArfGAP with SH3 Domain, Ankyrin Repeat and PH Domain 1 (ASAP1) expression both *in vivo* and *in cellulo*.[4] Depletion of eIF5B in maraba virus infected and uninfected U2OS cells resulted in reduced Bcl-xL expression at both the transcriptional and translational levels.[73] This suggests eIF5B plays a role in regulating apoptosis during oncolytic virus treatment.[73] Depletion of eIF5B reduced tumor mass and propagation in lewis lung carcinoma (LLC) and non-small cell lung cancer (NSLC) cell lines, respectively, demonstrating the dependence of cancer cells on eIF5B for growth and proliferation.[5] In line with these findings, high levels of eIF5B under heme depletion induce translation of integrated stress response (ISR) dependent PD-L1, which inhibits T-cell activity. This clearly indicates that eIF5B promotes the survival of LLC and NSLC malignancies.[5] Additionally, under serum deprivation in the THP1 cell line, an acute increase in eIF5B levels is observed.[18] When eIF5B is depleted, global translation is reserved and early G0 phase prohibition occurs, indicating the regulatory role of eIF5B in the cell cycle.[18] eIF5B also regulates developmental pathways, in particular the mammalian target of rapamycin (mTOR) and mitogen-activated protein kinase (MAPK)

pathways, which are activated by epidermal growth factor receptor (EGFR).[50] Thus, these studies highlight that depletion of eIF5B disrupts many pathways, alluding to its importance in oncogenesis.

1.2.10. Inhibitors of eIF5B

Considering eIF5B role in cancer cells, it is emerging as a therapeutic target for cancer treatment. Recent studies have identified small molecules and proteins that could inhibit the activity of eIF5B. For example, a small molecule denoted LWW31 was identified using biopanning assay, which was suggested to bind and inhibit eIF5B activity, and lower the viability of cancer cells.[74] Similarly, ribavirin triphosphate, a guanosine triphosphate analogue, has been hypothesized to inhibit the activity of eIF5B, but yet to be tested experimentally.[75] In addition to small molecules, proteins like Puf6p and HIV-1 matrix have been identified, which have shown to repress the function of eIF5B in yeast and human respectively.[76, 77] These promising works highlight that further research is required to test and identify clinically relevant compounds targeting eIF5B.

The research works summarized in the above sections clearly illustrate that eIF5B is essential for non-canonical translation initiation and cancer survival. In addition to eIF5B, eIF4E is another initiation factor that has implications in several cancers (head and neck, prostate, ovarian, blood, and oesophagal cancers),[6-9, 78] which will be elaborated further in the following sections.

1.3. Eukaryotic translation initiation factor 4E (eIF4E)

eIF4E is an mRNA binding protein and a subunit of the eIF4F complex (Figure 1.4a).[79] This Pacman shaped cap-binding protein was discovered in 1976 by Filipowicz

and Ochoa.[80] eIF4E helps recruit the ribosome onto the mRNA during canonical translation initiation by interacting with the 5′-terminal cap, which consists of 7-methylguanosine (m^7G).[81-83] This mechanism can be primarily attributed to the ability of eIF4E to interact with modified guanosine.[84-86] Specifically, introduction of methyl group at the N7 position

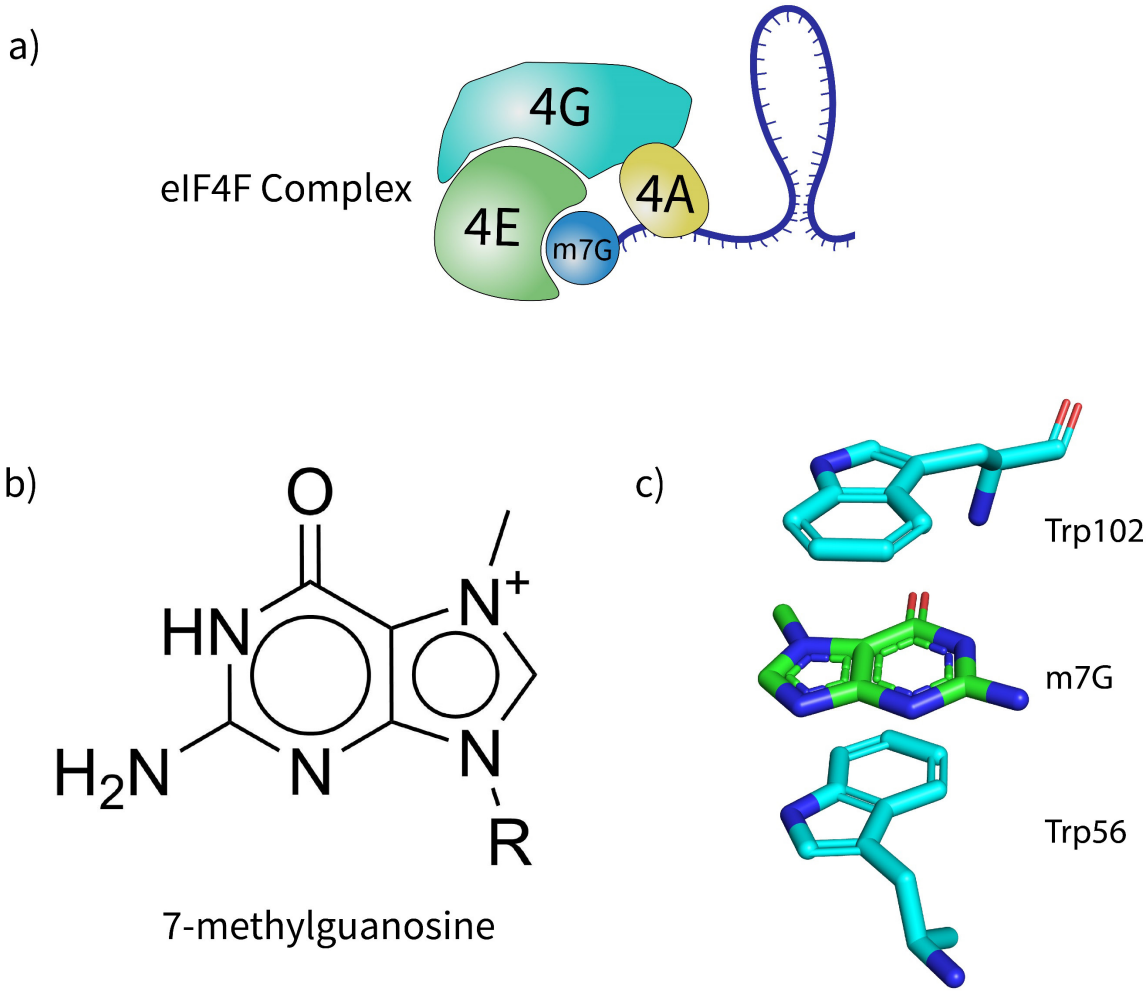

Figure 1.4 a) eIF4F complex interacts with the m^7G cap at the 5′-terminal of mRNA to recruit the 40S subunit. b) Chemical structure of m^7G (R=ribose). c) m^7G base stacks between two tryptophan residues of eIF4E (PDB ID: 1IPC).

gives guanine of m^7G cap a net positive charge, and helps m^7G intercalate between Trp56 and Trp102 (Figure 1.4c). This interaction is important for recruiting the ribosome onto the mRNA during translation initiation.[87] Apart from ribosomal recruitment, eIF4E also

regulates the activity of eIF4A during unwinding of the 5′ untranslated region (5′ UTR) of mRNA.[81] Although eIF4E plays a central role in global protein synthesis, overexpression of eIF4E only influences the expression of a subset of proteins, but not house-keeping genes.[3, 85, 88] It has been well established that eIF4E over-expression often transforms cells, and numerous cancers have shown abnormal levels of eIF4E.[7, 89, 90] This characteristic of eIF4E often leads to aberrant mRNA translation in cancer cells, facilitating proliferation and survival.[89-91] Such functions of eIF4E are possible due to interactions with the 5′-terminal m^7G cap. The importance of this interaction in selective transport and expression of certain mRNAs, and the associated roles in cell proliferation and survival are illustrated in the following section.

1.3.1. eIF4E role in mRNA degradation and transport

Although eIF4E has been predominantly found in the initiation complex, localization occurs in other subcellular regions such as stress granules, processing bodies (P-bodies), and the nucleus.[92-94] Except for eIF4E, P-bodies do not contain other initiation factors and ribosomes.[93] eIF4E prevents the degradation of certain mRNA in P-bodies. In contrast, in stress granules, eIF4E is found in the eIF4F complex along with other translational machinery and non-translating mRNA.[94-97] Often, mRNA is transported from stress granules to processing bodies and vice versa depending on conditions in the cell.[93, 98] eIF4E transports mRNA from the nucleus to the cytoplasm with the help of leucine-rich pentatricopeptide repeat cassette protein (LRPPRC) and chromosome region maintenance protein 1 (CRM1; Figure 1.5).[99-101] eIF4E has been reported to interact with ~3,500 5′ capped mRNAs in the nucleus, and this activity does not affect normal eIF4E function in the cytoplasm.[100, 102] Some of the notable eIF4E-dependent mRNAs include, but are not

limited to, cyclin D1, serine/threonine-protein kinase pim-1 (Pim1), cyclin E1, cellular Myc (c-myc), and ornithine decarboxylase (ODC).[99, 100] However, constitutively expressed mRNA such as Glyceraldehyde 3-phosphate dehydrogenase (GAPDH), b-actin and Lamin are unaffected by eIF4E levels.[103] All eIF4E sensitive mRNAs contain a ~50 nucleotide eIF4E sensitive element (4ESE) at the 3′ UTR. In general, eIF4E regulates the export of 4ESE containing mRNA.[100, 104, 105] However, eIF4E can also regulate both the export and translation of specific mRNA such as ODC due to the presence of secondary structures at

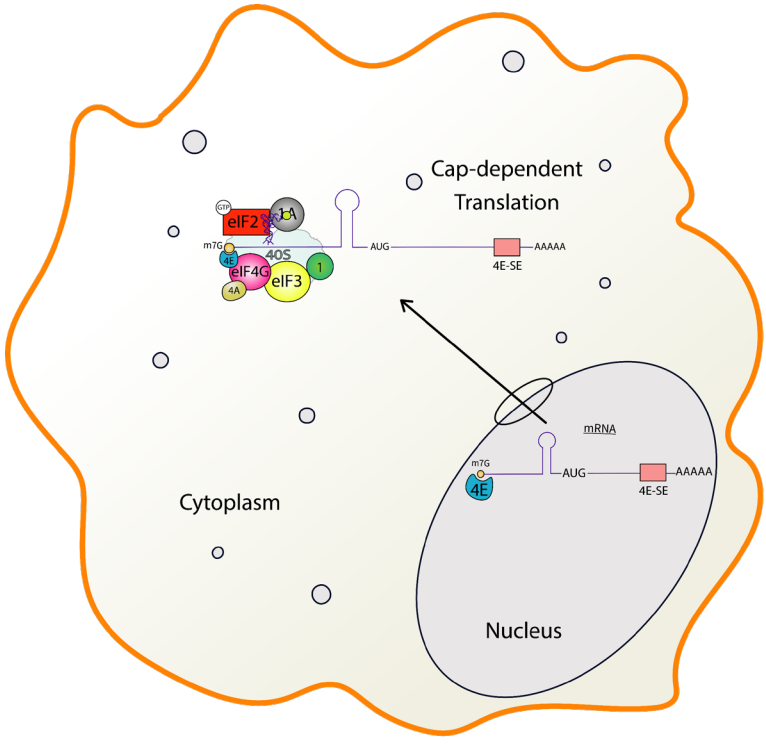

Figure 1.5 eIF4E promotes the export of eIF4E sensitive elements (4E-SE) containing mRNA from the nucleus to cytosol. eIF4E also initiates translation in the cytoplasm as a part of the eIF4F complex.

5′ UTR in addition to 4ESE.[7, 106, 107] Additionally, Vascular endothelial growth factor (VEGF) mRNA is comprised of 5′ UTR secondary structure instead of 4ESE, resulting in regulation at only the translational level.[7] All of the above eIF4E functions are achieved

due to interactions with m^7G, either in presence or absence of the ribosome.[87] There are certain exceptions, like histone H4 mRNA, that directly interact with eIF4E without the requirement of m^7G cap.[108]

1.3.2. eIF4E regulators

eIF4E has two notable binding regions, a concave cap-binding site and a conserved dorsal surface for consensus eIF4E-motif interaction.[3, 109, 110] For example, importin-8 competes with the m^7G cap to interact with eIF4E, displacing the mRNA.[111] The interaction between importin-8 and eIF4E is important for recycling eIF4E from the cytoplasm to the nucleus.[111] Proteins that bind to the dorsal surface include homeodomain-containing transcription factor (HoxA9), eukaryotic translation initiation factor 4G (eIF4G), omeobox-leucine zipper protein (Hox11), bicoid, eukaryotic translation initiation factor 4E binding protein 1 (4E-BP1), empty spiracles homeobox 2 (Emx2), Hsp27, proline-rich homeodomain (PRH), engrailed 2, and orthodenticle homeobox 2 (OTX2).[3, 112, 113] Most of these proteins interact through eIF4E-binding motif YXXXXLϕ (X represents any four amino acids and ϕ represents a single hydrophobic amino acid), reducing the affinity of eIF4E for eIF4G.[3, 112] Additionally, 4E-transporter (4E-T) also interacts with eIF4E through eIF4E-binding motif, promoting nuclear localization.[114] On the other hand, 4E-BP1 binds to eIF4E and prevents interaction with eIF4G hindering translation intiation.[115] There are other proteins like human antigen R (HuR), which also helps stabilize the eIF4E-cap interaction.[7] All these studies suggest that eIF4E can be regulated through competitive and non-competitive binding, which is critical for recycling or inhibiting its activity.

Apart from being regulated through competitive and non-competitive binding, eIF4E is also regulated through MAP kinase-interacting serine/threonine-protein kinase (Mnk)/eIF4E pathway, where eIF4E is phosphorylated by Mnk1/2.[116, 117] When Mnk is inhibited, there is a reduction of phosphorylated eIF4E levels in cancer cells.[118] Phosphorylation of eIF4E is essential for tumor progression and metastasis in prostate and breast cancer, respectively.[119, 120] In contrast, Phosphatidylinositol 3-kinase/protein kinase B/mammalian target of rapamycin complex 1 (PI3K/Akt/mTORC1) pathway can regulate eIF4E function by phosphorylating eIF4E-binding proteins (4E-BPs). These proteins bind to eIF4E to seclude its association with other eIF4F subunits, preventing translation. Inhibiting mTOR leads to the upregulation of eIF4E in colon cancer, but inhibiting both mTOR and Mnk has a profound effect on cellular progression in brain and prostate cancers.[87, 121] This suggests an interrelation between the PI3K-AKT-mTOR and Mnk/eIF4E pathways, where eIF4E could act as the connecting link. Together, these results suggest that various proteins regulate eIF4E interactions with the m^7G cap through allosteric or orthosteric binding. However, cancer cells with upregulated eIF4E are often unaffected by these regulatory proteins, the details of which are discussed in the following section.

1.3.3. eIF4E as a potential oncogene

Studies have shown that eIF4E is elevated in at least 30% of various cancers, including prostate, ovarian, colorectum, head and neck, breast, oesophagal and uterine cervix cancers.[6-9, 78] Aberrant levels of eIF4E have been associated with poor patient prognosis in ovarian, breast, and oesophagal cancers as it upregulates proteins involved in chemoresistance, cell cycle progression, tumor growth, metastasis, and survival.[7, 9, 78, 122-

[125] Some of the proto-oncogenic proteins upregulated due to eIF4E overexpression are nibrin (NBS1), mouse double minute 2 homolog (mdm2), cyclin D1, Pim1, cyclin E1, c-myc, ODC, survivin, and Pim-1.[3, 6] As mentioned in the previous section, while cyclin D1, Pim1, c-myc, ODC, are modulated post-transcriptionally during mRNA export, others are regulated at the translational level. However, eIF4E function could distinctly be affected depending on tissue type due to a difference in localization.[126] In acute myeloid leukemia (AML), eIF4E is concentrated in the nucleus and promotes mRNA transport, whereas cytoplasmic accumulation of eIF4E is high in lymphoma, which promotes translation.[127] Both functions are necessary for the oncogenic activity of eIF4E, and mutational studies of eIF4E cap-binding sites have indicated its inability to export transcripts, regulate translation, and ultimately prevents the oncogenic transformation.[3] Overall, these studies suggest that the ability of eIF4E to promote proliferation and survival of cancer cells was possible due to its cap-binding activity, signifying the necessity to limit eIF4E interaction with the m^7G cap.

1.3.4. Inhibitors of eIF4E

Since the interaction between eIF4E and m^7G cap is essential for mRNA transport and translation initiation, guanosine analogues can compete with m^7G to prevent the interaction with eIF4E. For example, ribavirin (RBV), and its metabolic form, RTP have been successful in binding and suppressing eIF4E-mediated oncogenic transformation.[85] However, the binding mode of RBV and RTP is yet to be identified in the cap binding site. In addition, oligopeptides such as 4E-BP mimetic and GnRH–4EBP fusion peptides prevent eIF4E activity by disrupting the interaction between eIF4E and eIF4G.[128-130] Although these works are promising, further research is necessary to increase the

specificity of these molecules for eIF4E. Especially, RBV and RTP, which have also been proposed to bind other proteins.[75, 131, 132]

1.4. Thesis overview

The information presented in Chapter 1 suggests an overexpression of eIF5B and eIF4E augments the translation of a subset of mRNAs, which facilitate the survival of cancer cells. Therefore, targeting eIF4E and eIF5B is a promising treatment strategy. This thesis uses a combination of in silico and in cellulo techniques to gain a fundamental understanding of the interactions of small molecules with eIF5B and identify potential small molecule binding sites. In addition, although eIF4E has been screened previously for select inhibitors (e.g., cap-analogues),[85] this thesis provides the currently missing structural information for small molecule binding to eIF4E, including the primary residues involved.

In Chapter 2, the half-maximal inhibitory concentration of RBV with or without eIF5B knockdown has been determined for glioblastoma cell line U343, and patient-derived brain tumor-initiating cells (BTICs) BT25 and BT48. Pro-apoptotic cytokine TNF-related apoptosis-inducing ligand (TRAIL) in combination with RBV has also been tested on these cell lines to determine the effect on cell viability. Furthermore, to understand the effect of RBV on eIF5B levels, western blot analysis has been performed to assess the levels of eIF5B and its downstream targets XIAP, Bcl-xL, cIAP1, $cFLIP_L$, $cFLIP_s$, and NRF2. This work complements other experimental studies showing that effect of RBV varies among different glioblastoma cell lines.[133] Next, MD simulations were used to corroborate experimental data by determining whether interactions between eIF5B and RTP are favorable. As human eIF5B structure is not available in the Protein Data Bank (PDB), homology modeling has been initially employed to generate the model for the C-

terminal region of human eIF5B-GTP using yeast eIF5B as a template. The quality of the eIF5B model has been validated and used for MD studies to determine the structural variations in each domain under polar environment. Blind docking and subsequent MD simulations were used to investigate the stability of LWW31 binding to eIF5B. Together, the findings presented in Chapter 2 uncover whether RBV affects eIF5B function in cellulo and provide information about the conformational dynamics of eIF5B-ligand complexes.

In Chapter 3, MD simulations were used to study the stability of m^7GTP, RBV and RTP in the cap-binding site of eIF4E since experimental data exists regarding the eIF4E binding affinity of these cap-analogues. The initial MD simulations of eIF4E-m^7GTP validate the computational methodology, which were then reliably applied to study the binding mode of RBV and RTP. MD simulations on eIF4E-RTP were performed to uncover the reasons for previously reported RTP flexibility in the binding pocket of eIF4E based on NMR studies,[134] and how the flexibility leads to the differences in the binding site stacking contacts for RTP and m^7GTP. Additionally, although affinity studies have suggested that RBV and RTP both bind to eIF4E,[85] there is not much information on how the absence of triphosphate tail affects RBV binding. Taken together, the information obtained from Chapter 3 can be used to rationalize existing experimental data and thereby provide a greater understanding of the binding of cap-analogues to eIF4E.

Finally, Chapter 4 summarized the thesis work with concluding remarks and provides future directions for targeting other regions of eIF5B and the phosphorylated form of eIF4E. Overall, this thesis provides the structure and conformational dynamics of eIF5B and eIF5B-ligand complexes (RTP and LWW31), and the first structural details of the

binding mode of RBV and RTP inhibitors in the cap-binding site of eIF4E. This information could be useful for the future design of improved eIF5B and eIF4E inhibitors.

1.5. References

1. Sharma, D. K.; Bressler, K.; Patel, H.; Balasingam, N.; Thakor, N., Role of Eukaryotic Initiation Factors during Cellular Stress and Cancer Progression. *Journal of Nucleic Acids* **2016,** *2016*, 8235121.

2. Ross, J. A.; Dungen, K. V.; Bressler, K. R.; Fredriksen, M.; Khandige Sharma, D.; Balasingam, N.; Thakor, N., Eukaryotic initiation factor 5B (eIF5B) provides a critical cell survival switch to glioblastoma cells via regulation of apoptosis. *Cell Death & Disease* **2019,** *10* (2), 57.

3. Borden, K. L., The eukaryotic translation initiation factor eIF4E wears a "cap" for many occasions. *Translation* **2016,** *4* (2), e1220899.

4. Wang, Z. G.; Zheng, H.; Gao, W.; Han, J.; Cao, J. Z.; Yang, Y.; Li, S.; Gao, R.; Liu, H.; Pan, Z. Y.; Fu, S. Y.; Gu, F. M.; Xing, H.; Ni, J. S.; Yan, H. L.; Ren, H.; Zhou, W. P., eIF5B increases ASAP1 expression to promote HCC proliferation and invasion. *Oncotarget* **2016,** *7* (38), 62327-62339.

5. Suresh, S.; Chen, B.; Zhu, J.; Golden, R. J.; Lu, C.; Evers, B. M.; Novaresi, N.; Smith, B.; Zhan, X.; Schmid, V.; Jun, S.; Karacz, C. M.; Peyton, M.; Zhong, L.; Wen, Z.; Sathe, A. A.; Xing, C.; Behrens, C.; Wistuba, I. I.; Xiao, G.; Xie, Y.; Fu, Y.-X.; Minna, J. D.; Mendell, J. T.; O'Donnell, K. A., eIF5B drives integrated stress response-dependent translation of PD-L1 in lung cancer. *Nature Cancer* **2020,** *1* (5), 533-545.

6. Borden, K. L. B.; Culjkovic-Kraljacic, B., Ribavirin as an anti-cancer therapy: acute myeloid leukemia and beyond? *Leukemia Lymphoma* **2010,** *51* (10), 1805-1815.

7. Culjkovic, B.; Borden, K. L., Understanding and Targeting the Eukaryotic Translation Initiation Factor eIF4E in Head and Neck Cancer. *Journal of oncology* **2009,** *2009*, 981679.

8. D'Abronzo, L. S.; Ghosh, P. M., eIF4E Phosphorylation in Prostate Cancer. *Neoplasia* **2018,** *20* (6), 563-573.

9. Liu, T.; Li, R.; Zhao, H.; Deng, J.; Long, Y.; Shuai, M. T.; Li, Q.; Gu, H.; Chen, Y. Q.; Leng, A. M., eIF4E promotes tumorigenesis and modulates chemosensitivity to cisplatin in esophageal squamous cell carcinoma. *Oncotarget* **2016,** *7* (41), 66851-66864.

10. Zheng, J.; Li, X.; Zhang, C.; Zhang, Y., eIF4E Overexpression Is Associated with Poor Prognoses of Ovarian Cancer. *Analytical Cellular Pathology* **2020,** *2020*, 8984526.

11. Clark, J. J.; Orban, Z. J.; Carlson, H. A., Predicting binding sites from unbound versus bound protein structures. *Scientific Reports* **2020,** *10* (1), 15856.

12. Wang, D. F.; Helquist, P.; Wiech, N. L.; Wiest, O., Toward selective histone deacetylase inhibitor design: homology modeling, docking studies, and molecular

dynamics simulations of human class I histone deacetylases. *Journal of Medicinal Chemistry* **2005,** *48* (22), 6936-6947.

13. Ravindranath, B. S.; Vishnu Vinayak, S.; Chandra Mohan, V., RNR inhibitor binding studies of Chlamydia felis: insights from in silico molecular modeling, docking, and simulation studies. *Journal of Biomolecular Structure and Dynamics* **2021**, 1-13.

14. Pestova, T. V.; Lomakin, I. B.; Lee, J. H.; Choi, S. K.; Dever, T. E.; Hellen, C. U., The joining of ribosomal subunits in eukaryotes requires eIF5B. *Nature* **2000,** *403* (6767), 332-5.

15. Roll-Mecak, A.; Cao, C.; Dever, T. E.; Burley, S. K., X-Ray structures of the universal translation initiation factor IF2/eIF5B: conformational changes on GDP and GTP binding. *Cell* **2000,** *103* (5), 781-792.

16. Lee, J. H.; Pestova, T. V.; Shin, B. S.; Cao, C.; Choi, S. K.; Dever, T. E., Initiation factor eIF5B catalyzes second GTP-dependent step in eukaryotic translation initiation. *Proceedings of the National Academy of Sciences* **2002,** *99* (26), 16689-16694.

17. Merrick, W. C.; Kemper, W. M.; Anderson, W. F., Purification and characterization of homogeneous initiation factor M2A from rabbit reticulocytes. *Journal of Biological Chemistry* **1975,** *250* (14), 5556-5562.

18. Lee, S.; Truesdell, S. S.; Bukhari, S. I.; Lee, J. H.; LeTonqueze, O.; Vasudevan, S., Upregulation of eIF5B controls cell-cycle arrest and specific developmental stages. *Proceedings of the National Academy of Sciences* **2014,** *111* (41), E4315-E4322.

19. Ross, J. A.; Ahn, B. Y.; King, J.; Bressler, K. R.; Senger, D. L.; Thakor, N., Eukaryotic initiation factor 5B (eIF5B) regulates temozolomide-mediated apoptosis in brain tumour stem cells (BTSCs). *Biochemistry and Cell Biology* **2020,** *98* (6), 647-652.

20. Lee, J. H.; Choi, S. K.; Roll-Mecak, A.; Burley, S. K.; Dever, T. E., Universal conservation in translation initiation revealed by human and archaeal homologs of bacterial translation initiation factor IF2. *Proceedings of the National Academy of Sciences* **1999,** *96* (8), 4342-4347.

21. Choi, S. K.; Lee, J. H.; Zoll, W. L.; Merrick, W. C.; Dever, T. E., Promotion of met-tRNAiMet binding to ribosomes by yIF2, a bacterial IF2 homolog in yeast. *Science* **1998,** *280* (5370), 1757-1760.

22. Shin, B. S.; Maag, D.; Roll-Mecak, A.; Arefin, M. S.; Burley, S. K.; Lorsch, J. R.; Dever, T. E., Uncoupling of initiation factor eIF5B/IF2 GTPase and translational activities by mutations that lower ribosome affinity. *Cell* **2002,** *111* (7), 1015-1025.

23. Fringer, J. M.; Acker, M. G.; Fekete, C. A.; Lorsch, J. R.; Dever, T. E., Coupled release of eukaryotic translation initiation factors 5B and 1A from 80S ribosomes following subunit joining. *Molecular and Cellular Biology* **2007,** *27* (6), 2384-2397.

24. Pisareva, V. P.; Pisarev, A. V., eIF5 and eIF5B together stimulate 48S initiation complex formation during ribosomal scanning. *Nucleic Acids Research* **2014,** *42* (19), 12052-12069.

25. Pestova, T. V.; Kolupaeva, V. G.; Lomakin, I. B.; Pilipenko, E. V.; Shatsky, I. N.; Agol, V. I.; Hellen, C. U., Molecular mechanisms of translation initiation in eukaryotes. *Proceedings of the National Academy of Sciences* **2001,** *98* (13), 7029-7036.

26. Huang, B. Y.; Fernandez, I. S., Long-range interdomain communications in eIF5B regulate GTP hydrolysis and translation initiation. *Proceedings of the National Academy of Sciences* **2020,** *117* (3), 1429-1437.

27. Nag, N.; Lin, K. Y.; Edmonds, K. A.; Yu, J.; Nadkarni, D.; Marintcheva, B.; Marintchev, A., eIF1A/eIF5B interaction network and its functions in translation initiation complex assembly and remodeling. *Nucleic Acids Research* **2016,** *44* (15), 7441-7456.

28. Shin, B.-S.; Acker, M. G.; Kim, J.-R.; Maher, K. N.; Arefin, S. M.; Lorsch, J. R.; Dever, T. E., Structural integrity of {alpha}-helix H12 in translation initiation factor eIF5B is critical for 80S complex stability. *RNA* **2011,** *17* (4), 687-696.

29. Holcik, M., Could the eIF2alpha-Independent Translation Be the Achilles Heel of Cancer? *Frontiers in Oncology* **2015,** *5*.

30. Thakor, N.; Holcik, M., IRES-mediated translation of cellular messenger RNA operates in eIF2alpha- independent manner during stress. *Nucleic Acids Research* **2012,** *40* (2), 541-552.

31. Lebaron, S.; Schneider, C.; van Nues, R. W.; Swiatkowska, A.; Walsh, D.; Bottcher, B.; Granneman, S.; Watkins, N. J.; Tollervey, D., Proofreading of pre-40S ribosome maturation by a translation initiation factor and 60S subunits. *Nature Structural & Molecular Biology* **2012,** *19* (8), 744-753.

32. Woolford, J. L., Jr.; Baserga, S. J., Ribosome biogenesis in the yeast Saccharomyces cerevisiae. *Genetics* **2013,** *195* (3), 643-681.

33. Strunk, B. S.; Novak, M. N.; Young, C. L.; Karbstein, K., A translation-like cycle is a quality control checkpoint for maturing 40S ribosome subunits. *Cell* **2012,** *150* (1), 111-121.

34. Lin, K. Y.; Nag, N.; Pestova, T. V.; Marintchev, A., Human eIF5 and eIF1A Compete for Binding to eIF5B. *Biochemistry* **2018,** *57* (40), 5910-5920.

35. Paulin, F. E. M.; Campbell, L. E.; O'Brien, K.; Loughlin, J.; Proud, C. G., Eukaryotic translation initiation factor 5 (eIF5) acts as a classical GTPase-activator protein. *Current Biology* **2001,** *11* (1), 55-59.

36. Pisarev, A. V.; Kolupaeva, V. G.; Pisareva, V. P.; Merrick, W. C.; Hellen, C. U.; Pestova, T. V., Specific functional interactions of nucleotides at key -3 and +4 positions

flanking the initiation codon with components of the mammalian 48S translation initiation complex. *Genes & Development* **2006,** *20* (5), 624-636.

37. Unbehaun, A.; Borukhov, S. I.; Hellen, C. U.; Pestova, T. V., Release of initiation factors from 48S complexes during ribosomal subunit joining and the link between establishment of codon-anticodon base-pairing and hydrolysis of eIF2-bound GTP. *Genes & Development* **2004,** *18* (24), 3078-3093.

38. Majumdar, R.; Maitra, U., Regulation of GTP hydrolysis prior to ribosomal AUG selection during eukaryotic translation initiation. *EMBO J* **2005,** *24* (21), 3737-3746.

39. Jennings, M. D.; Kershaw, C. J.; White, C.; Hoyle, D.; Richardson, J. P.; Costello, J. L.; Donaldson, I. J.; Zhou, Y.; Pavitt, G. D., eIF2beta is critical for eIF5-mediated GDP-dissociation inhibitor activity and translational control. *Nucleic Acids Research* **2016,** *44* (20), 9698-9709.

40. Jennings, M. D.; Pavitt, G. D., eIF5 has GDI activity necessary for translational control by eIF2 phosphorylation. *Nature* **2010,** *465* (7296), 378-381.

41. Fernandez, I. S.; Bai, X. C.; Hussain, T.; Kelley, A. C.; Lorsch, J. R.; Ramakrishnan, V.; Scheres, S. H. W., Molecular architecture of a eukaryotic translational initiation complex. *Science* **2013,** *342* (6160), 1240585.

42. Wang, J.; Wang, J.; Shin, B. S.; Kim, J. R.; Dever, T. E.; Puglisi, J. D.; Fernandez, I. S., Structural basis for the transition from translation initiation to elongation by an 80S-eIF5B complex. *Nature Communications* **2020,** *11* (1), 5003.

43. Choi, S. K.; Olsen, D. S.; Roll-Mecak, A.; Martung, A.; Remo, K. L.; Burley, S. K.; Hinnebusch, A. G.; Dever, T. E., Physical and functional interaction between the eukaryotic orthologs of prokaryotic translation initiation factors IF1 and IF2. *Molecular and Cellular Biology* **2000,** *20* (19), 7183-7191.

44. Sorensen, H. P.; Hedegaard, J.; Sperling-Petersen, H. U.; Mortensen, K. K., Remarkable conservation of translation initiation factors: IF1/eIF1A and IF2/eIF5B are universally distributed phylogenetic markers. *IUBMB Life* **2001,** *51* (5), 321-327.

45. Yu, Y.; Marintchev, A.; Kolupaeva, V. G.; Unbehaun, A.; Veryasova, T.; Lai, S. C.; Hong, P.; Wagner, G.; Hellen, C. U.; Pestova, T. V., Position of eukaryotic translation initiation factor eIF1A on the 40S ribosomal subunit mapped by directed hydroxyl radical probing. *Nucleic Acids Research* **2009,** *37* (15), 5167-5182.

46. Olsen, D. S.; Savner, E. M.; Mathew, A.; Zhang, F.; Krishnamoorthy, T.; Phan, L.; Hinnebusch, A. G., Domains of eIF1A that mediate binding to eIF2, eIF3 and eIF5B and promote ternary complex recruitment in vivo. *The EMBO journal* **2003,** *22* (2), 193-204.

47. Acker, M. G.; Shin, B.-S.; Dever, T. E.; Lorsch, J. R., Interaction between eukaryotic initiation factors 1A and 5B is required for efficient ribosomal subunit joining. *Journal of Biological Chemistry* **2006,** *281* (13), 8469-8475.

48. Wang, J.; Johnson, A. G.; Lapointe, C. P.; Choi, J.; Prabhakar, A.; Chen, D. H.; Petrov, A. N.; Puglisi, J. D., eIF5B gates the transition from translation initiation to elongation. *Nature* **2019,** *573* (7775), 605-608.

49. Kuhle, B.; Ficner, R., eIF5B employs a novel domain release mechanism to catalyze ribosomal subunit joining. *The EMBO Journal* **2014,** *33* (10), 1177-1191.

50. Jiang, X.; Jiang, X.; Feng, Y.; Xu, R.; Wang, Q.; Deng, H., Proteomic Analysis of eIF5B Silencing-Modulated Proteostasis. *PLOS ONE* **2016,** *11* (12), e0168387.

51. Kim, E.; Kim, J. H.; Seo, K.; Hong, K. Y.; An, S. W. A.; Kwon, J.; Lee, S.-J. V.; Jang, S. K., eIF2A, an initiator tRNA carrier refractory to eIF2α kinases, functions synergistically with eIF5B. *Cellular and molecular life sciences : CMLS* **2018,** *75* (23), 4287-4300.

52. Pestova, T. V.; de Breyne, S.; Pisarev, A. V.; Abaeva, I. S.; Hellen, C. U., eIF2-dependent and eIF2-independent modes of initiation on the CSFV IRES: a common role of domain II. *EMBO J* **2008,** *27* (7), 1060-1072.

53. Yamamoto, H.; Unbehaun, A.; Loerke, J.; Behrmann, E.; Collier, M.; Burger, J.; Mielke, T.; Spahn, C. M., Structure of the mammalian 80S initiation complex with initiation factor 5B on HCV-IRES RNA. *Nature Structural & Molecular Biology* **2014,** *21* (8), 721-727.

54. Adams, S. L.; Safer, B.; Anderson, W. F.; Merrick, W. C., Eukaryotic initiation complex formation. Evidence for two distinct pathways. *Journal of Biological Chemistry* **1975,** *250* (23), 9083-9089.

55. Zoll, W. L.; Horton, L. E.; Komar, A. A.; Hensold, J. O.; Merrick, W. C., Characterization of mammalian eIF2A and identification of the yeast homolog. *Journal of Biological Chemistry* **2002,** *277* (40), 37079-37087.

56. Holcik, M.; Sonenberg, N.; Korneluk, R. G., Internal ribosome initiation of translation and the control of cell death. *Trends in Genetics* **2000,** *16* (10), 469-473.

57. Shatsky, I.; Terenin, I.; Dmitriev, S.; Andreev, D., Eukaryotic translation initiation machinery can operate in a prokaryotic-like mode without eIF2. *Nature Precedings* **2008**.

58. Terenin, I. M.; Dmitriev, S. E.; Andreev, D. E.; Shatsky, I. N., Eukaryotic translation initiation machinery can operate in a bacterial-like mode without eIF2. *Nature Structural & Molecular Biology* **2008,** *15* (8), 836-841.

59. Yoon, A.; Peng, G.; Brandenburger, Y.; Zollo, O.; Xu, W.; Rego, E.; Ruggero, D., Impaired control of IRES-mediated translation in X-linked dyskeratosis congenita. *Science* **2006,** *312* (5775), 902-906.

60. Thakor, N.; Smith, M. D.; Roberts, L.; Faye, M. D.; Patel, H.; Wieden, H. J.; Cate, J. H. D.; Holcik, M., Cellular mRNA recruits the ribosome via eIF3-PABP bridge to initiate internal translation. *RNA Biology* **2017,** *14* (5), 553-567.

61. LaCasse, E. C.; Mahoney, D. J.; Cheung, H. H.; Plenchette, S.; Baird, S.; Korneluk, R. G., IAP-targeted therapies for cancer. *Oncogene* **2008,** *27* (48), 6252-6275.

62. Perrelet, D.; Ferri, A.; MacKenzie, A. E.; Smith, G. M.; Korneluk, R. G.; Liston, P.; Sagot, Y.; Terrado, J.; Monnier, D.; Kato, A. C., IAP family proteins delay motoneuron cell death in vivo. *European Journal of Neuroscience* **2000,** *12* (6), 2059-2067.

63. Deniz, N.; Lenarcic, E. M.; Landry, D. M.; Thompson, S. R., Translation initiation factors are not required for Dicistroviridae IRES function in vivo. *RNA* **2009,** *15* (5), 932-946.

64. Kerr, C. H.; Ma, Z. W.; Jang, C. J.; Thompson, S. R.; Jan, E., Molecular analysis of the factorless internal ribosome entry site in Cricket Paralysis virus infection. *Scientific Reports* **2016,** *6* (1), 37319.

65. Chew, G. L.; Pauli, A.; Schier, A. F., Conservation of uORF repressiveness and sequence features in mouse, human and zebrafish. *Nature Communications* **2016,** *7* (1), 11663.

66. Dever, T. E.; Feng, L.; Wek, R. C.; Cigan, A. M.; Donahue, T. F.; Hinnebusch, A. G., Phosphorylation of initiation factor 2 alpha by protein kinase GCN2 mediates gene-specific translational control of GCN4 in yeast. *Cell* **1992,** *68* (3), 585-596.

67. Pakos-Zebrucka, K.; Koryga, I.; Mnich, K.; Ljujic, M.; Samali, A.; Gorman, A. M., The integrated stress response. *EMBO reports* **2016,** *17* (10), 1374-1395.

68. Ross, J. A.; Bressler, K. R.; Thakor, N., Eukaryotic Initiation Factor 5B (eIF5B) Cooperates with eIF1A and eIF5 to Facilitate uORF2-Mediated Repression of ATF4 Translation. *International Journal of Molecular Sciences* **2018,** *19* (12), 4032.

69. Chen, H. H.; Tarn, W. Y., uORF-mediated translational control: recently elucidated mechanisms and implications in cancer. *RNA Biology* **2019,** *16* (10), 1327-1338.

70. Barbosa, C.; Peixeiro, I.; Romao, L., Gene expression regulation by upstream open reading frames and human disease. *PLOS Genetics* **2013,** *9* (8), e1003529.

71. Bressler, K. R.; Ross, J. A.; Ilnytskyy, S.; Vanden Dungen, K.; Taylor, K.; Patel, K.; Zovoilis, A.; Kovalchuk, I.; Thakor, N., Depletion of eukaryotic initiation factor 5B (eIF5B) reprograms the cellular transcriptome and leads to activation of endoplasmic

reticulum (ER) stress and c-Jun N-terminal kinase (JNK). *Cell Stress Chaperones* **2021,** *26* (1), 253-264.

72. Murakami, R.; Singh, C. R.; Morris, J.; Tang, L.; Harmon, I.; Takasu, A.; Miyoshi, T.; Ito, K.; Asano, K.; Uchiumi, T., The Interaction between the Ribosomal Stalk Proteins and Translation Initiation Factor 5B Promotes Translation Initiation. *Molecular and Cellular Biology* **2018,** *38* (16), e00067-18.

73. Hassanzadeh, G.; Naing, T.; Graber, T.; Jafarnejad, S. M.; Stojdl, D. F.; Alain, T.; Holcik, M., Characterizing Cellular Responses During Oncolytic Maraba Virus Infection. *International Journal of Molecular Sciences* **2019,** *20* (3), 580.

74. Wu, C.-Y.; Wang, D.-H.; Wang, X.; Dixon, S. M.; Meng, L.; Ahadi, S.; Enter, D. H.; Chen, C.-Y.; Kato, J.; Leon, L. J.; Ramirez, L. M.; Maeda, Y.; Reis, C. F.; Ribeiro, B.; Weems, B.; Kung, H.-J.; Lam, K. S., Rapid Discovery of Functional Small Molecule Ligands against Proteomic Targets through Library-Against-Library Screening. *ACS combinatorial science* **2016,** *18* (6), 320-329.

75. Galmozzi, E.; Aghemo, A.; Colombo, M., Eukaryotic initiation factor 5B: a new player for the anti-hepatitis C virus effect of ribavirin? *Medical Hypotheses* **2012,** *79* (4), 471-473.

76. Wilson, S. A.; Sieiro-Vazquez, C.; Edwards, N. J.; Iourin, O.; Byles, E. D.; Kotsopoulou, E.; Adamson, C. S.; Kingsman, S. M.; Kingsman, A. J.; Martin-Rendon, E., Cloning and characterization of hIF2, a human homologue of bacterial translation initiation factor 2, and its interaction with HIV-1 matrix. *The Biochemical Journal* **1999,** *342 (Pt 1)*, 97-103.

77. Deng, Y.; Singer, R. H.; Gu, W., Translation of ASH1 mRNA is repressed by Puf6p-Fun12p/eIF5B interaction and released by CK2 phosphorylation. *Genes & Development* **2008,** *22* (8), 1037-1050.

78. Zheng, J.; Li, X. Q.; Zhang, C. Y.; Zhang, Y. Q., eIF4E Overexpression Is Associated with Poor Prognoses of Ovarian Cancer. *Analytical Cellular Pathology* **2020,** *2020*, 8984526.

79. Sonenberg, N.; Hinnebusch, A. G., Regulation of translation initiation in eukaryotes: mechanisms and biological targets. *Cell* **2009,** *136* (4), 731-745.

80. Filipowicz, W.; Furuichi, Y.; Sierra, J. M.; Muthukrishnan, S.; Shatkin, A. J.; Ochoa, S., A protein binding the methylated 5'-terminal sequence, m7GpppN, of eukaryotic messenger RNA. *Proceedings of the National Academy of Sciences* **1976,** *73* (5), 1559-63.

81. Feoktistova, K.; Tuvshintogs, E.; Do, A.; Fraser, C. S., Human eIF4E promotes mRNA restructuring by stimulating eIF4A helicase activity. *Proceedings of the National Academy of Sciences* **2013,** *110* (33), 13339-13344.

82. Sonenberg, N., eIF4E, the mRNA cap-binding protein: from basic discovery to translational research. *Biochemistry and Cell Biology* **2008,** *86* (2), 178-183.

83. Patel, S.; Athirasala, A.; Menezes, P. P.; Ashwanikumar, N.; Zou, T.; Sahay, G.; Bertassoni, L. E., Messenger RNA Delivery for Tissue Engineering and Regenerative Medicine Applications. *Tissue Engineering Part A* **2019,** *25* (1-2), 91-112.

84. Liu, W. Z.; Zhao, R.; McFarland, C.; Kieft, J.; Niedzwiecka, A.; Jankowska-Anyszka, M.; Stepinski, J.; Darzynkiewicz, E.; Jones, D. N. M.; Davis, R. E., Structural Insights into Parasite eIF4E Binding Specificity for m(7)G and m(2,2,7)G mRNA Caps. *Journal of Biological Chemistry* **2009,** *284* (45), 31336-31349.

85. Kentsis, A.; Topisirovic, I.; Culjkovic, B.; Shao, L.; Borden, K. L., Ribavirin suppresses eIF4E-mediated oncogenic transformation by physical mimicry of the 7-methyl guanosine mRNA cap. *Proceedings of the National Academy of Sciences* **2004,** *101* (52), 18105-18110.

86. Filipowicz, W.; Bhattacharyya, S. N.; Sonenberg, N., Mechanisms of post-transcriptional regulation by microRNAs: are the answers in sight? *Nature Reviews Genetics* **2008,** *9* (2), 102-114.

87. Batool, A.; Aashaq, S.; Andrabi, K. I., Eukaryotic initiation factor 4E (eIF4E): A recap of the cap-binding protein. *Journal of Cellular Biochemistry* **2019,** *120* (9), 14201-14212.

88. De Benedetti, A.; Harris, A. L., eIF4E expression in tumors: its possible role in progression of malignancies. *The International Journal of Biochemistry & Cell Biology* **1999,** *31* (1), 59-72.

89. De Benedetti, A.; Graff, J. R., eIF-4E expression and its role in malignancies and metastases. *Oncogene* **2004,** *23* (18), 3189-3199.

90. Truitt, M. L.; Conn, C. S.; Shi, Z.; Pang, X.; Tokuyasu, T.; Coady, A. M.; Seo, Y.; Barna, M.; Ruggero, D., Differential Requirements for eIF4E Dose in Normal Development and Cancer. *Cell* **2015,** *162* (1), 59-71.

91. Yoshizawa, A.; Fukuoka, J.; Shimizu, S.; Shilo, K.; Franks, T. J.; Hewitt, S. M.; Fujii, T.; Cordon-Cardo, C.; Jen, J.; Travis, W. D., Overexpression of Phospho-eIF4E Is Associated with Survival through AKT Pathway in Non-Small Cell Lung Cancer. *Clinical Cancer Research* **2010,** *16* (1), 240-248.

92. Lejbkowicz, F.; Goyer, C.; Darveau, A.; Neron, S.; Lemieux, R.; Sonenberg, N., A fraction of the mRNA 5' cap-binding protein, eukaryotic initiation factor 4E, localizes to the nucleus. *Proceedings of the National Academy of Sciences* **1992,** *89* (20), 9612-9616.

93. Decker, C. J.; Parker, R., P-bodies and stress granules: possible roles in the control of translation and mRNA degradation. *Cold Spring Harbor Perspectives in Biology* **2012,** *4* (9), a012286.

94. Sukarieh, R.; Sonenberg, N.; Pelletier, J., The eIF4E-binding proteins are modifiers of cytoplasmic eIF4E relocalization during the heat shock response. *American Journal of Physiology-Cell Physiology* **2009,** *296* (5), C1207-C1217.

95. Eulalio, A.; Behm-Ansmant, I.; Izaurralde, E., P bodies: at the crossroads of post-transcriptional pathways. *Nature Reviews Molecular Cell Biology* **2007,** *8* (1), 9-22.

96. Brengues, M.; Parker, R., Accumulation of polyadenylated mRNA, Pab1p, eIF4E, and eIF4G with P-bodies in Saccharomyces cerevisiae. *Mol Biol Cell* **2007,** *18* (7), 2592-602.

97. Jain, S.; Wheeler, J. R.; Walters, R. W.; Agrawal, A.; Barsic, A.; Parker, R., ATPase-Modulated Stress Granules Contain a Diverse Proteome and Substructure. *Cell* **2016,** *164* (3), 487-498.

98. Campos-Melo, D.; Hawley, Z. C. E.; Droppelmann, C. A.; Strong, M. J., The Integral Role of RNA in Stress Granule Formation and Function. *Frontiers in Cell and Developmental Biology* **2021,** *9*.

99. Topisirovic, I.; Siddiqui, N.; Lapointe, V. L.; Trost, M.; Thibault, P.; Bangeranye, C.; Pinol-Roma, S.; Borden, K. L. B., Molecular dissection of the eukaryotic initiation factor 4E (eIF4E) export-competent RNP. *EMBO J* **2009,** *28* (8), 1087-1098.

100. Culjkovic, B.; Topisirovic, I.; Skrabanek, L.; Ruiz-Gutierrez, M.; Borden, K. L. B., eIF4E is a central node of an RNA regulon that governs cellular proliferation. *Journal of Cell Biology* **2006,** *175* (3), 415-426.

101. Volpon, L.; Culjkovic-Kraljacic, B.; Sohn, H. S.; Blanchet-Cohen, A.; Osborne, M. J.; Borden, K. L. B., A biochemical framework for eIF4E-dependent mRNA export and nuclear recycling of the export machinery. *RNA* **2017,** *23* (6), 927-937.

102. Culjkovic-Kraljacic, B.; Fernando, T. M.; Marullo, R.; Calvo-Vidal, N.; Verma, A.; Yang, S. N.; Tabbo, F.; Gaudiano, M.; Zahreddine, H.; Goldstein, R. L.; Patel, J.; Taldone, T.; Chiosis, G.; Ladetto, M.; Ghione, P.; Machiorlatti, R.; Elemento, O.; Inghirami, G.; Melnick, A.; Borden, K. L. B.; Cerchietti, L., Combinatorial targeting of nuclear export and translation of RNA inhibits aggressive B-cell lymphomas. *Blood* **2016,** *127* (7), 858-868.

103. Davis, M. R.; Delaleau, M.; Borden, K. L. B., Nuclear eIF4E Stimulates 3 '-End Cleavage of Target RNAs. *Cell Reports* **2019,** *27* (5), 1397-1408.e4.

104. Culjkovic, B.; Topisirovic, I.; Borden, K. L. B., Controlling gene expression through RNA regulons - The role of the eukaryotic translation initiation factor eIF4E. *Cell Cycle* **2007,** *6* (1), 65-69.

105. Culjkovic, B.; Topisirovic, I.; Skrabanek, L.; Ruiz-Gutierrez, M.; Borden, K. L. B., eIF4E promotes nuclear export of cyclin D1 mRNAs via an element in the 3 ' UTR. *Journal of Cell Biology* **2005,** *169* (2), 245-256.

106. Leppek, K.; Das, R.; Barna, M., Functional 5' UTR mRNA structures in eukaryotic translation regulation and how to find them. *Nature Reviews Molecular Cell Biology* **2018,** *19* (3), 158-174.

107. Leppek, K.; Fujii, K.; Quade, N.; Susanto, T. T.; Boehringer, D.; Lenarcic, T.; Xue, S.; Genuth, N. R.; Ban, N.; Barna, M., Gene- and Species-Specific Hox mRNA Translation by Ribosome Expansion Segments. *Molecular Cell* **2020,** *80* (6), 980-995.e13.

108. Martin, F.; Barends, S.; Jaeger, S.; Schaeffer, L.; Prongidi-Fix, L.; Eriani, G., Cap-Assisted Internal Initiation of Translation of Histone H4. *Molecular Cell* **2011,** *41* (2), 197-209.

109. Marcotrigiano, J.; Gingras, A. C.; Sonenberg, N.; Burley, S. K., Cap-dependent translation initiation in eukaryotes is regulated by a molecular mimic of elF4G. *Molecular Cell* **1999,** *3* (6), 707-716.

110. Matsuo, H.; Li, H.; McGuire, A. M.; Fletcher, C. M.; Gingras, A. C.; Sonenberg, N.; Wagner, G., Structure of translation factor eIF4E bound to m7GDP and interaction with 4E-binding protein. *Nature structural & molecular biology* **1997,** *4* (9), 717-724.

111. Volpon, L.; Culjkovic-Kraljacic, B.; Osborne, M. J.; Ramteke, A.; Sun, Q. X.; Niesman, A.; Chook, Y. M.; Borden, K. L. B., Importin 8 mediates m(7)G cap-sensitive nuclear import of the eukaryotic translation initiation factor eIF4E. *Proceedings of the National Academy of Sciences* **2016,** *113* (19), 5263-5268.

112. Mader, S.; Lee, H.; Pause, A.; Sonenberg, N., The Translation Initiation-Factor Eif-4e Binds to a Common Motif Shared by the Translation Factor Eif-4-Gamma and the Translational Repressors 4e-Binding Proteins. *Molecular and Cellular Biology* **1995,** *15* (9), 4990-4997.

113. Papadopoulos, E.; Jenni, S.; Kabha, E.; Takrouri, K. J.; Yi, T. F.; Salvi, N.; Luna, R. E.; Gavathiotis, E.; Mahalingam, P.; Arthanari, H.; Rodriguez-Mias, R.; Yefidoff-Freedman, R.; Aktas, B. H.; Chorev, M.; Halperin, J. A.; Wagner, G., Structure of the eukaryotic translation initiation factor eIF4E in complex with 4EGI-1 reveals an allosteric mechanism for dissociating eIF4G. *Proceedings of the National Academy of Sciences* **2014,** *111* (31), E3187-E3195.

114. Dostie, J.; Ferraiuolo, M.; Pause, A.; Adam, S. A.; Sonenberg, N., A novel shuttling protein, 4E-T, mediates the nuclear import of the mRNA 5 ' cap-binding protein, eIF4E. *EMBO J* **2000,** *19* (12), 3142-3156.

115. von der Haar, T.; Ball, P. D.; McCarthy, J. E. G., Stabilization of eukaryotic initiation factor 4E binding to the mRNA 5 '-cap by domains of eIF4G. *Journal of Biological Chemistry* **2000,** *275* (39), 30551-30555.

116. Ueda, T.; Watanabe-Fukunaga, R.; Fukuyama, H.; Nagata, S.; Fukunaga, R., Mnk2 and Mnk1 are essential for constitutive and inducible phosphorylation of eukaryotic initiation factor 4E but not for cell growth or development. *Molecular and Cellular Biology* **2004,** *24* (15), 6539-6549.

117. Ueda, T.; Sasaki, M.; Elia, A. J.; Chio, II; Hamada, K.; Fukunaga, R.; Mak, T. W., Combined deficiency for MAP kinase-interacting kinase 1 and 2 (Mnk1 and Mnk2) delays tumor development. *Proceedings of the National Academy of Sciences* **2010,** *107* (32), 13984-13990.

118. Wen, Q. Y.; Wang, W. Y.; Luo, J. D.; Chu, S. Z.; Chen, L. J.; Xu, L. N.; Zang, H. J.; Alnemah, M. M.; Ma, J.; Fan, S. Q., CGP57380 enhances efficacy of RAD001 in non-small cell lung cancer through abrogating mTOR inhibition-induced phosphorylation of eIF4E and activating mitochondrial apoptotic pathway. *Oncotarget* **2016,** *7* (19), 27787-27801.

119. Furic, L.; Rong, L. W.; Larsson, O.; Koumakpayi, I. H.; Yoshida, K.; Brueschke, A.; Petroulakis, E.; Robichaud, N.; Pollak, M.; Gaboury, L. A.; Pandolfi, P. P.; Saad, F.; Sonenberg, N., eIF4E phosphorylation promotes tumorigenesis and is associated with prostate cancer progression. *Proceedings of the National Academy of Sciences* **2010,** *107* (32), 14134-14139.

120. Hernandez, G.; Ramirez, J. L.; Pedroza-Torres, A.; Herrera, L. A.; Jimenez-Rios, M. A., The Secret Life of Translation Initiation in Prostate Cancer. *Front Genet* **2019,** *10*.

121. Morita, M.; Gravel, S. P.; Hulea, L.; Larsson, O.; Pollak, M.; St-Pierre, J.; Topisirovic, I., mTOR coordinates protein synthesis, mitochondrial activity and proliferation. *Cell Cycle* **2015,** *14* (4), 473-480.

122. Lu, C. W.; Makala, L.; Wu, D. Q.; Cai, Y. F., Targeting translation: eIF4E as an emerging anticancer drug target. *Expert Rev Mol Med* **2016,** *18*, e2.

123. Assouline, S.; Culjkovic, B.; Cocolakis, E.; Rousseau, C.; Beslu, N.; Amri, A.; Caplan, S.; Leber, B.; Roy, D. C.; Miller, W. H.; Borden, K. L. B., Molecular targeting of the oncogene eIF4E in acute myeloid leukemia (AML): a proof-of-principle clinical trial with ribavirin. *Blood* **2009,** *114* (2), 257-260.

124. Polunovsky, V. A.; Rosenwald, I. B.; Tan, A. T.; White, J.; Chiang, L.; Sonenberg, N.; Bitterman, P. B., Translational control of programmed cell death: Eukaryotic translation initiation factor 4E blocks apoptosis in growth-factor-restricted fibroblasts with physiologically expressed or deregulated Myc. *Molecular and Cellular Biology* **1996,** *16* (11), 6573-6581.

125. Coleman, L. J.; Peter, M. B.; Teall, T. J.; Brannan, R. A.; Hanby, A. M.; Honarpisheh, H.; Shaaban, A. M.; Smith, L.; Speirs, V.; Verghese, E. T.; McElwaine, J. N.; Hughes, T. A., Combined analysis of eIF4E and 4E-binding protein expression predicts breast cancer survival and estimates eIF4E activity. *British Journal of Cancer* **2009,** *100* (9), 1393-1399.

126. Osborne, M. J.; Borden, K. L. B., The eukaryotic translation initiation factor eIF4E in the nucleus: taking the road less traveled. *Immunological Reviews* **2015,** *263* (1), 210-223.

127. Topisirovic, I.; Guzman, M. L.; McConnell, M. J.; Licht, J. D.; Culjkovic, B.; Neering, S. J.; Jordan, C. T.; Borden, K. L. B., Aberrant eukaryotic translation initiation factor 4E-dependent mRNA transport impedes hematopoietic differentiation and contributes to leukemogenesis. *Molecular and Cellular Biology* **2003,** *23* (24), 8992-9002.

128. Ko, S. Y.; Guo, H.; Barengo, N.; Naora, H., Inhibition of Ovarian Cancer Growth by a Tumor-Targeting Peptide That Binds Eukaryotic Translation Initiation Factor 4E. *Clinical Cancer Research* **2009,** *15* (13), 4336-4347.

129. Herbert, T. P.; Fåhraeus, R.; Prescott, A.; Lane, D. P.; Proud, C. G., Rapid induction of apoptosis mediated by peptides that bind initiation factor eIF4E. *Current Biology* **2000,** *10* (13), 793-796.

130. Yang, H.; Li, L. W.; Shi, M.; Wang, J. H.; Xiao, F.; Zhou, B.; Diao, L. Q.; Long, X. L.; Liu, X. L.; Xu, L., In vivo study of breast carcinoma radiosensitization by targeting eIF4E. *Biochemical and Biophysical Research Communications* **2012,** *423* (4), 878-883.

131. Braun-Sand, S. B.; Peetz, M., Inosine monophosphate dehydrogenase as a target for antiviral, anticancer, antimicrobial and immunosuppressive therapeutics. *Future Medicinal Chemistry* **2010,** *2* (1), 81-92.

132. De la Cruz-Hernandez, E.; Medina-Franco, J. L.; Trujillo, J.; Chavez-Blanco, A.; Dominguez-Gomez, G.; Perez-Cardenas, E.; Gonzalez-Fierro, A.; Taja-Chayeb, L.; Duenas-Gonzalez, A., Ribavirin as a tri-targeted antitumor repositioned drug. *Oncology Reports* **2015,** *33* (5), 2384-2392.

133. Ogino, A.; Sano, E.; Ochiai, Y.; Yamamuro, S.; Tashiro, S.; Yachi, K.; Ohta, T.; Fukushima, T.; Okamoto, Y.; Tsumoto, K.; Ueda, T.; Yoshino, A.; Katayama, Y., Efficacy of ribavirin against malignant glioma cell lines. *Oncology Letters* **2014,** *8* (6), 2469-2474.

134. Volpon, L.; Osborne, M. J.; Zahreddine, H.; Romeo, A. A.; Borden, K. L., Conformational changes induced in the eukaryotic translation initiation factor eIF4E by a clinically relevant inhibitor, ribavirin triphosphate. *Biochemical and Biophysical Research Communications* **2013,** *434* (3), 614-619.

Chapter 2: The Interactions of Eukaryotic Translation Initiator Factor 5B (eIF5B) with RTP and LWW31: A Combined in cellulo and in silico Investigation

2.1. Introduction

eIF5B is a multi-domain protein that catalyzes the association of 40S and 60S ribosomal subunits during translation initiation in eukaryotes (Figure 2.1a).[1-3] Recent studies have implicated eIF5B's role in non-canonical translation,[4-6] which prevents apoptosis in certain cancer cells by promoting the synthesis of anti-apoptotic and immune-suppressing proteins.[5, 6] High expression of eIF5B allows cancer cells such as hepatocellular carcinoma (HCC), glioblastoma multiforme (GBM), and lung adenocarcinoma (LUAD) survive under treatment conditions.[4, 6, 7] However, among them, GBM is the most aggressive form of cancers.[8, 9] Testing effective small molecules against eIF5B in GBM cells could obviate the translation of eIF5B dependent proteins, making cells susceptible to apoptosis and immune response.

Previous studies on eIF5B have suggested that ligands like ribavirin triphosphate (RTP) and LWW31 could inhibit eIF5B.[10] However, RTP cannot permeate through the cell membrane due to its large size.[11] Therefore, ribavirin (RBV), a precursor of RTP, is generally used for cell culture studies.[12] Once inside the cell, RBV is phosphorylated to RTP by adenosine kinase (Figure 2.1b).[11, 13] LWW31 is another small molecule suggested to bind in the N-terminus region of eIF5B (1–586 residues; Figure 2.1c). However, there is no concrete evidence to attribute inhibition of eIF5B to binding in this region.[14] Therefore, LWW31 should also be tested against the functional C-terminal region of eIF5B to identify the binding sites.

Interestingly, computational biology tools like homology modeling, molecular docking, and molecular dynamics (MD) simulations have been proven to help obtain insights into structural changes of proteins and identify ligand binding sites even in the absence of a crystal structure.[15-17] Therefore, computational biology techniques provide the structural information about the interactions of ligands like LWW31 and RTP in the C-terminal region of eIF5B, which currently lacks an X-ray crystal structure.

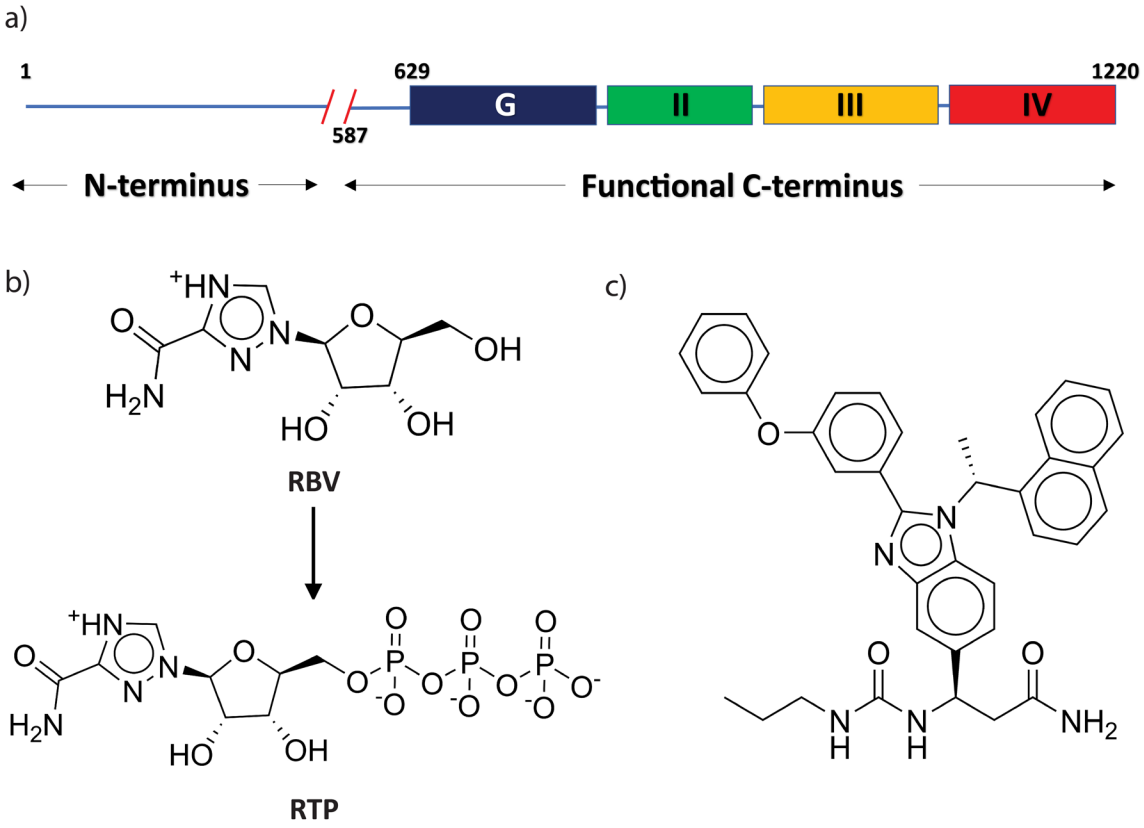

Figure 2.1 Different domains and small molecules targeting eIF5B. a) Functional part of eIF5B represented with different domains in the C-terminus region (629–1220 residues). b) Chemical structure of RBV and RTP where RBV is converted to RTP upon entering the cell. c) Chemical structure of LWW31.

In addition to understanding the ligand binding sites, it is important to study the structural changes of eIF5B since flexibility could affect the pocket formation on the

surface of a protein.[18] Previous experimental work on yeast shows that eIF5B adopts different conformations in the presence and the absence of the ribosome.[19, 20] In the presence of the ribosome, D1 and D3 establish interactions to catalyze GTP hydrolysis.[19] However, when eIF5B leaves the ribosome, D3 moderately rotates by disrupting the interaction with D1, which in turn increases D4 flexibility.[19] In the absence of wet bench biochemical experimental information, computational tools such as MD simulations can help determine whether human eIF5B undergoes structural changes like yeast eIF5B.

In this chapter, cell viability studies are employed to determine the half-maximal inhibitory concentration (IC_{50}) of RBV with or without pro-apoptotic cytokine treatment in three GBM cell lines, U343, BT25, and BT48. Western blot experiments are then used to assess the effect of RBV on eIF5B and its downstream targets in U343 and BT48 cells. Although ribavirin has other targets like eukaryotic initiation factor 4E (eIF4E), inosine 5'-phosphate dehydrogenase (IMPDH), and histone methyltransferase zeste homolog 2 (EZH2), its effect on these proteins has been studied in other cancers.[21-24] Therefore the present work is solely focused on understanding the effect of RBV on eIF5B. In addition to in cellulo approaches, MD simulations are employed to characterize RTP binding to eIF5B and corroborate the western blot results. While homology modeling was used to predict the structure of the C-terminus region of human eIF5B, MD simulations were used to provide insights into the flexibility of eIF5B in the absence of the ribosome. The broader flexibility of eIF5B uncovered using MD simulations, is necessary information for the future rational design of eIF5B-targeting ligands. Finally, docking calculations and MD simulations are used to identify potential binding sites and determine the stability of LWW31 binding in the C-terminal region of eIF5B, respectively.

2.2. Materials and Methods

2.2.1. Experimental materials and methods

2.2.1.1. Cell lines and reagents

BT25, BT48, and U343 cell lines were used for cell culture studies. Serum-free media was used for BT25 and BT48 cells, supplementing additionally with heparin sulfate (2 μg/ml; R&D Systems), fibroblast growth factor 2 (FGF-2; 20 ng/ml; R&D Systems), and epidermal growth factor (EGF; 20 ng/ml; Peprotech). Cells were propagated in a T25 flask in a humidified incubator at 37°C and 5% CO_2. Cell passage was done at regular intervals, and spheroid BT25 and BT48 cells were dissociated into single-cell suspension using accutase (Innovative Cell Technologies), which reformed spheroids upon incubation. For monolayer culturing of brain tumor initiating cells (BTICs), plates were coated with 1 μg/cm^2 laminin (Millipore Sigma) before seeding cells. Dulbecco's modified eagle medium (DMEM; HyClone) was used for U343 cell line, supplementing with 1% penicillin-streptomycin (Gibco), 10% fetal bovine serum (Gibco), 25 mmol L^{-1} glucose (Thermo Scientific), 1 mmol L^{-1} sodium pyruvate (Thermo Scientific), and 4 mmol L^{-1} L-glutamine (Thermo Scientific). TRAIL was obtained from Sigma-Aldrich. Lipofectamine RNAiMAX (Invitrogen, USA) and Opti-MEM (Gibco) were used to prepare transfection mixtures based on the instructions provided by the manufacturing company. Finally, sieIF5B (Invitrogen; HSS114469/70/71) and control siRNA (Qiagen; 297705515) were diluted to a working concentration of 20 μM and used for cell viability studies.

2.2.1.2. Cell viability assay

For assessing cell viability of BT25 and BT48 cells, 13,000 cells/well were seeded in a 96 well plate and incubated for 24 or 48 hours. After incubation, cells were treated

with five concentrations of ribavirin (0.1–1000 μM; Sigma-Aldrich) using a 10-fold dilution series, and further incubated for 96 hours. Furthermore, to study the effect of RBV and TRAIL treatment, cells were treated with TRAIL (100 ng/mL; Sigma-Aldrich) after 2h of RBV treatment. Finally, alamarBlue assay (Resazurin sodium salt; Sigma-Aldrich) was performed after 96 hours of incubation to determine the cell viability. Cytation 5 plate imager (BioTek) was used to evaluate the fluorescence (excitation, 560 nm; emission, 590 nm), and results obtained were normalized to control. In order to knockdown eIF5B in BTICs, cells were grown as a monolayer by seeding 13,000 cells/well on a laminin-coated 96 well plate and incubated for 24 hours. After incubation, cells were transfected and incubated further for 24 hours. Finally, control and eIF5B-depleted cells were treated with different concentrations of RBV (0.1-1000 μM). Cell viability of eIF5B knockdown cells was performed using alamarBlue assay after 96 hours of incubation. A similar cell viability protocol was used for U343 cell viability studies with varying cell seeding number and incubation times. For U343 cells, 10,000 cells/well were seeded in a 96 well plate, and incubated for 72 hours after RBV treatment. For knockdown studies, U343 cells were reverse transfected and treated with RBV after 24 hours. Upon RBV treatment, cells were incubated for 72 hours after which alamarBlue assay was performed. Dilutions for ribavirin were performed using phosphate buffer saline (PBS), and control wells were treated with PBS. All experiments were performed in three biological replicates. However, eIF5B depleted cell viability assays were performed in three technical replicates.

2.2.1.3. Immunoblotting

BT48 cells were seeded at 400,000 cells/well in BTICs medium containing a 6-well plate. For U343 cell line 300,000 cells/well were seeded in a 6-well plate. All the cell lines

were treated with RBV 24 hours after seeding. The concentration of RBV used for immunoblotting experiments was based on the IC_{50} value obtained for BT48, whereas for U343, it was 100 μM. Cells were harvested after 96 and 72 hours of incubation for U343 and BT48 cells, respectively. Harvested cells were lysed in radioimmunoprecipitation assay lysis (RIPA) buffer containing protease inhibitors. The protein concentration of the obtained lysate was estimated using Bradford assay. Once the concentration was determined, 15 μg and 20 μg of protein was loaded in sodium dodecyl sulfate-polyacrylamide gel electrophoresis (SDS-PAGE) for BT48 and U343, respectively. A protein dual color standard (Bio-Rad) was also added to one of the wells during SDS-PAGE. Separated proteins were transferred onto a nitrocellulose membrane (cytiva lifesciences). All blots were probed with primary antibodies including, eIF5B (ProteinTech), Bcl-xL (Cell Signalling Technology), XIAP (Cell Signalling Technology), c-FLIP (Cell Signalling Technology), cIAP1 (Abcam), and Nrf2 (Abcam; Table A.1). Furthermore, same blots were probed with a secondary antibody (anti-rabbit-HRP conjugate; Abcam; Table A.1) and bands were quantified in imager (AI600 imager, GE) using densitometry method. All proteins quantified were normalized to β-actin, which was detected with an anti-actin rhodamine antibody (Abcam).

2.2.1.4. Statistical analysis

All the data was quantified using GraphPad Prism 9, and statistical significance was calculated using unpaired, two-tailed t-test by setting the threshold value at $p \leq 0.05$. GraphPad Prism 9 was used to calculate half maximal inhibitory concentration (IC_{50}) for all alamarBlue assays. IC_{50} was calculated using non-linear regression analysis, with X axis

as log of dose and Y axis varying from 0 to 100, normalized to control. All quantitative data represented are mean ± standard error of the mean, unless indicated.

2.2.2. Computational Methods

2.2.2.1. Apo-eIF5B and eIF5B-GTP model building

Human eIF5B was modeled using UCSF chimera (version 1.14), which has an interface for MODELLER (version 9.22).[25-28] Since the N-terminus (1–628) of eIF5B is intrinsically disordered and less conserved than the C-terminus region,[29] eIF5B model containing amino acid residues 629–1220 was constructed. NCBI protein-BLAST (blastp) was used to obtain crystal structures similar to the target sequence from the Protein Data Bank (PDB).[30] Two templates were selected from the blastp results. While the first eIF5B template does not have GTP and Mg^{2+} bound, the second eIF5B template has a GTP and Mg^{2+} but lacks domains 3 and 4. Therefore, both structures were used as templates to enhance structure prediction. The first template is the crystal structure of eIF5B from *Saccharomyces cerevisiae* (yeast; PDB ID: 3WBI), which showed a sequence identity of 52% (314 residue (human eIF5B) hits out of 602 residues (yeast eIF5B)) to the human eIF5B amino acid sequence. The second template is the crystal structure of eIF5B from *Chaetomium thermophilum* (fungus; PDB ID: 4NCN), which showed a sequence identity of 57% (256 residue (human eIF5B) hits out of 447 residues (yeast eIF5B)) to the human eIF5B amino acid sequence. From two templates, MODELLER generated five eIF5B-GTP models, but only one structure with the best normalized discrete optimized protein energy (zDOPE) score was selected for subsequent docking and MD studies.

The MODELLER generated eIF5B-GTP model (MOD eIF5B-GTP) was refined using the GalaxyRefine web-based server,[31] and the output was validated using

Ramachandran plot (RC plot).[32] Outliers observed in RC plot were removed and relooped using the loop refinement protocol in MODELLER.[25, 28] The final relooped output was validated using VERIFY 3D, ERRAT, PROCHECK, and Quality Estimate analyses to determine the accuracy of the predicted structure.[32-36] Additionally, a full structure of human eIF5B was obtained from the AlphaFold (AF eIF5B-GTP) database and the first 628 amino acids were removed, with the goal to validate the initial human eIF5B model generated by MODELLER (Figure A.8).[37] Finally, apo-eIF5B model was generated by removing GTP from MOD eIF5B-GTP model in PyMOL (version 2.3.2).

2.2.2.2. eIF5B-RTP and LWW31 model building

Since RTP is a GTP analogue, it has been hypothesized by Galmozzi and colleagues that RTP competes with GTP to bind to eIF5B.[10] Therefore, GTP in the MOD eIF5B-GTP model was modified to a eIF5B-RTP model using PyMOL (version 2.3.2).[38]

To generate the eIF5B-GTP-LWW31 model in the absence of information about the three-dimensional structure and the precise eIF5B binding site for LWW31, the structure of LWW31 was initially constructed using GaussView 6 and optimized with B3LYP/6-31G(d) in the gas phase. Furthermore, the optimized LWW31 structure was used to search the potential energy surface of LWW31 with respect to all key torsional angles using AMBER95 in HyperChem. Subsequently, structures obtained from HyperChem were re-optimized with B3LYP-D3(BJ)/6-31G(d,p) to determine the relative energies using Gaussian 16 (G16 Rev. C.01).[39] The lowest energy conformation of LWW31 was used for docking studies and to generate RESP charges for the force field description.

Prior to docking, minimization, heating, and equilibration was performed for MOD eIF5B-GTP to remove steric clashes and poor geometric features. Post equilibration, the first 100 ns of the trajectory (details of MD are explained in next sub-section) was clustered (with respect to the protein backbone) and submitted for docking studies. Although the AF eIF5B-GTP model could have been used for docking, the structure became available later (July 2021). Blind docking was carried out using AutoDock Vina to determine the binding site of LWW31 to eIF5B.[40] PDBQT files of eIF5B and LWW31 were generated using AutoDock Tools (ADT; version 1.5.6), which were used as input files for AutoDock Vina.[41, 42] Blind docking was performed using grid dimensions that include the entire eIF5B (size x = 76, size y = 82, and size z = 102). An exhaustiveness of 100 was implemented, and the top two eIF5B-GTP-LWW31 structures were considered for MD simulations.

2.2.2.3. Molecular dynamics simulation protocol

The MOD eIF5B-GTP, AF eIF5B-GTP, apo-eIF5B, eIF5B-RTP, and eIF5B-GTP-LWW31 models were generated as described above and used for MD studies. Parameters for eIF5B in these models was described using AMBERff14SB.[43] Parameters for GTP were adopted from the AMBER parameter database.[44] Charges for RTP were obtained from restrained electrostatic potential (RESP) charge calculations using the geometry optimized with B3LYP/6-31+G(d) in implicit solvent (IEFPCM; water) as implemented in Gaussian 16 (G16 Rev. C.01).[39] Atom types were assigned for RTP and LWW31 using Antechamber with missing parameters being supplemented by GAFF.[45, 46] Each of the 5 models (namely MOD eIF5B-GTP, AF eIF5B-GTP, apo-eIF5B, eIF5B-RTP, and eIF5B-GTP-LWW31) were solvated in tleap using the TIP4PEW water model in an octahedral box,[45] with each edge of the box being 10.0 Å away from the edge of the solute in every direction. All

models were neutralized and then brought to a physiological salt concentration (150 mM) via the addition of Na^+ and Cl^- ions.

Each system was minimized over four stages. The first stage used 4,000 and 1,000 steps of steepest descent and conjugate gradient optimization algorithms, respectively. The last three stages used 2,000 and 1,000 steps of steepest descent and conjugate gradient optimization algorithms, respectively. In the first minimization stage, the solvent was relaxed, while restraints were applied to all other atoms. In the second stage, all hydrogen atoms were minimized. In the third stage, all atoms except solute were minimized, and no restraints were applied in the final step. A force constant of 100 kcal/(mol $Å^2$) was used for restraints in the three stages of minimization. After minimization, each system was gradually heated from 10 K to 310 K in six increments that increased the temperature by 50 K in each step. A restraint of 25 kcal/(mol $Å^2$) was applied on the solute during all heating steps. Finally, the restraints on the solute were gradually removed in five increments, using four equal reductions in the force constant from 20 to 5 kcal/mol $Å^2$, and a final reduction from 5 to 1.5 kcal/mol $Å^2$. Each incremental step was run for 20 ps. The particle-mesh Ewald method was used for long-range electrostatic interactions, and a non-bonded cut-off of 10 Å was implemented for all simulations. MD simulations on MOD eIF5B-GTP, apo-eIF5B, and eIF5B-GTP-LWW31 were performed for 1,000 ns in triplicate using the AMBER18 suite. However, prior to MD simulation, MOD eIF5B-GTP system was equilibrated for a 213 ns. Additionally, only a single 1,000 ns MD simulations was run for the AF eIF5B-GTP complex, whereas RTP in the eIF5B-RTP complex was displaced from the eIF5B binding site within the first 50 ns at which time the simulation was terminated.

Post trajectory analyses for all replicates were done independently using cpptraj,[47] including the root-mean-square deviation (RMSD), root-mean-square fluctuation (RMSF), hydrogen-bond analysis (HBA), distance analysis, clustering, and solvent accessible surface area (SASA) of the protein. The RMSD of the protein backbone and ligand heavy atoms were calculated for all protein-ligand systems with respect to initial model (prior to minimization). The backbone RMSF of the protein was calculated to identify the ordered and flexible regions. The percentage occupancy of hydrogen bonds between the protein and ligand were calculated using an angle cut off of 120° and a distance cut off of 3.4 Å. For the clustering analysis, the Heiragglo algorithm was used to generate the representative structures. Representative structures of the eIF5B-LWW31 complex were used as inputs for the protein-ligand interaction profiler (PLIP) to analyze non-covalent interactions.[48]

2.2.2.4. Free energy calculations

The molecular mechanics generalized born surface area (MM-GBSA) method was employed to carry out free energy calculations. MM-GBSA is one of the effective methods to quantify the binding affinity between a protein and ligand from the trajectory data.[49] Equations for calculating the binding free energy ($\Delta G_{binding}$) are given below

$$\Delta Gbinding = \Delta GR + L - (\Delta GR + \Delta GL) = \Delta EMM + \Delta Gsol - T\Delta S$$

$$\Delta EMM = \Delta Eint + \Delta EvdW + \Delta Eelec$$

$$\Delta Gsol = \Delta GGB + \Delta GSA$$

From the equation, ΔG_{R+L} is the free energy of the protein and ligand complex, whereas ΔG_R and ΔG_L are the free energies of the protein and ligand, respectively. The sum of these values is equal to the sum of the molecular mechanical interaction (ΔE_{MM}), solvation

(ΔG_{sol}), and the change in the conformation entropy ($-T\Delta S$). ΔE_{MM} is the sum of van der Wresiduesls (ΔE_{vdW}), intermolecular interactions (ΔE_{int}) and electrostatic terms (ΔE_{elec}) (Eq. 2), while ΔG_{sol} is the sum of the polar and non-polar terms (Eq. 3). Parmed was used to generate prmtop input files. For each system, 20,000 snapshots spanning over 1,000 ns were used to calculate the free binding energy of all protein-ligand complexes.

2.3. Results

2.3.1. Cytotoxic effect of RBV, with or without TRAIL, varies in different GBM cell lines

BT25, BT48 and U343 cells were treated with RBV (24 h after seeding) to evaluate the cytotoxicity. The concentration of RBV used for the study ranges from 0.1 μM to 1 mM. As shown in Figure 2.2a, RBV treatment did not affect the viability of BT25 cells at lower concentrations, but a significant reduction in viability was observed at higher concentrations. In contrast, upon RBV treatment, a dose-dependent reduction in viability was observed in BT48 cells (Figure 2.2b). Additionally, U343 showed no noticeable reduction in cell viability even at high RBV concentrations (Figure 2.2c). Overall, BT25 and BT48 showed IC_{50} values of 187.48 μM and 147.63 μM, respectively (Table 2.1). Taken together, these results suggest that RBV treatment has a varying effect on different cell lines, specifically U343, which did not show robust effect even at high RBV concentrations.

In previous studies, TRAIL had a profound impact on the viability of eIF5B depleted GBM cells.[6] Therefore, experiments were carried out to determine whether RBV and TRAIL treatment has a similar impact on cell viability. Before determining the combined effect of RBV and TRAIL, the cell viability of TRAIL treatment alone was

assessed in BT25, BT48, and U343 cells. The TRAIL concentration (100 ng/ml) used for the experiment was based on the previous study on GBM cell lines.[6] The cytotoxic effect of TRAIL was determined under two treatment conditions, early (TRAIL treated 24 h after seeding) or late (TRAIL treated 48 h after seeding). The early treatment results suggested that TRAIL has a significant impact on BT25 cell viability compared to control, reducing

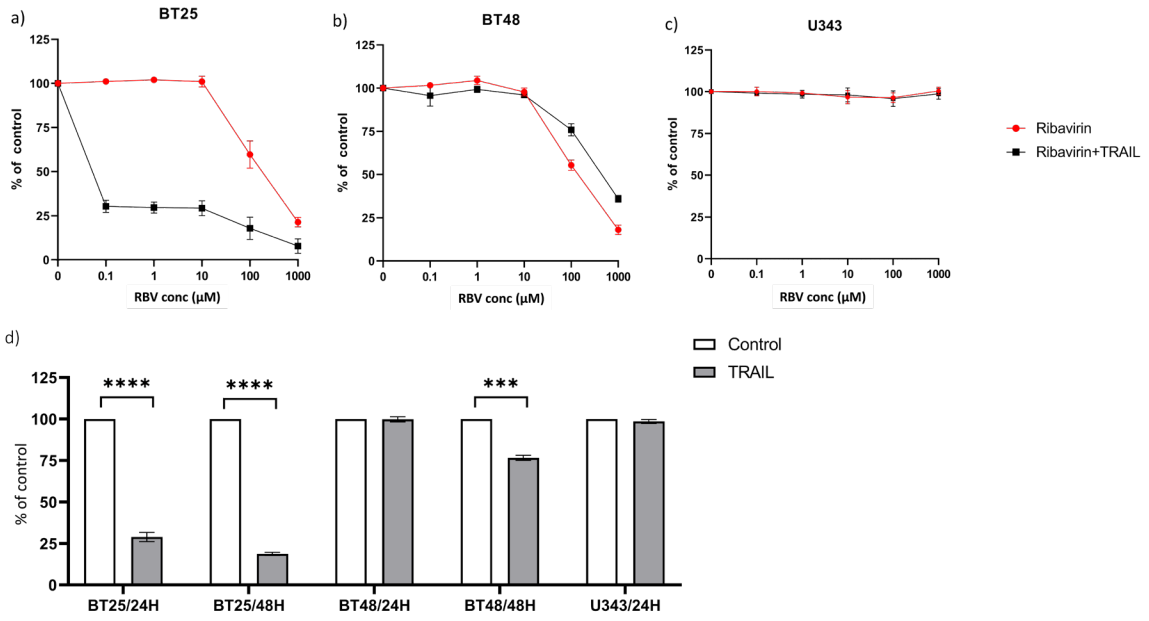

Figure 2.2 The inhibitory effect of RBV with or without TRAIL tested in three different cell lines, a) BT25, b) BT48, and c) U343. Cells were treated with TRAIL (100 ng/mL) 2 h after the addition of RBV. d) Control cells treated with PBS, and test cells treated with TRAIL at different timepoints 24h (early) or 48 h (late) after seeding. TRAIL concentration used was 100 ng/mL. Unlike BT25 and BT48 cells, U343 cells do not grow as spheroids. Therefore, 48h timepoint was not considered for U343 cells. At 0 µM, cells were treated with neither RBV nor TRAIL. Data shown here is an average ± SEM of three independent biological replicates; ***, $p < 0.001$; ****, $p < 0.0001$.

Table 2.1 IC_{50} of BT25 and BT48 cell lines when RBV is treated with or without TRAIL. Since U343 did not show any change, IC_{50} is not shown here.

Cell line	**IC_{50} of Ribavirin (µM)**	**IC_{50} of Ribavirin (µM) in the presence of TRAIL**
BT25	187.48	ND
BT48	147.63	463.55

viability to 29% (Figure 2.2d). In contrast, BT48 cells showed resistance to early TRAIL treatment with no effect on cell viability (Figure 2.2d). Under late treatment conditions, TRAIL further reduced the cell viability of BT25 cells to 19%, and interestingly, TRAIL significantly reduced the cell viability of BT48 cells to 77% (Figure 2.2d). However, U343 cells showed resistance to TRAIL treatment (Figure 2.2d). These results indicate that TRAIL shows greater cytotoxicity against BT25 cells and inhibits BT48 cells when the treatment is delayed.

2.3.2. TRAIL does not enhance the activity of RBV in BT48 and U343 cells

To evaluate the combined effect of RBV and TRAIL treatment on cell viability, BT25, BT48 and U343 cells were treated with both ligands 24 h after seeding. Compared to RBV treatment alone, TRAIL and RBV treated BT25 cells showed cell viability below 50% at all concentrations, and the reduction was predominantly due to TRAIL (Figure 2.2a,d). Because of the extremely low cell viability, the IC_{50} was not determined for BT25 cells. In contrast, compared to RBV treatment alone, RBV treated BT48 and U343 cells had little to no effect upon exposure to TRAIL (Figure 2.2b,c). While BT48 cells showed a IC_{50} of 147.63 μM with RBV treatment, the IC_{50} increased to 463.55 μM when RBV and TRAIL drugs were used (Figure 2.2b, Table 2.1). Taken together, these results indicate that the combined treatment of TRAIL and RBV does not amplify the cytotoxicity of RBV in BT25 and U343 cells, and RBV and TRAIL treatment augments the viability in BT48 cells, increasing the IC_{50} value.

2.3.3. BT25 and BT48 cells show increased resistance when RBV treatment is delayed

BT25 and BT48 cells were treated with RBV (48 h after seeding) to determine the inhibitory effect of late RBV treatment. Compared to early RBV treatment (Figure 2.2a,b), both BT25 and BT48 cells exhibited increased resistance to late RBV treatment (Figure 2.3a,b). This was evident from the IC_{50} of RBV in BT25 and BT48, which showed 840.00 µM and 473.58 µM, respectively (Table 2.2), indicating that RBV has a varying cell viability effect depending on the time of treatment.

Interestingly, a combination of late RBV and TRAIL (ligands treated after 48 hours) led to the further reduction of cell viability in BT25 (Figure 2.3a). This data correlates with the late TRAIL treatment data (Figure 2.2d), indicating the viability reduction observed is due to TRAIL treatment alone (Figure 2.3a). Additionally, TRAIL augmented the viability of RBV treated BT48 cells at higher concentrations as compared to cells without TRAIL (Figure 2.3b).

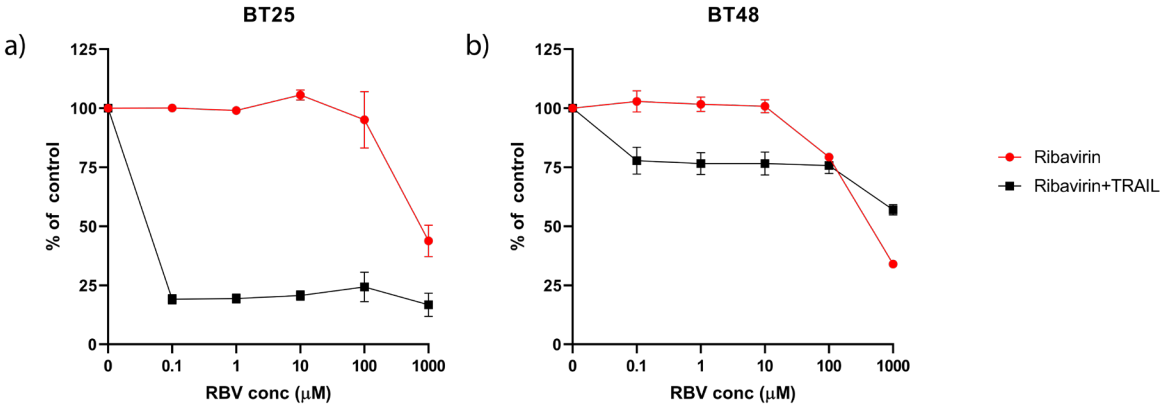

Figure 2.3 Inhibitory effect of Late RBV treatment with or without TRAIL tested in a) BT25 and b) BT48 cell lines. TRAIL concentration used for the cell viability studies was 100 ng/mL, and at 0 µM, cells were treated with neither RBV nor TRAIL. Data shown here is an average ± SEM of three independent biological replicates.

Table 2.2 IC_{50} values of BT25 and BT48 cell lines when RBV is treated late, with or without TRAIL.

Cell line	Ribavirin IC_{50} (μM)	IC_{50} of Ribavirin (μM) in the presence of TRAIL
BT25	840.00	ND
BT48	473.58	ND

2.3.4. eIF5B knockdown does not enhance the activity of RBV in BT25 and BT48 cells

Since the combination of RBV and TRAIL did not amplify the cytotoxicity of RBV substantially, its influence on cell viability in eIF5B depleted BT25, BT48, and U343 cells was evaluated. Before assessing RBV effect, the viability of all eIF5B depleted cells alone was determined. Consistent with previous studies, silencing eIF5B did not affect the viability of BT25, BT48 and U343 cells (Figure 2.4).[6, 50] Furthermore, depleting eIF5B in BT25 and BT48 cells did not enhance the activity of RBV, compared to control cells (Figure 2.5a,b). Overall, RBV treatment in eIF5B depleted BT25, and BT48 cells showed IC_{50} values of 288.76 μM, and 959.24 μM, respectively (Table 2.3), which is high compared to RBV treated siC BT25 and BT48 cells, which showed 61.36 μM and 336.52

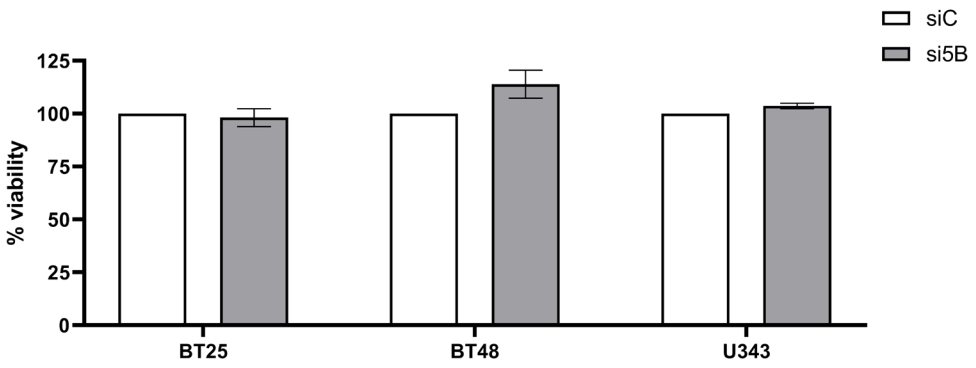

Figure 2.4 Different GBM cell lines treated with either control siRNA or eIF5B siRNA. si5B treated cells were normalized to control and shown as percentage alamarBlue activity.

μM, respectively (Table 2.3). eIF5B depleted U343 cells were resistant to RBV treatment, showing no effect on the cell viability (Figure 2.5c). Levels of eIF5B were quantified in U343 cells to ensure that the knockdown of eIF5B was robust. The results implied a robust reduction in levels of eIF5B in RBV treated and eIF5B depleted U343 cells (Figure A.1). Overall, the data derived indicates that silencing eIF5B in BT25 and BT48 cells do not enhance the cytotoxicity of RBV.

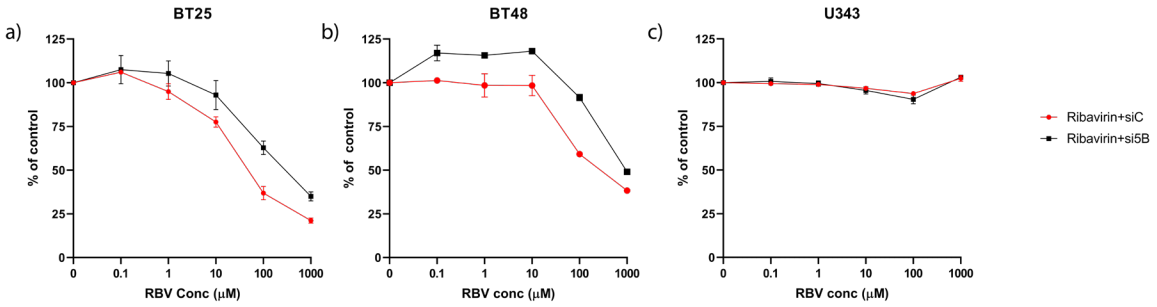

Figure 2.5 siC or si5B treated GBM cells treated with RBV after 24 and 48 h in a) BT25, b) BT48, and c) U343 cells. si5B and RBV treated cells were normalized to control and shown as a percentage of alamarBlue activity.

Table 2.3 IC_{50} values of si5B knockdown BT25 and BT48 cell lines treated with RBV.

Cell line	IC_{50} of Ribavirin (μM) in control cells	IC_{50} of Ribavirin (μM) in eIF5B depleted cells
BT25	61.36	288.76
BT48	336.52	959.24

2.3.5. Monolayer BT25 and BT48 cells are more sensitive to RBV over spheroid cells

Since growth conditions for spheroid and monolayer cells vary, the inhibitory effect of RBV could also vary. To assess this, the cell viability effect of RBV was assessed in spheroid and monolayer forms of BT25 and BT48 cells. As shown in Figure 2.6a, while

monolayer BT25 cells were more sensitive to RBV at low concentrations, spheroid BT25 cells were relatively more resistant. Although the viability of spheroid BT25 cells reduced at high concentrations, it was not substantial compared to monolayered cells (Figure 2.6a). Overall, the IC_{50} value of RBV for spheroid and monolayered BT25 cells was 840.00 µM and 61.36 µM, respectively (Table 2.4). In contrast, both monolayer and spheroid BT48 cells were resistant to RBV at lower concentrations until 10 µM. However, the cell viability of BT48 cells reduced drastically at 100 µM concentration in monolayer cells compared to spheroid cells (Figure 2.6b). The IC_{50} value of RBV for spheroid and monolayered BT48 cells was 473.58 µM and 336.52 µM, respectively (Table 2.4). Both BT25 and BT48 cell viability results suggest that RBV is more efficient at inhibiting monolayered BTICs cells than spheroid cells.

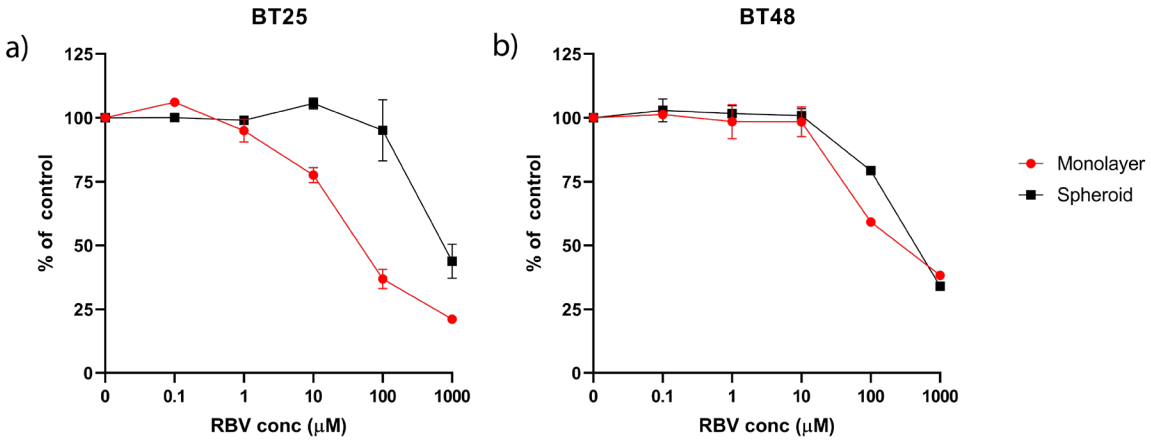

Figure 2.6 Comparison of alamarBlue activity between monolayered and spheroid forms of a) BT25 and b) BT48 cells. Cells were treated with RBV (48 h after seeding), and results are shown as a percentage of control.

Table 2.4 IC_{50} values of RBV treated BT25 and BT48 cell lines cultures either in monolayer or spheroid.

Cell line	IC_{50} of RBV (µM) for monolayer culture	IC_{50} of RBV (µM) for spheroid culture
BT25	61.36	840.00
BT48	336.52	473.58

2.3.6. No significant changes in levels of eIF5B dependent proteins in RBV treated BT48 and U343 cells

Since TRAIL treatment was not enhancing the activity of RBV, western blot experiments were carried to determine the levels of eIF5B and eIF5B dependent proteins in RBV treated BT48 and U343 cells. BT48 and U343 cells showed no significant changes in levels of eIF5B, Bcl-xL, XIAP, cIAP1, $cFLIP_L$, and $cFLIP_s$ (Figure 2.7a–d). However, levels of NRF2 was reduced in RBV treated BT48 cells but not in U343 cells (Figure 2.7b,d). Overall, this data suggests that the expression of eIF5B and eIF5B dependent proteins except NRF2 is not affected in the presence of RBV in BT48 and U343 cells.

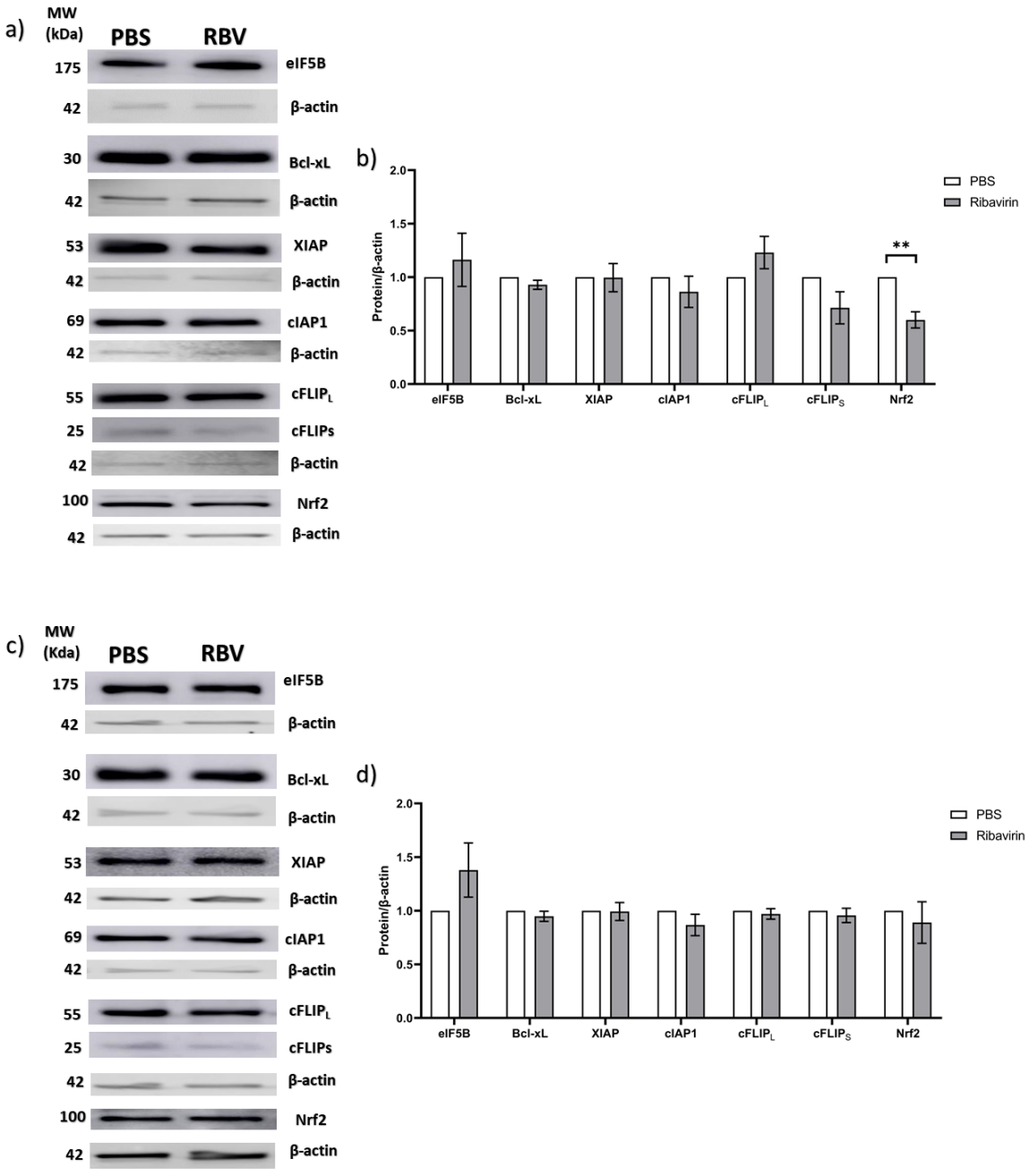

Figure 2.7 a) Representative blot images of eIF5B, Bcl-xL, XIAP, cIAP1, cFLIP$_L$ cFLIP$_S$, and NRF2 and b) their quantification in RBV treated BT48 cells. c) Representative blot images of aforementioned proteins and d) their quantification in RBV treated U343 cells. Values represented here are normalized to β-actin. Data shown is an average ± SEM of three independent biological replicates; **, $p < 0.01$.

2.3.7. MD simulations provide insight into human eIF5B structural dynamics

2.3.7.1. Human eIF5B sequence analysis and model building

To computationally study the binding of either RTP or LWW31 to eIF5B, structural information about human eIF5B is necessary. Therefore, eIF5B-GTP modeling was carried out to generate a reliable protein model for MD simulation and subsequent molecular docking studies. The MOD eIF5B-GTP model generated using MODELLER showed an estimated RMSD of 2.3 Å with respect to the template with 100% query cover and a zDOPE value of –0.6 (Figure 2.8a, A.2). A previous study on protein modeling has suggested that a zDOPE score of –0.5 or below indicates that the protein model generated adopts a native-like conformation,[51] implying the human eIF5B model is reliable. However, the RC plot showed 2 residues in the disallowed region of the model (Figure A.3), which was reduced to 1 through refinement and loop remodeling (Figure 2.8b, Table 2.5). In general, high quality RC plot would show <1% outliers,[52] and the RC plot generated for MOD eIF5B-GTP displayed only 0.2% outliers (Table 2.5). Furthermore, 93.9% of the residues were in the most favorable regions for the model, with previous work estimating that a high-quality structure has more than 90% of residues in the most favorable regions.[53] The eIF5B model also passed other validation analyses including ERRAT, Verify3D, and QMEAN, confirming the good quality of the model (Figure A.4a–c). Finally, the eIF5B model is within the Z-score mean value of other protein crystal structures in the PDB with similar residue number, again supporting its reliability (Figure 2.8c). Overall, using homology modeling, the first human eIF5B model was generated, which will be used to study the characteristics and ligand docking in the following sections.

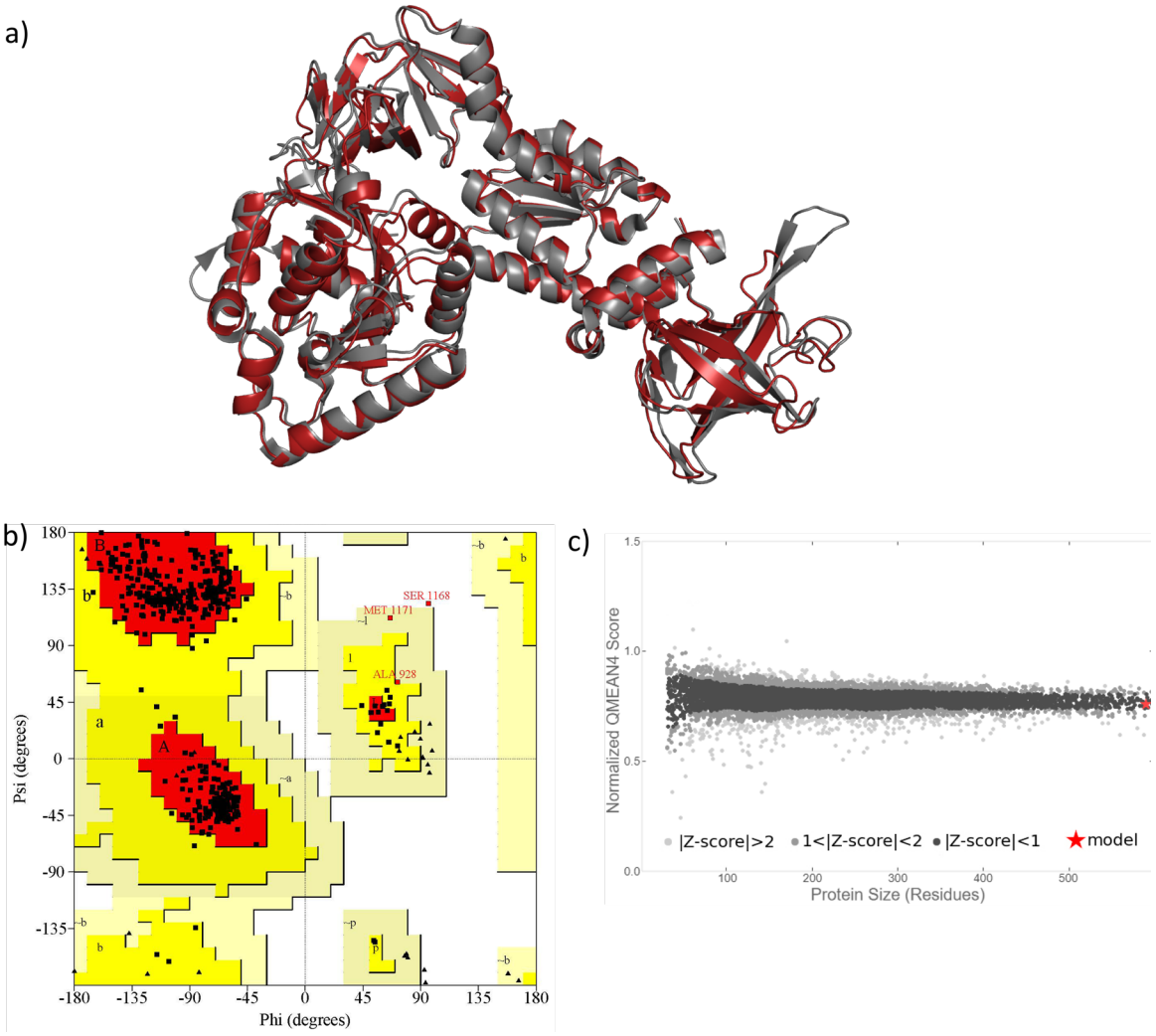

Figure 2.8 eIF5B validation and structure superposition. a) Superposition of the human eIF5B (brick red) model with the yeast eIF5B (grey) template. b) Ramachandran plot (RC plot) showing favorable and unfavorable regions for the human eIF5B model. The core region containing the most favoured regions is shown in red, while the additional allowed regions are shown in yellow. c) Comparison of the human eIF5B model with other nonredundant structures available in the protein data bank.

Table 2.5 The statistics of the RC plot (Figure 2.8b), showing allowed and disallowed regions after refinement and loop remodeling.

RC Plot Statistics		
Residues in most favoured regions [A,B,L]	494	93.9%
Residues in additional allowed regions [a,b,l,p]	29	5.5%

Residues in generously allowed regions [~a,~b,~l,~p]	2	0.4%
Residues in disallowed regions	1	0.2%
Number of non-glycine and non-proline residues	526	100.0%
Number of end-residues (Excluding Gly and Pro)	2	
Number of glycine residues (shown as triangles)	36	
Number of proline residues	28	
Total number of residues	592	

2.3.7.2. D3 and D4 influence the dynamics of human eIF5B

RMSD analysis of the protein backbone (N, C, CA) and the ligand heavy atoms was monitored in the MOD eIF5B-GTP model with respect to the refined initial structure. The

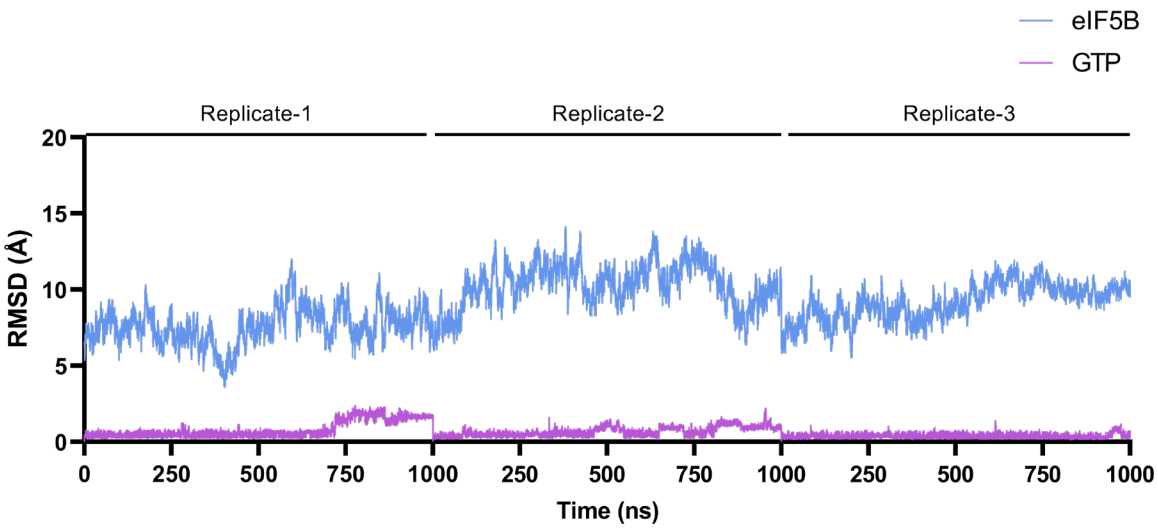

Figure 2.9 Shown here is the RMSD of eIF5B (blue) and GTP (magenta) in the MOD eIF5B-GTP complex.

eIF5B model exhibited high structural variations throughout the simulation in all replicates (RMSD = 9.0 ± 1.7 Å; Figure 2.9, Table A.2), suggesting that eIF5B is highly dynamic in solution. However, GTP in the binding site of eIF5B did not show substantial structural variations (RMSD = 0.6 ± 0.4 Å; Figure 2.9, Table A.2), suggesting stable interactions with

eIF5B. Furthermore, structural variations of individual domains were calculated to determine which domain(s) contribute to the high variations in the eIF5B structure. RMSD analysis suggested that D2 of eIF5B is the most stable domain, whereas D3 and D4 show high structural variations in all and two replicates, respectively (Figure 2.10a–f).

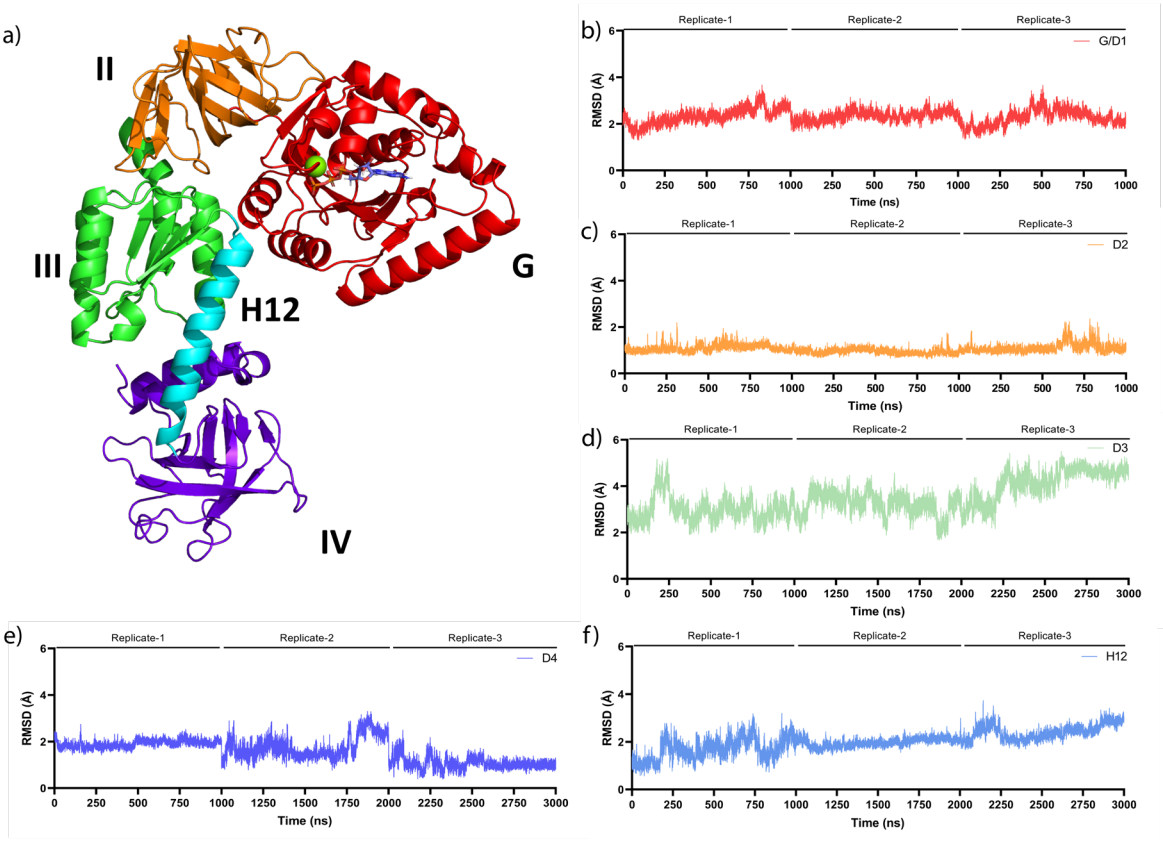

Figure 2.10 RMSD data of eIF5B represented in three replicates. a) The domains of the eIF5B model represented in different colors, including H12, each color corresponds to RMSD data of each domain shown in b) G/D1, c) D2, d) D3, e) D4, and f) H12.

Additionally, RMSF analysis suggested that most residues of D4 and some residues of D3 exhibit higher flexibility than D1 and D2 (Figure A.5a–d). These results are consistent with experimental studies on yeast eIF5B that showed resolving D4 is challenging due to its flexibility in solution.[19] The results also suggest that GTP forms a stable complex with eIF5B, with the contacts being formed are explained further in the following section.

2.3.7.3. Contacts driving the stability of GTP in eIF5B-GTP complex

Before understanding which residues contribute to the GTP stability in the binding pocket of human eIF5B, the flexibility of the binding pocket was determined when GTP is bound. Four regions make up the binding pocket of eIF5B, namely G1, G2, G3, and G4, which correspond to residues 638–646, 702–705, 756–759, and 824–826, respectively (Figure 2.11a).[54] Compared to apo-eIF5B, these four regions are less flexible in the presence of GTP (Figure 2.11b). However, binding of GTP increased the flexibility of residues 666–670 in the switch-I region (Figure 2.11b), which is stabilized by the H14 of rRNA during ribosomal association.[20, 54] Among the four regions, GTP established hydrogen bonds with G1, G3, and G4 regions, but not G2. Specifically, GTP forms hydrogen bond contacts with 645, 657, 665, 756, 759, and 826 (Figure A.6), contributing to the overall stability of GTP in the binding site of eIF5B. In addition to these residues, GTP is also stabilized by Mg^{2+} ion, which showed a consistent coordination with the β- (distance = 1.91 ± 0.05 Å) and γ-phosphate (distance = 1.88 ± 0.04 Å) oxygens of GTP throughout the simulation (Figure 2.11a; Table A3). Although GTP forms stable interactions in D1, the absence of GTP did not affect the overall stability of D1 in apo-eIF5B (Figure A.7). These results suggest that GTP does not affect the global flexibility, but rather only the surrounding regions in the binding site of human eIF5B.

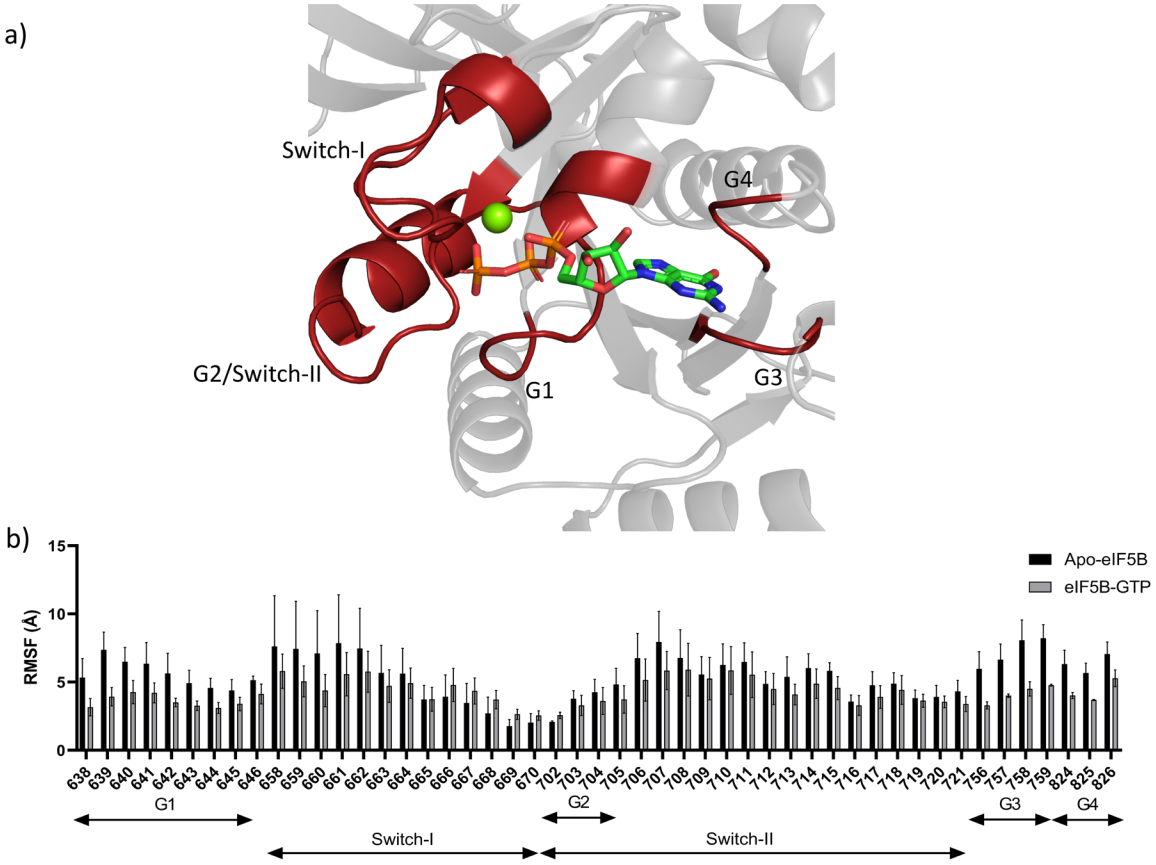

Figure 2.11 Representative structure of the eIF5B-GTP complex, highlighting a) the GTP (green), Mg^{2+} (green sphere), and residues of eIF5B (brick red) making up the binding pocket. b) Flexibility of the binding pocket residues in apo-eIF5B and eIF5B-GTP.

2.3.7.4. Human eIF5B adopts a unique conformation off-ribosome

In yeast, after eIF5B completes ribosomal association and tRNAi positioning, Tyr837 (human Tyr1063) is oriented towards His480 (human His706),[55] which is believed to be important for GTP hydrolysis. However, in the absence of the ribosome, interactions between D1 and D3 of eIF5B are broken, which impacts the distance between His706 of D1 and Tyr1063 of D3.[19, 20] To test this, the distance between His706 and Tyr1063 was calculated for the MOD eIF5B-GTP human model. The average distance between these two residues in MOD eIF5B-GTP (distance = 18.6 ± 3.2 Å) was more than the interacting

distance observed in the cryo-EM structure of yeast eIF5B on the ribosome (distance = 6.5 Å; Figure 2.12a,b).[55] Furthermore, the cryo-EM structure of yeast eIF5B was superimposed with the MD representative structure of the MOD eIF5B-GTP model. D3 and D4 of the eIF5B model rotated 81° compared to yeast eIF5B bound to the ribosome (Figure 2.12c), and this rotation is 21° greater than what was previously observed in other eukaryotes.[20] Nevertheless, it is important to consider that the eIF5B structure comparison involves two different organisms, which may have inherent structural differences. To address these differences and to further validate the human eIF5B model, a structure was retrieved from the recently established AlphaFold database, which is discussed in the following section.

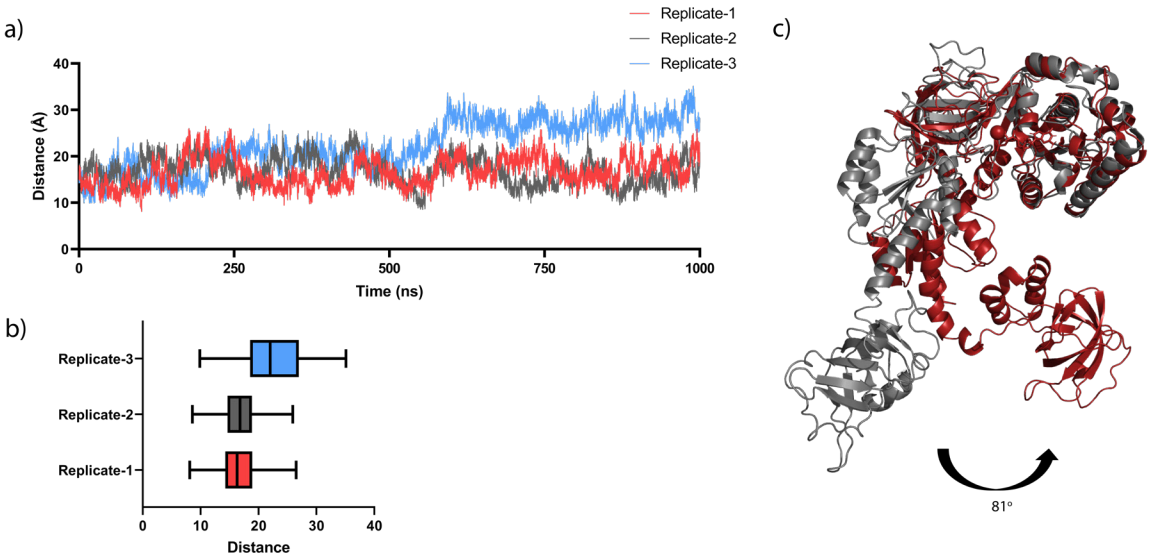

Figure 2.12 Influence of the eIF5B conformation on the distance between His706 and Tyr1063. Distance between His706 and Tyr1063 throughout each simulation replicate a) as a function of time and b) shown as box and whisker plots. c) Superimposition of isolated human eIF5B model (brick red) and yeast eIF5B (grey, PDB ID 6WOO) on the ribosome by the G-domain.

A second model of human eIF5B, the AF eIF5B-GTP model, was chosen to compare the rotational differences of the eIF5B structure in the presence and absence of

the ribosome. Since the conformation adopted by the AF eIF5B-GTP model is very similar to yeast eIF5B bound to the ribosome (Figure A.8), it was hypothesized that AF eIF5B-GTP undergoes structural changes like yeast eIF5B in a polar environment to attain a conformation similar to MOD eIF5B-GTP. RMSD analysis of the MD trajectories for AF eIF5B-GTP indicated that the complex is highly dynamic during the first 500 ns but stabilizes at higher RMSD for the remainder of the MD simulation (RMSD = 7.4 ± 0.9 Å, Figure 2.13a). Since a high RMSD indicated a shift in the conformation, the impact on the surface area of eIF5B was calculated, which revealed a gradual increase of SASA at ~350

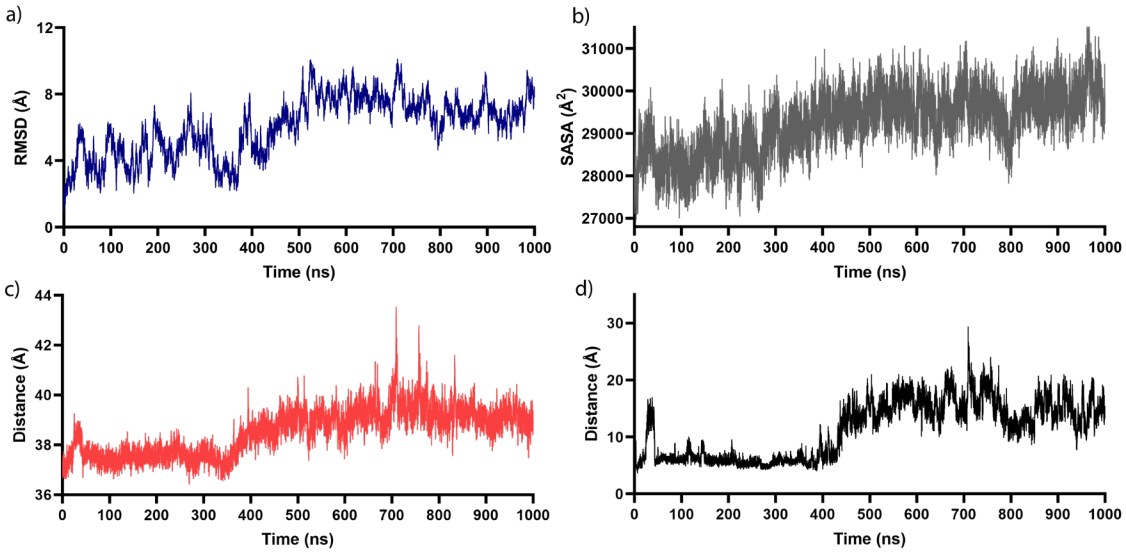

Figure 2.13 a) RMSD shows AF eIF5B is more dynamic in the first 500 ns. b) SASA increases gradually from 350 ns until 500 ns, indicating an increase in the surface area of eIF5B. c) The distance between D1 and D3 gradually increases from 350 to 500 ns. d) The distance between His706 and Tyr1063 abruptly increases at ~450 ns due to conformational changes in D3.

ns prior to the shift in the RMSD at ~450 ns (Figure 2.13b). Consistent with the SASA results, the distance between D1 and D3 gradually increased at ~350 ns, implying disruption of interactions (Figure 2.13c). This change in distance between the two domains

significantly impacted the distance between His706 and Tyr1063 after ~450 ns (Figure 2.13d, A.9), which ultimately led the structure of AF eIF5B-GTP to adopt a conformation similar to MOD eIF5B-GTP in solution (Figure A.10). Compared to the initial AF eIF5B-GTP model (prior to minimization), D3 and D4 rotated approximately 61° and 92°, respectively, by the end of the MD simulation (Figure 2.14a,b). Additionally, D3 and D4 are displaced approximately by 16 Å and 22 Å from their initial position. Overall, the results revealed that the combined rotation of D3 and D4 is 78° compared to the initial structure (prior to minimization), which is similar to the rotation (81°) observed in MOD eIF5B-GTP (Figure A.11). Like yeast eIF5B, the unique conformation adopted by the MOD eIF5B-GTP and AF eIF5B-GTP models due to the rotation of D3 and D4 could prevent GTP hydrolysis in the absence of the ribosome. Since both models adopt similar structures, the MOD eIF5B-GTP model was used for subsequent ligand docking studies.

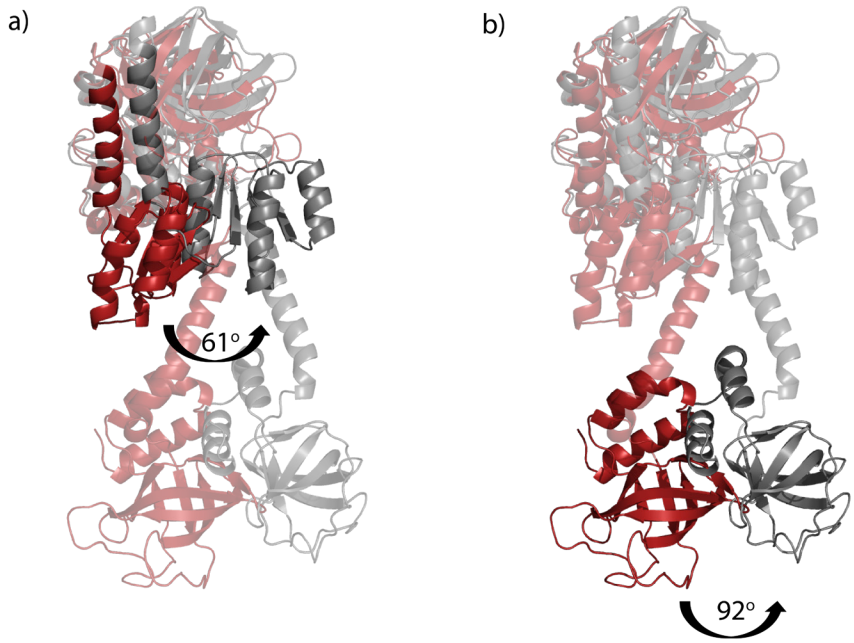

Figure 2.14 Superimposition of the initial (grey) and final structures of the AF eIF5B model with respect to G-domain. a) D3 rotated 61° from the initial AF eIF5B-GTP model. b) D4 rotated 92° from the initial AF eIF5B-GTP model.

2.3.8. Interactions of RTP and LWW31 with human eIF5B

2.3.8.1. RTP might not be an inhibitor of eIF5B

The experimental results presented previously have shown that ribavirin failed to affect the function of eIF5B. Therefore, to understand whether an interaction between RTP and eIF5B is possible, MD simulations were performed. In the MOD eIF5B-GTP representative structure, GTP was modified to RTP to generate the eIF5B-RTP model (Figure 2.15a). Following 50 ns MD simulation, RTP failed to form a stable complex with eIF5B (Figure 2.15b) and was instead displaced from the binding pocket due to repulsive forces between the cationic 1,2,4-triazole-3-carboxamide ring of RTP and the basic amino acids Lys647, Lys757, and His826 in the binding pocket (Figure 2.15b). The displacement of RTP during the MD simulations corroborates the western blot results, which clearly

showed that ribavirin does not affect the cellular levels of either eIF5B or its downstream targets.

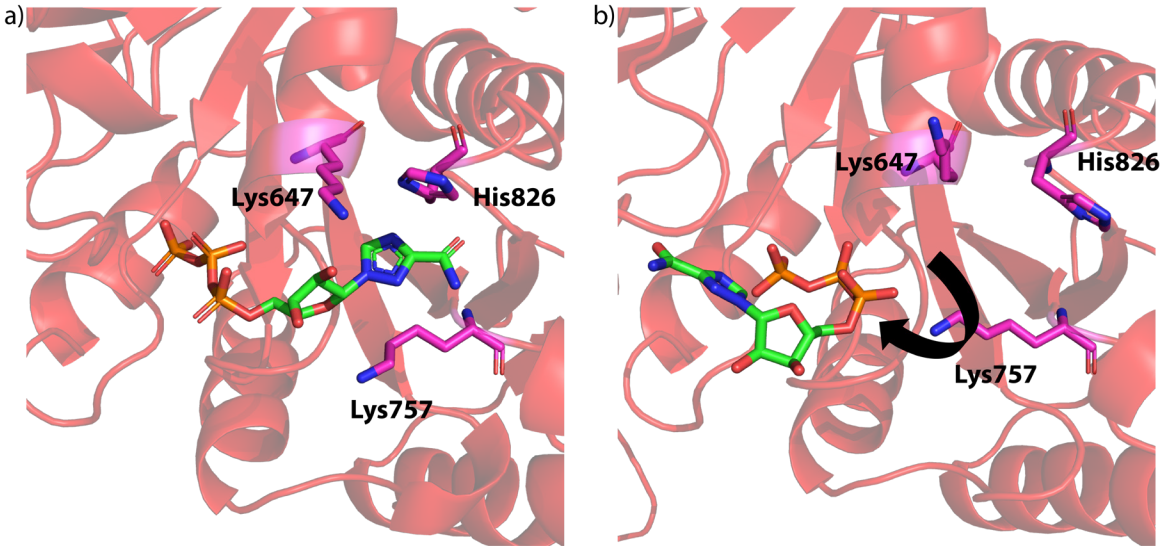

Figure 2.15 RTP interaction with eIF5B in eIF5B-RTP model. a) Key residues shown in the binding site, with RTP replaced by GTP. b) The positively charged triazole ring of RTP is displaced from the binding site due to the presence of basic amino acids. Hydrogen atoms are not shown for better visualization.

2.3.8.2. Molecular docking of LWW31 with eIF5B-GTP

As previous experimental studies have suggested LWW31 binds to eIF5B,[14] docking calculations were carried out against the conserved C-terminus region of eIF5B using AutoDock Vina to predict the binding site of LWW31. Based on an empirical scoring function, five binding sites were identified (Table 2.6). Although top four binding sites were considered for MD simulations initially, only the top two binding sites were able to form a stable complex, (binding affinity = –9.6 kcal/mol), namely, binding site-I (BS-I), which is found in the G-domain (Figure 2.16a), and binding site-II (BS-II), which is found

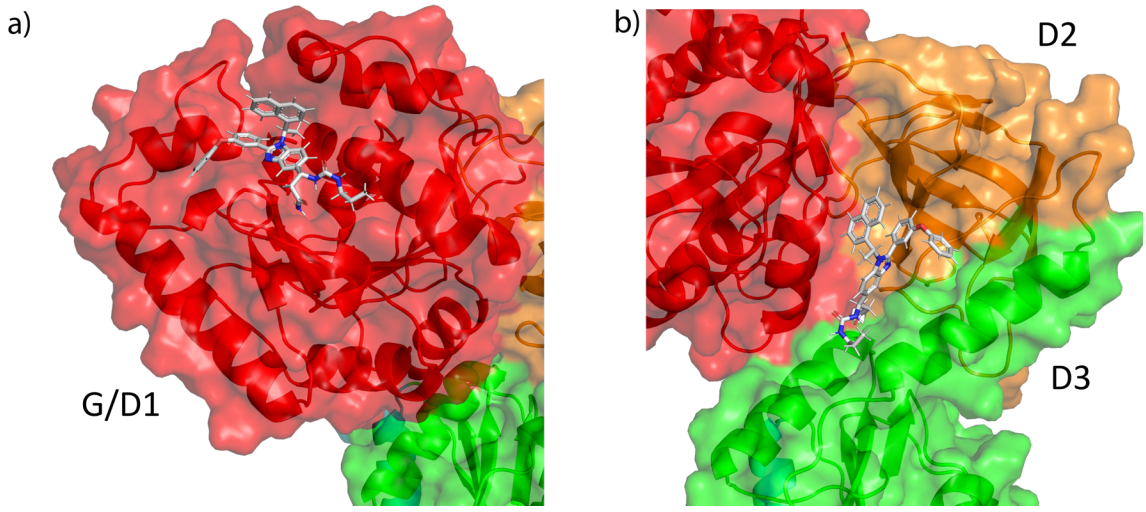

Figure 2.16 Surface representation of the top two eIF5B binding sites of LWW31. a) LWW31 BS-I occurs in D1, showing a deep groove. b) LWW31 BS-II occurs in a shallow pocket at the interdomain space of D2 and D3.

in the interdomain space of D2 and D3 (Figure 2.16b). The depth and hydrophobicity of BS-I is high compared to the BS-II (Figure 2.16a,b). MD simulations suggested that the stability of eIF5B in the presence of LWW31 in either BS-I (RMSD = 8.2 ± 1.7 Å; Figure 2.17a) or BS-II (RMSD = 6.6 ± 1.6 Å; Figure 2.17b) is comparable. However, the stability of LWW31 in BS-I is modestly better (0.67 ± 0.30 Å) than BS-II (0.79 ± 0.28 Å). Although LWW31 in BS-I and BS-II result in the same binding energy based on docking calculations, MD simulations suggest that LWW31 in BS-I forms a more stable complex with eIF5B.

Table 2.6 eIF5B binding affinities predicted by AutoDock Vina for LWW31.

Mode	Affinity (kcal/mol)	Distance from best mode	
		RMSD l.b.[a]	RMSD u.b.[a]
1	–9.6	0	0
2	–9.6	33.387	38.157
3	–9.5	39.361	41.513
4	–9.5	45.302	48.665
5	–9.3	50.711	54.11

[a]RMSD l.b. (lower bound) and u.b. (upper bound) of LWW31

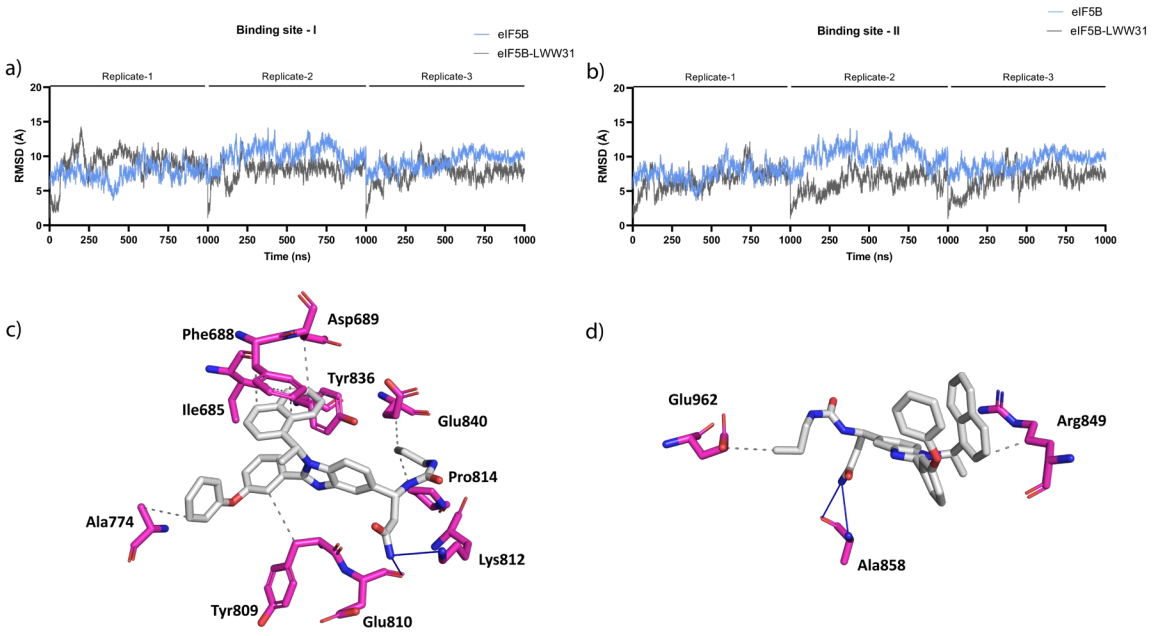

Figure 2.17 Stability of eIF5B-LWW31 complexes and key interactions. RMSD data for eIF5B when LWW31 is bound to a) BS-I and b) BS-II. Key interactions of LWW31 in c) BS-I and d) BS-II. Hydrogen atoms are not shown for better visualization.

Representative structures of LWW31 in both binding sites were submitted to PLIP to visualize the key interactions. Hydrophobic interactions are the driving forces promoting the stability of LWW31 in BS-I (Figure 2.17c). Specifically, Ile685, Phe688, Asp689, Ala774, Tyr809, and Tyr836 formed hydrophobic contacts with the aromatic groups of LWW31, whereas Glu840 and Pro814 of eIF5B showed hydrophobic contacts with the hydrocarbon tail of LWW31, which was further correlated by a lower polar solvation energy (ΔE_{polar} = 27.35 ± 1.49 kcal/mol) and better non-polar contributions ($\Delta E_{non\text{-}pol}$ = –58.79 ± 0.92 kcal/mol) to the binding free energy (Figure 2.17c, Table A.4). In addition to hydrophobic interactions, LWW31 was stabilized by two intermolecular hydrogen bonds with Glu810 and Lys812, giving LWW31 an overall free binding energy (ΔG_{bind} = –31.43 ± 1.32 kcal/mol; Figure 2.17c, Table 2.7, A.4). In contrast, LWW31 in BS-II had fewer

contacts with eIF5B compared to BS-I, with a higher polar solvation energy (ΔE_{polar} = 40.06 ± 2.28 kcal/mol; Table 2.7). While BS-I showed eight hydrophobic contacts, side chains of Arg849 and Glu962 of BS-II form two hydrophobic contacts with LWW31 (Table A.5). Additionally, LWW31 in BS-II establishes two hydrogen bonds with the backbone of Ala858, giving a total free binding energy (ΔG_{bind} = –26.17 ± 1.33 kcal/mol; Table A.5, Figure 2.18a) lower than LWW31 in BS-I (ΔG_{bind} = –31.43 ± 1.32 kcal/mol; Table 2.7, Figure 2.18a). These interactions indicate that LWW31 in BS-I is more favourable than LWW31 in BS-II due to the deeper binding pocket and more contacts (Table 2.6; Figure 2.17a,b). Furthermore, the druggability of these two binding pockets was assessed using Pockdrug. The Pockdrug program gives a druggability score from 0 to 1, with 1 being most favorable.[56] PockDrug assigned LWW31 BS-I with a score of 0.91 (Figure A.12) , but did not predict BS-II to be a druggable pocket, implying BS-I as the most favorable binding site for LWW31.

Binding free energy calculations were also carried out to determine whether LWW31 binding to eIF5B reduces GTP affinity. The results suggested that binding free energy of GTP is unaffected when LWW31 is bound either to BS-I (ΔG_{bind} = –97.02 ± 6.42 kcal/mol, Figure 2.18b) or BS-II (ΔG_{bind} = –96.29 ± 13.10 kcal/mol, Figure 2.18b) compared to the absence of LWW31 (ΔG_{bind} = –101.26 ± 6.01 kcal/mol). Additionally, GTP affinity to Mg^{2+} is also unaffected in the presence and absence of LWW31 either in BS-I or BS-II (Figure A.13).

Table 2.7 Free binding energies (kcal/mol) of GTP and LWW31 to eIF5B.

Ligand	GTP (LWW31 absent)	GTP (LWW31 bound to BS-I)	GTP (LWW31 bound to BS-II)	LWW31 (BS-I)	LWW31 (BS-II)
ΔE_{vdW}	–24.53 ± 1.36	–24.45 ± 0.78	–23.95 ± 1.63	–45.93 ± 1.56	–43.91 ± 2.33
ΔE_{elec}	–825.94 ± 23.36	–815.94 ± 3.06	–816.25 ± 34.75	–12.85 ± 1.67	–22.32 ± 3.24
ΔG_{GB}	755.04 ± 17.61	749.26 ± 2.60	749.72 ± 23.58	33.25 ± 1.39	45.82 ± 1.99
ΔG_{SA}	–5.85 ± 0.10	–5.88 ± 0.05	–5.82 ± 0.09	–5.90 ± 0.20	–5.76 ± 0.30
ΔE_{nonpol}	–850.46 ± 23.31	–840.39 ± 3.77	–840.20 ± 36.35	–58.79 ± 0.92	–66.23 ± 0.95
ΔE_{polar}	749.20 ± 17.54	743.38 ± 2.64	743.90 ± 23.50	27.35 ± 1.49	40.06 ± 2.28
ΔG_{bind}	–101.26 ± 6.01	–97.02 ± 6.42	–96.29 ± 13.10	–31.43 ± 1.32	–26.17 ± 1.33

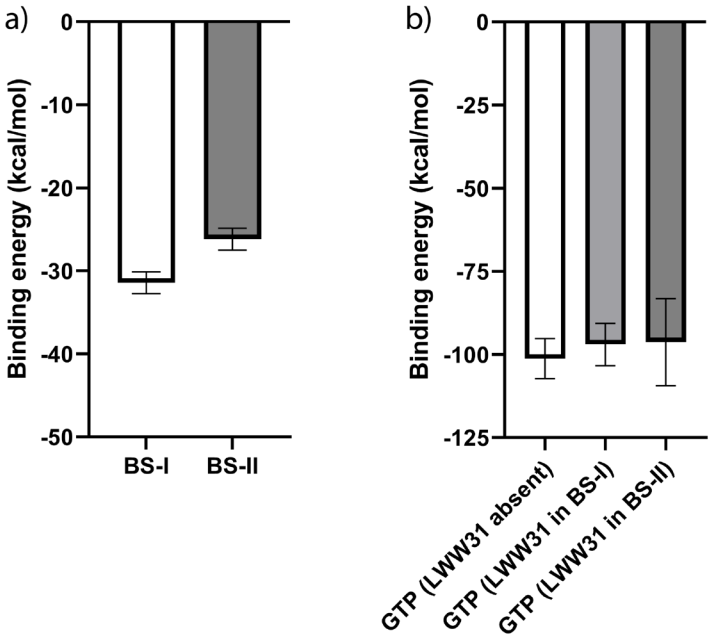

Figure 2.18 Binding free energies of LWW31 and GTP to eIF5B. a) LWW31 shows more favourable binding to BS-I over BS-II. b) Binding free energy of GTP when LWW31 is bound to BS-I (grey) or BS-II (dark grey). Data shown here is an average ± SEM of three replicates.

2.4. Discussion

In this chapter, the experimental work helps demonstrate whether RBV inhibits eIF5B's function. The cell viability effect of RBV was evaluated in different GBM cell lines. BT48 cells showed reduced viability when treated with RBV, followed by BT25 cells (Figure 2.2a, 2.3a). While BT25 and BT48 responded to RBV treatment, U343 responded neither to RBV nor TRAIL treatments (Figure 2.2c). Previous studies suggested that depleting eIF5B sensitizes cells for TRAIL mediated apoptosis.[6] In the present study, TRAIL did not enhance the activity of RBV in decreasing the cell viability of GBM cells (Figure 2.2a–c). This indicates that RBV might not bind to eIF5B or affect its function. Additionally, the decrease in cell viability with the combination of RBV and TRAIL treatment in BT25 cells was due to TRAIL alone (Figure 2.2d). Having said that, the activity of RBV also depends on several factors, including RBV permeability, dimerization, metabolism via adenosine kinase to phosphorylated form, and half-life in GBM as they vary between cells.[11, 57]

The cell viability effect of early and late treatment of RBV was also assessed for BT25 and BT48 cells, which indicated that both cell lines are more resistant to delayed RBV treatment (Figure 2.3a,b). Additionally, the results also suggest that early treatment of RBV prevents the formation of hypoxic tumor microenvironment in BT25 and BT48 cells, but these hypoxic spheres could be established when RBV is treated late. The hypoxic environment usually initiates alternative translation for survival,[58, 59] and RBV might not have much impact on viability under such conditions. Additionally, the permeability of RBV would be better for monolayered cells over spheroid cells.

To further gain confidence in the cell viability data, western blot analysis was performed to determine levels of eIF5B and its downstream targets in cellulo. Levels of Bcl-xL, XIAP, cIAP1, $cFLIP_L$, and $cFLIP_s$ were determined, and these results also indicate that neither eIF5B nor eIF5B dependent proteins are affected by RBV treatment in BT48 and U343 cells (Figure 2.7a,b). Interestingly, NRF2 in the BT48 cell line was an exception, which was downregulated upon RBV treatment (Figure 2.7b). The downregulation of NRF2 could be due to VEGF, a protein regulated by eIF4E at the translational level.[60, 61] In general, RBV treatment inhibits eIF4E function preventing the translation of VEGF.[12] A previous study demonstrated an interplay between VEGF and NRF2 proteins, as low levels of VEGF elevate oxidative stress.[62] These studies imply that the change in NRF2 protein levels might be eIF4E-mediated. However, the levels of NRF2 are unaffected in U343 cell line, and further experiments are required to determine why NRF2 levels are unaffected under RBV treatment in U343 cells. Additionally, unaffected levels of eIF5B-dependent proteins also indicate that eIF5B translation is independent of eIF4E.

Consistent with western blot experiments, MD simulations showed that the eIF5B-RTP complex is not stable, with RTP being displaced from the binding pocket within as little as 50 ns. Although RTP was previously hypothesized to compete with GTP to prevent eIF5B function, the charge of the RTP ring was not properly taken into account in these previous suggestions.[10] Since ribavirin has a high pK_a value, the cationic triazole of RTP is positively charged at physiological pH.[12] Furthermore, the eIF5B binding pocket, in which RTP was proposed to bind, has charged amino acids Lys646 and Lys757 (Figure 2.15a). As a result, when GTP was replaced with RTP and MD simulations performed, the cationic triazole of RTP formed repulsive interactions with the lysine residues in the binding pocket

(Figure 2.15b). These results are consistent with the experimental study, which suggested that neither eIF5B nor eIF5B-dependent protein levels were altered upon ribavirin treatment in BT48 and U343 cell lines, indicating that RTP is not an orthosteric non-covalent inhibitor of eIF5B.

Apart from experimental and computational studies on ribavirin binding to eIF5B, the overall conformational dynamics of eIF5B and eIF5B interactions with LWW31 are elucidated in the chapter. Homology modeling and MD simulations provided the first structural model of human eIF5B. The MD simulations predicted that the overall stability of the MOD eIF5B-GTP model is low in the absence of the ribosome. Additionally, RMSF analysis suggested that the D4 of MOD eIF5B-GTP is the most flexible of all domains (Figure A.5d), agreeing with previous crystallographic studies that showed lower electron density for D4 in the absence of the ribosome,[19] which was observed for both prokaryotic and eukaryotic homologs of human eIF5B.[19, 63] In general, D4 of eIF5B could be stabilized when recruited onto the ribosome due to interactions with initiator tRNA and initiation factors like eIF1A, eIF5, and eIF2A.[64-66] The regions of D4 interacting with these initiation factors, if discovered, could be appealing targets to test small molecules.

The flexibility of the GTP binding site was also compared between apo-eIF5B and eIF5B-GTP. The data reveals that the flexibility of most residues in the binding site is reduced when GTP is bound, except for residues in the switch-I region. Although switch-I showed high flexibility in apo-eIF5B, GTP binding further increased this flexibility (Figure 2.11b). Release of switch-I could be necessary for eIF5B when GTP is bound as this region interacts with helix 14 (H14) of 18S rRNA during ribosomal subunit association.[20, 54] Using MD simulations, the current chapter demonstrates for the first time that human eIF5B

undergoes conformational changes off-ribosome similar to yeast eIF5B (Figure A.9a,b). This conformation is possible when interactions between D1 and D3 are broken, and D3 rotates, which has also been previously observed in yeast eIF5B.[20, 29]

Results from AutoDock vina uncovered two binding sites with the same binding affinity for LWW31 ($\Delta G = -9.6$ kcal/mol, Table 2.6). Subsequent MD simulations and free energy calculations on the eIF5B-LWW31 complex revealed that BS-I is a more favorable binding site than the BS-II. This data was further corroborated using druggability software, PockDrug, which also predicted BS-I as a more favourable binding site (Figure A.12). Together, these results suggest that BS-I is the possible binding site for LWW31 in the C-terminus region of eIF5B.

However, there are certain properties of LWW31 that can be tuned in future studies to yield an improved eIF5B inhibitor to treat GBM. Specifically, to be an effective drug, a molecule needs to permeate through the blood-brain barrier (BBB). Usually molecules below 400-600 Da pass the BBB, making LWW31 relatively large molecule (~612 Da) that falls just above the permissible limit.[67] Additionally, LWW31 is non-polar, making it less soluble, and the aromatic groups of LWW31 can form intramolecular interactions. Specifically, the bulky naphthalene group in LWW31 intermittently makes intramolecular contacts with Benzimidazole, which can disrupt the interaction with eIF5B (Figure 2.17d). Therefore, modifying these aromatic groups could improve intermolecular non-covalent interactions and increase the permeability for the BBB. Nevertheless, apart from GBM, LWW31 is still a promising compound for targeting elevated levels of eIF5B in other cancers such as HCC, LUAD, and prostate cancers that do not require crossing of BBB.

2.5. Conclusion

In this chapter, a unique approach was employed to vet the favourability of ribavirin triphosphate interaction to bind to eIF5B by combining modeling like protein modeling, docking, and MD simulations with experimental techniques like cell viability and western blotting techniques. Although RTP has been suggested to compete with GTP to bind in the G-domain, quantification of eIF5B and its downstream targets suggested that RBV does not affect the function of eIF5B. MD simulations corroborated the western blot results further, indicating that the interaction between RTP and eIF5B is unfavourable. Specifically, interactions between eIF5B and RTP are not possible due to the charged triazole ring of RTP, which makes repulsive contacts with surrounding basic residues Lys647 and Lys757 of eIF5B.

Using homology modeling and structural validation tools, the first human eIF5B model was generated, which was used to study eIF5B structural dynamics and ligand binding. In addition to providing insight into domain release mechanism, studying the dynamics of human eIF5B also helped identify the most favorable binding site in D1 for LWW31. Overall, this chapter highlighted how a combination of cell, molecular and computational biology can accelerate the understanding of ligand binding to eIF5B. Thus, the complementary work presented in this chapter offers an interdisciplinary approach to identify promising compounds for oncogenic proteins that lack X-ray crystal structures.

2.6. References

1. Pestova, T. V.; Lomakin, I. B.; Lee, J. H.; Choi, S. K.; Dever, T. E.; Hellen, C. U., The joining of ribosomal subunits in eukaryotes requires eIF5B. *Nature* **2000,** *403* (6767), 332-335.

2. Lee, J. H.; Pestova, T. V.; Shin, B. S.; Cao, C.; Choi, S. K.; Dever, T. E., Initiation factor eIF5B catalyzes second GTP-dependent step in eukaryotic translation initiation. *Proceedings of the National Academy of Sciences* **2002,** *99* (26), 16689-16694.

3. Nag, N.; Lin, K. Y.; Edmonds, K. A.; Yu, J.; Nadkarni, D.; Marintcheva, B.; Marintchev, A., eIF1A/eIF5B interaction network and its functions in translation initiation complex assembly and remodeling. *Nucleic Acids Research* **2016,** *44* (15), 7441-7456.

4. Suresh, S.; Chen, B.; Zhu, J.; Golden, R. J.; Lu, C.; Evers, B. M.; Novaresi, N.; Smith, B.; Zhan, X.; Schmid, V.; Jun, S.; Karacz, C. M.; Peyton, M.; Zhong, L.; Wen, Z.; Sathe, A. A.; Xing, C.; Behrens, C.; Wistuba, I. I.; Xiao, G.; Xie, Y.; Fu, Y.-X.; Minna, J. D.; Mendell, J. T.; O'Donnell, K. A., eIF5B drives integrated stress response-dependent translation of PD-L1 in lung cancer. *Nature Cancer* **2020,** *1* (5), 533-545.

5. Smith, R. C. L.; Kanellos, G.; Vlahov, N.; Alexandrou, C.; Willis, A. E.; Knight, J. R. P.; Sansom, O. J., Translation initiation in cancer at a glance. *Journal of Cell Science* **2021,** *134* (1).

6. Ross, J. A.; Dungen, K. V.; Bressler, K. R.; Fredriksen, M.; Khandige Sharma, D.; Balasingam, N.; Thakor, N., Eukaryotic initiation factor 5B (eIF5B) provides a critical cell survival switch to glioblastoma cells via regulation of apoptosis. *Cell Death & Disease* **2019,** *10* (2), 57.

7. Wang, Z. G.; Zheng, H.; Gao, W.; Han, J.; Cao, J. Z.; Yang, Y.; Li, S.; Gao, R.; Liu, H.; Pan, Z. Y.; Fu, S. Y.; Gu, F. M.; Xing, H.; Ni, J. S.; Yan, H. L.; Ren, H.; Zhou, W. P., eIF5B increases ASAP1 expression to promote HCC proliferation and invasion. *Oncotarget* **2016,** *7* (38), 62327-62339.

8. Hanif, F.; Muzaffar, K.; Perveen, K.; Malhi, S. M.; Simjee, S. U., Glioblastoma Multiforme: A Review of its Epidemiology and Pathogenesis through Clinical Presentation and Treatment. *Asian Pacific journal of cancer prevention : APJCP* **2017,** *18* (1), 3-9.

9. Carr, M. T.; Hochheimer, C. J.; Rock, A. K.; Dincer, A.; Ravindra, L.; Zhang, F. L.; Opalak, C. F.; Poulos, N.; Sima, A. P.; Broaddus, W. C., Comorbid Medical Conditions as Predictors of Overall Survival in Glioblastoma Patients. *Scientific Reports* **2019,** *9* (1), 20018.

10. Galmozzi, E.; Aghemo, A.; Colombo, M., Eukaryotic initiation factor 5B: a new player for the anti-hepatitis C virus effect of ribavirin? *Medical Hypotheses* **2012,** *79* (4), 471-473.

11. Borden, K. L. B.; Culjkovic-Kraljacic, B., Ribavirin as an anti-cancer therapy: acute myeloid leukemia and beyond? *Leukemia Lymphoma* **2010,** *51* (10), 1805-1815.

12. Kentsis, A.; Topisirovic, I.; Culjkovic, B.; Shao, L.; Borden, K. L., Ribavirin suppresses eIF4E-mediated oncogenic transformation by physical mimicry of the 7-methyl guanosine mRNA cap. *Proceedings of the National Academy of Sciences* **2004,** *101* (52), 18105-18110.

13. Bengsch, B.; Thimme, R., Ribavirin ante portas: Uptake transporters into hepatocytes dissected. *Journal of Hepatology* **2010,** *52* (4), 469-471.

14. Wu, C.-Y.; Wang, D.-H.; Wang, X.; Dixon, S. M.; Meng, L.; Ahadi, S.; Enter, D. H.; Chen, C.-Y.; Kato, J.; Leon, L. J.; Ramirez, L. M.; Maeda, Y.; Reis, C. F.; Ribeiro, B.; Weems, B.; Kung, H.-J.; Lam, K. S., Rapid Discovery of Functional Small Molecule Ligands against Proteomic Targets through Library-Against-Library Screening. *ACS combinatorial science* **2016,** *18* (6), 320-329.

15. Ravindranath, B. S.; Vishnu Vinayak, S.; Chandra Mohan, V., RNR inhibitor binding studies of Chlamydia felis: insights from in silico molecular modeling, docking, and simulation studies. *Journal of Biomolecular Structure and Dynamics* **2021**, 1-13.

16. Wang, D. F.; Helquist, P.; Wiech, N. L.; Wiest, O., Toward selective histone deacetylase inhibitor design: homology modeling, docking studies, and molecular dynamics simulations of human class I histone deacetylases. *Journal of Medicinal Chemistry* **2005,** *48* (22), 6936-6947.

17. Valente, R. P. d. P.; Souza, R. C. d.; de Medeiros Muniz, G.; Ferreira, J. E. V.; de Miranda, R. M.; e Lima, A. H. L.; Vianez Junior, J. L. d. S. G., Using Accelerated Molecular Dynamics Simulation to elucidate the effects of the T198F mutation on the molecular flexibility of the West Nile virus envelope protein. *Scientific Reports* **2020,** *10* (1), 9625.

18. Stank, A.; Kokh, D. B.; Fuller, J. C.; Wade, R. C., Protein Binding Pocket Dynamics. *Accounts of Chemical Research* **2016,** *49* (5), 809-815.

19. Zheng, A.; Yu, J.; Yamamoto, R.; Ose, T.; Tanaka, I.; Yao, M., X-ray structures of eIF5B and the eIF5B-eIF1A complex: the conformational flexibility of eIF5B is restricted on the ribosome by interaction with eIF1A. *Acta Crystallographica Section D* **2014,** *70* (12), 3090-3098.

20. Yamamoto, H.; Unbehaun, A.; Loerke, J.; Behrmann, E.; Collier, M.; Burger, J.; Mielke, T.; Spahn, C. M., Structure of the mammalian 80S initiation complex with initiation factor 5B on HCV-IRES RNA. *Nature structural & molecular biology* **2014,** *21* (8), 721-727.

21. De la Cruz-Hernandez, E.; Medina-Franco, J. L.; Trujillo, J.; Chavez-Blanco, A.; Dominguez-Gomez, G.; Perez-Cardenas, E.; Gonzalez-Fierro, A.; Taja-Chayeb, L.;

Duenas-Gonzalez, A., Ribavirin as a tri-targeted antitumor repositioned drug. *Oncology Reports* **2015,** *33* (5), 2384-2392.

22. Zhou, S.; Liu, R.; Baroudy, B. M.; Malcolm, B. A.; Reyes, G. R., The effect of ribavirin and IMPDH inhibitors on hepatitis C virus subgenomic replicon RNA. *Virology* **2003,** *310* (2), 333-342.

23. Kraljacic, B. C.; Arguello, M.; Amri, A.; Cormack, G.; Borden, K., Inhibition of eIF4E with ribavirin cooperates with common chemotherapies in primary acute myeloid leukemia specimens. *Leukemia* **2011,** *25* (7), 1197-1200.

24. Volpin, F.; Casaos, J.; Sesen, J.; Mangraviti, A.; Choi, J.; Gorelick, N.; Frikeche, J.; Lott, T.; Felder, R.; Scotland, S. J.; Eisinger-Mathason, T. S. K.; Brem, H.; Tyler, B.; Skuli, N., Use of an anti-viral drug, Ribavirin, as an anti-glioblastoma therapeutic. *Oncogene* **2017,** *36* (21), 3037-3047.

25. Fiser, A.; Do, R. K.; Sali, A., Modeling of loops in protein structures. *Protein Science* **2000,** *9* (9), 1753-1773.

26. Sali, A.; Blundell, T. L., Comparative protein modelling by satisfaction of spatial restraints. *Journal of Molecular Biology* **1993,** *234* (3), 779-815.

27. Pettersen, E. F.; Goddard, T. D.; Huang, C. C.; Couch, G. S.; Greenblatt, D. M.; Meng, E. C.; Ferrin, T. E., UCSF Chimera--a visualization system for exploratory research and analysis. *Journal of Computational Chemistry* **2004,** *25* (13), 1605-1612.

28. Yang, Z.; Lasker, K.; Schneidman-Duhovny, D.; Webb, B.; Huang, C. C.; Pettersen, E. F.; Goddard, T. D.; Meng, E. C.; Sali, A.; Ferrin, T. E., UCSF Chimera, MODELLER, and IMP: an integrated modeling system. *Journal of Structural Biology* **2012,** *179* (3), 269-278.

29. Kuhle, B.; Ficner, R., eIF5B employs a novel domain release mechanism to catalyze ribosomal subunit joining. *The EMBO Journal* **2014,** *33* (10), 1177-1191.

30. Altschul, S. F.; Gish, W.; Miller, W.; Myers, E. W.; Lipman, D. J., Basic local alignment search tool. *Journal of Molecular Biology* **1990,** *215* (3), 403-410.

31. Heo, L.; Park, H.; Seok, C., GalaxyRefine: Protein structure refinement driven by side-chain repacking. *Nucleic Acids Research* **2013,** *41* (W1), W384-W388.

32. Laskowski, R. A.; MacArthur, M. W.; Moss, D. S.; Thornton, J. M., PROCHECK: a program to check the stereochemical quality of protein structures. *Journal of Applied Crystallography* **1993,** *26* (2), 283-291.

33. Lüthy, R.; Bowie, J. U.; Eisenberg, D., Assessment of protein models with three-dimensional profiles. *Nature* **1992,** *356* (6364), 83-85.

34. Bowie, J. U.; Lüthy, R.; Eisenberg, D., A method to identify protein sequences that fold into a known three-dimensional structure. *Science* **1991,** *253* (5016), 164-170.

35. Colovos, C.; Yeates, T. O., Verification of protein structures: patterns of nonbonded atomic interactions. *Protein Science* **1993,** *2* (9), 1511-1519.

36. Benkert, P.; Biasini, M.; Schwede, T., Toward the estimation of the absolute quality of individual protein structure models. *Bioinformatics* **2011,** *27* (3), 343-350.

37. Jumper, J.; Evans, R.; Pritzel, A.; Green, T.; Figurnov, M.; Ronneberger, O.; Tunyasuvunakool, K.; Bates, R.; Zidek, A.; Potapenko, A.; Bridgland, A.; Meyer, C.; Kohl, S. A. A.; Ballard, A. J.; Cowie, A.; Romera-Paredes, B.; Nikolov, S.; Jain, R.; Adler, J.; Back, T.; Petersen, S.; Reiman, D.; Clancy, E.; Zielinski, M.; Steinegger, M.; Pacholska, M.; Berghammer, T.; Bodenstein, S.; Silver, D.; Vinyals, O.; Senior, A. W.; Kavukcuoglu, K.; Kohli, P.; Hassabis, D., Highly accurate protein structure prediction with AlphaFold. *Nature* **2021,** *596* (7873), 583-589.

38. Schrodinger, LLC, The PyMOL Molecular Graphics System, Version 1.8. 2015.

39. Frisch, M. J.; Trucks, G. W.; Schlegel, H. B.; Scuseria, G. E.; Robb, M. A.; Cheeseman, J. R.; Scalmani, G.; Barone, V.; Petersson, G. A.; Nakatsuji, H.; Li, X.; Caricato, M.; Marenich, A. V.; Bloino, J.; Janesko, B. G.; Gomperts, R.; Mennucci, B.; Hratchian, H. P.; Ortiz, J. V.; Izmaylov, A. F.; Sonnenberg, J. L.; Williams; Ding, F.; Lipparini, F.; Egidi, F.; Goings, J.; Peng, B.; Petrone, A.; Henderson, T.; Ranasinghe, D.; Zakrzewski, V. G.; Gao, J.; Rega, N.; Zheng, G.; Liang, W.; Hada, M.; Ehara, M.; Toyota, K.; Fukuda, R.; Hasegawa, J.; Ishida, M.; Nakajima, T.; Honda, Y.; Kitao, O.; Nakai, H.; Vreven, T.; Throssell, K.; Montgomery Jr., J. A.; Peralta, J. E.; Ogliaro, F.; Bearpark, M. J.; Heyd, J. J.; Brothers, E. N.; Kudin, K. N.; Staroverov, V. N.; Keith, T. A.; Kobayashi, R.; Normand, J.; Raghavachari, K.; Rendell, A. P.; Burant, J. C.; Iyengar, S. S.; Tomasi, J.; Cossi, M.; Millam, J. M.; Klene, M.; Adamo, C.; Cammi, R.; Ochterski, J. W.; Martin, R. L.; Morokuma, K.; Farkas, O.; Foresman, J. B.; Fox, D. J. *Gaussian 16 Rev. C.01*, Wallingford, CT, 2016.

40. Trott, O.; Olson, A. J., AutoDock Vina: improving the speed and accuracy of docking with a new scoring function, efficient optimization, and multithreading. *Journal of computational chemistry* **2010,** *31* (2), 455-461.

41. Morris, G. M.; Huey, R.; Lindstrom, W.; Sanner, M. F.; Belew, R. K.; Goodsell, D. S.; Olson, A. J., AutoDock4 and AutoDockTools4: Automated docking with selective receptor flexibility. *Journal of Computational Chemistry* **2009,** *30* (16), 2785-2791.

42. Sanner, M. F., Python: a programming language for software integration and development. *Journal of Molecular Graphics and Modelling* **1999,** *17* (1), 57-61.

43. Maier, J. A.; Martinez, C.; Kasavajhala, K.; Wickstrom, L.; Hauser, K. E.; Simmerling, C., ff14SB: Improving the Accuracy of Protein Side Chain and Backbone Parameters from ff99SB. *Journal of Chemical Theory and Computation* **2015,** *11* (8), 3696-3713.

44. Meagher, K. L.; Redman, L. T.; Carlson, H. A., Development of polyphosphate parameters for use with the AMBER force field. *Journal of Computational Chemistry* **2003,** *24* (9), 1016-1025.

45. Wang, J.; Wang, W.; Kollman, P. A.; Case, D. A., Automatic atom type and bond type perception in molecular mechanical calculations. *Journal of Molecular Graphics and Modelling* **2006,** *25* (2), 247-260.

46. Wang, J.; Wolf, R. M.; Caldwell, J. W.; Kollman, P. A.; Case, D. A., Development and testing of a general amber force field. *Journal of Computational Chemistry* **2004,** *25* (9), 1157-1174.

47. Roe, D. R.; Cheatham, T. E., 3rd, PTRAJ and CPPTRAJ: Software for Processing and Analysis of Molecular Dynamics Trajectory Data. *Journal of Chemical Theory and Computation* **2013,** *9* (7), 3084-3095.

48. Adasme, M. F.; Linnemann, K. L.; Bolz, S. N.; Kaiser, F.; Salentin, S.; Haupt, V. J.; Schroeder, M., PLIP 2021: expanding the scope of the protein-ligand interaction profiler to DNA and RNA. *Nucleic Acids Research* **2021,** *49* (W1), W530-W534.

49. Wang, E.; Sun, H.; Wang, J.; Wang, Z.; Liu, H.; Zhang, J. Z. H.; Hou, T., End-Point Binding Free Energy Calculation with MM/PBSA and MM/GBSA: Strategies and Applications in Drug Design. *Chemical Reviews* **2019,** *119* (16), 9478-9508.

50. Ross, J. A.; Ahn, B. Y.; King, J.; Bressler, K. R.; Senger, D. L.; Thakor, N., Eukaryotic initiation factor 5B (eIF5B) regulates temozolomide-mediated apoptosis in brain tumour stem cells (BTSCs). *Biochemistry and Cell Biology* **2020,** *98* (6), 647-652.

51. Shen, M. Y.; Sali, A., Statistical potential for assessment and prediction of protein structures. *Protein Science* **2006,** *15* (11), 2507-2524.

52. Emsley, P.; Lohkamp, B.; Scott, W. G.; Cowtan, K., Features and development of Coot. *Acta Crystallographica Section D* **2010,** *66* (4), 486-501.

53. Balaji, S.; Kalpana, R.; Shapshak, P., Paradigm development: comparative and predictive 3D modeling of HIV-1 Virion Infectivity Factor (Vif). *Bioinformation* **2006,** *1* (8), 290-309.

54. Roll-Mecak, A.; Cao, C.; Dever, T. E.; Burley, S. K., X-Ray structures of the universal translation initiation factor IF2/eIF5B: conformational changes on GDP and GTP binding. *Cell* **2000,** *103* (5), 781-792.

55. Huang, B. Y.; Fernandez, I. S., Long-range interdomain communications in eIF5B regulate GTP hydrolysis and translation initiation. *Proceedings of the National Academy of Sciences* **2020,** *117* (3), 1429-1437.

56. Hussein, H. A.; Borrel, A.; Geneix, C.; Petitjean, M.; Regad, L.; Camproux, A. C., PockDrug-Server: a new web server for predicting pocket druggability on holo and apo proteins. *Nucleic Acids Research* **2015,** *43* (W1), W436-W442.

57. Bordbar, A.; McCloskey, D.; Zielinski, D. C.; Sonnenschein, N.; Jamshidi, N.; Palsson, B. O., Personalized Whole-Cell Kinetic Models of Metabolism for Discovery in Genomics and Pharmacodynamics. *Cell Systems* **2015,** *1* (4), 283-292.

58. Uniacke, J.; Perera, J. K.; Lachance, G.; Francisco, C. B.; Lee, S., Cancer cells exploit eIF4E2-directed synthesis of hypoxia response proteins to drive tumor progression. *Cancer Research* **2014,** *74* (5), 1379-1389.

59. Ho, J. J. D.; Balukoff, N. C.; Cervantes, G.; Malcolm, P. D.; Krieger, J. R.; Lee, S., Oxygen-Sensitive Remodeling of Central Carbon Metabolism by Archaic eIF5B. *Cell Reports* **2018,** *22* (1), 17-26.

60. Yang, S. X.; Hewitt, S. M.; Steinberg, S. M.; Liewehr, D. J.; Swain, S. M., Expression levels of eIF4E, VEGF, and cyclin D1, and correlation of eIF4E with VEGF and cyclin D1 in multi-tumor tissue microarray. *Oncology Reports* **2007,** *17* (2), 281-287.

61. Batool, A.; Aashaq, S.; Andrabi, K. I., Eukaryotic initiation factor 4E (eIF4E): A recap of the cap-binding protein. *Journal of Cellular Biochemistry* **2019,** *120* (9), 14201-14212.

62. Kweider, N.; Fragoulis, A.; Rosen, C.; Pecks, U.; Rath, W.; Pufe, T.; Wruck, C. J., Interplay between vascular endothelial growth factor (VEGF) and nuclear factor erythroid 2-related factor-2 (Nrf2): implications for preeclampsia. *Journal of Biological Chemistry* **2011,** *286* (50), 42863-42872.

63. Eiler, D.; Lin, J.; Simonetti, A.; Klaholz, B. P.; Steitz, T. A., Initiation factor 2 crystal structure reveals a different domain organization from eukaryotic initiation factor 5B and mechanism among translational GTPases. *Proceedings of the National Academy of Sciences* **2013,** *110* (39), 15662-15667.

64. Wang, J.; Wang, J.; Shin, B. S.; Kim, J. R.; Dever, T. E.; Puglisi, J. D.; Fernandez, I. S., Structural basis for the transition from translation initiation to elongation by an 80S-eIF5B complex. *Nature Communications* **2020,** *11* (1), 5003.

65. Kim, E.; Kim, J. H.; Seo, K.; Hong, K. Y.; An, S. W. A.; Kwon, J.; Lee, S.-J. V.; Jang, S. K., eIF2A, an initiator tRNA carrier refractory to eIF2α kinases, functions synergistically with eIF5B. *Cellular and molecular life sciences : CMLS* **2018,** *75* (23), 4287-4300.

66. Lin, K. Y.; Nag, N.; Pestova, T. V.; Marintchev, A., Human eIF5 and eIF1A Compete for Binding to eIF5B. *Biochemistry* **2018,** *57* (40), 5910-5920.

67. Pardridge, W. M., Transport of small molecules through the blood-brain barrier: biology and methodology. *Advanced Drug Delivery Reviews* **1995,** *15* (1), 5-36.

Chapter 3: The Interactions of Eukaryotic Translation Initiation Factor 4E (eIF4E) with m^7GTP, RBV, and RTP: A MD Study

3.1. Introduction

eIF4E is a subunit of the eIF4F complex (eIF4E, 4G, and 4A), which binds to the 5′-terminal 7-methylguanosine (m^7G) cap of mRNA to recruit the 40S ribosome during cap-dependent translation (Figure 3.1a).[1-5] The cap-binding activity of eIF4E controls gene expression post-transcriptionally by regulating the transport of a subset of mRNA from the nucleus to the cytoplasm.[6-9] However, the same cap-binding activity augments the translation of vascular endothelial growth factor (VEGF), cyclin-D, and ornithine decarboxylase (ODC).[10] Therefore, eIF4E regulates gene expression at both the post-transcriptional and translational levels. However, high levels of eIF4E often promotes cancer cell proliferation and survival.[10, 11] Approximately 30% of cancers show elevated levels of eIF4E,[12-16] making eIF4E a desirable target for the development of inhibitory drugs.

Previous studies have shown that cap-analogues like ribavirin (RBV), ribavirin triphosphate (RTP), and 7-methylguanosine triphosphate (m^7GTP) inhibit eIF4E function by binding to the cap-binding site (Figure 3.1b–d).[17] Although it is known that RTP is synthesized inside the cell when RBV is metabolized by adenosine kinase,[15, 18-20] the extent of RBV to RTP conversion in cancer cells in uncertain. Studies have shown that RTP (K_d = 0.13 μM) has a similar binding affinity to eIF4E as m^7GTP (K_d = 0.19 μM) and a better binding affinity than RBV (K_d = 6.7 μM).[19] Additionally, viability experiments of RBV treated cancer cells showed promising results in terms of eIF4E inhibition.[19, 21] However, clinical trial data indicated that patients develop drug resistance over time (after four

months),[15] which could be due to reduced RBV metabolism. Therefore, it is essential to understand the interactions of both RBV and RTP with eIF4E until further experiments can confirm the dominant active form in cancer cells.

While a crystal structure for m^7GTP in complex with eIF4E is available (PDB ID: 1IPC),[22] very little structural information is known about RBV and RTP binding to eIF4E, including the primary residues involved. Additionally, although molecular dynamics (MD) simulations have been performed for the eIF4E-m^7GTP complex,[23] the simulations were short (800 ps), and primarily focussed on how m^7GTP and m^7GpppA/G affect the size of cap-binding pocket. Furthermore, there is no information on how RBV and RTP affect the flexibility of the C-terminus (203–211 residues), a region important for the regulation and stability of eIF4E.[24, 25] In the absence of experimental data, recent studies have proven that computational biology can be a useful tool for elucidating the dynamics of protein-ligand interactions.[26-28] For example, MD simulations have been successfully used for the structural prediction of the CYFIP1 peptide (CYFIP1p) with eIF4E,[29] predicting the binding mode and novel (electrostatic and hydrophobic) CYFIP1p–eIF4E contacts.[29] Therefore, MD simulations will be a useful tool to identify the binding modes of RBV and RTP to eIF4E, including the amino acid contacts that promote binding, with the goal to identify potential new designs of small molecule inhibitors.

In this chapter, atomic-level structural insights are provided for the eIF4E-m^7GTP, eIF4E-RTP, and eIF4E-RBV complexes using MD simulations. The eIF4E-m^7GTP complex was used to validate the computational approach through comparisons with the eIF4E-m^7GTP crystal structure (PDB ID: 1IPC),[22] affinity experiments,[19] and NMR studies.[30] Furthermore, structural changes induced by m^7GTP in the N and C-terminus

regions of eIF4E were investigated. The approach used to successfully study the eIF4E-m^{7}GTP complex was then applied to the eIF4E-RTP and eIF4E-RBV complexes for which

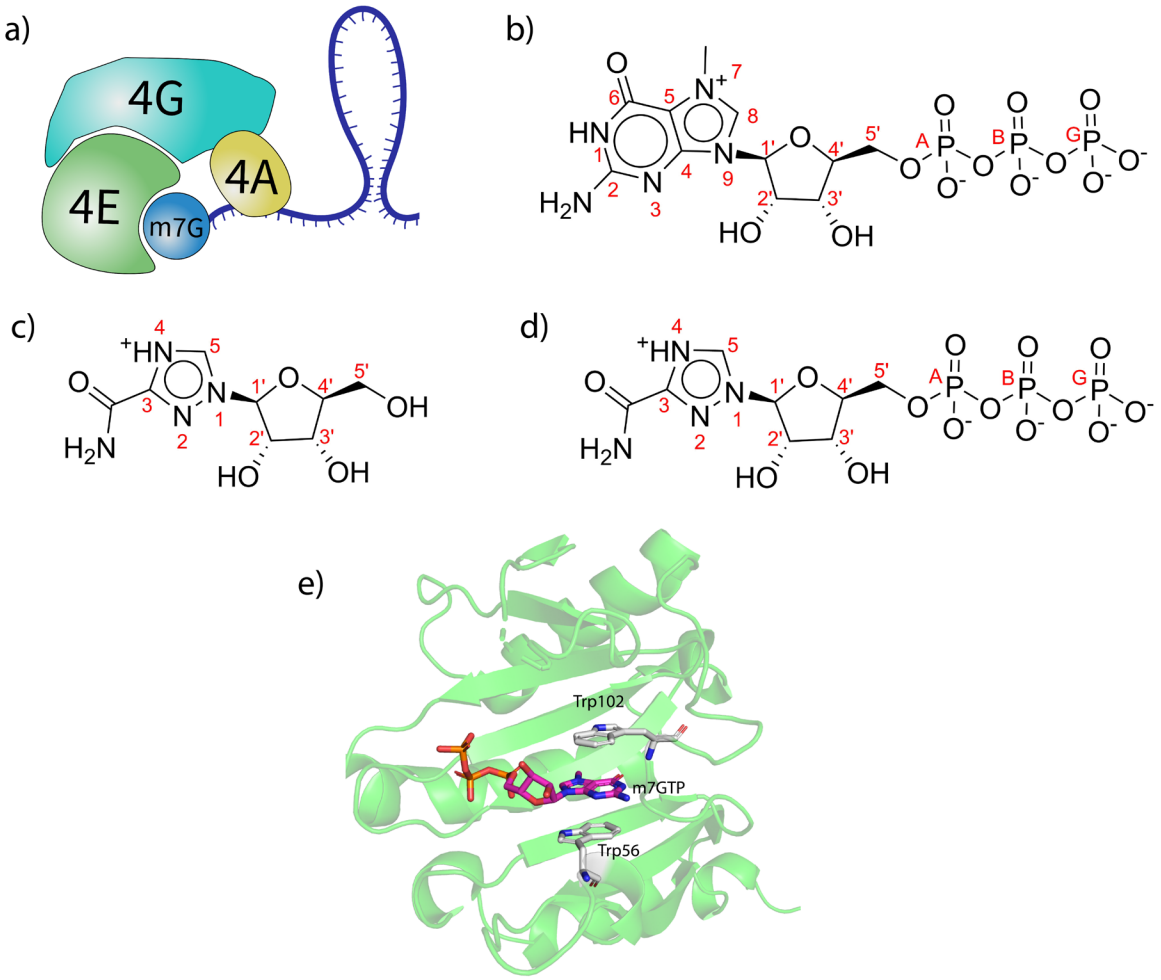

Figure 3.1 a) eIF4E in the eIF4F complex interacts with the 5′-terminal m^{7}G of mRNA to recruit on the 40S subunit. b) Structure of m^{7}GTP, c) RBV, and d) RTP. e) Crystal structure of the eIF4E-m^{7}GTP complex (PDB ID: 1IPC), highlighting m^{7}GTP stacked between two conserved tryptophan residues.

little structural information exists. MD simulations reveal the ligand–target interactions, system dynamics, and stability of RTP and RBV ligands in the cap-binding site of eIF4E. A focus was placed on determining how RTP and RBV bind within the cap-binding site as well as identifying differences and similarities compared to m^{7}GTP. Finally, binding free

energy calculations are used to compare the predicted binding affinities for m^7GTP, RTP, and RBV to eIF4E. Overall, the work reveals new structural information about the interactions between RBV or RTP and the cap-binding residues of eIF4E, which can be used in future work to develop better neoplastic drugs for the treatment of ovarian, breast, and head and neck cancers that show aberrant eIF4E expression.[31, 32]

3.2. Computational Methods

3.2.1. Ligand optimization:

The structure of RBV was optimized with B3LYP/6-31+G(d,p) in the gas phase, and charges were derived using the restrained electrostatic potential (RESP) method. Due to inherent instability in the gas phase resulting from the high charge of the triphosphate tail, parameterization of m^7GTP and RTP was carried out with B3LYP/6-31+G(d) calculations in implicit solvent (IEFPCM; water) using Gaussian 16 (Rev. C.01),[33] and charges were derived using the RESP method.

3.2.2. Molecular dynamics protocol:

The crystal structure of m^7GTP bound to eIF4E (PDB ID: 1IPC) was retrieved from the Protein Data Bank for MD studies (Figure 3.1e). Since the N-terminus region (1–27 residues) of eIF4E was not resolved,[22] amino acids 28–217 of eIF4E were included in the eIF4E-m^7GTP structure. Residues 206–210 of eIF4E were not resolved in the eIF4E-m^7GTP crystal structure. Thus, loop modeling was employed to construct this region using MODELLER.[34, 35] In the next step, the apo-eIF4E model was derived by deleting m^7GTP from the eIF4E-m^7GTP model. In the final step, since RBV and its metabolite, RTP, are

orthosteric inhibitors of the m^7G cap,[19, 30] m^7GTP in the eIF4E-m^7GTP model was modified to RTP or RBV using PyMOL (version 2.3.2).[36] Each model was then used for MD studies.

Minimization and heating protocols were adopted from Chapter 2. While the eIF4E-m^7GTP and eIF4E-RBV systems were equilibrated for an additional 500 ns compared to Chapter 2, the eIF4E-RTP complex was equilibrated for 100 ns, at which point each system was sufficiently stable. The remainder of the MD simulation protocol was adopted from Chapter 2, with 1000 ns MD simulations performed on each equilibrated system in triplicate.

Post-trajectory analyses and MM-GBSA calculations were performed for each trajectory as described in Chapter 2. However, since the crystal structure was used for eIF4E, the RMSD was calculated with respect to the backbone of the corresponding initial eIF4E-cap analogue structure (prior to minimization). Additionally, the RMSD for all ligands was calculated with respect to the heavy atoms of the ligands in the corresponding initial model (prior to minimization). Percentage occupancy of hydrogen bonds between the protein and ligand were calculated using an angle cut off of 120° and a distance cut off of 3.4 Å. Percentage occupancy for the stacking interactions were analyzed using an inhouse script that considered stacking to be present when the centers of mass of the two aromatic groups were within a distance of 5 Å, and the interplanar angles of the two aromatic groups were set between 0° and 30° or 150° and 180 °.

3.3. Results & Discussion

3.3.1. Predicted interactions in the eIF4E-m^{7}GTP complex are consistent with the crystal structure

The X-ray crystal structure of eIF4E-m^{7}GTP showed that the purine group of m^{7}GTP stacks between the side chains of Trp56 and Trp102 (Figure 3.2), and N1 and N2 of the m^{7}GTP nucleobase forms hydrogen bonds with the side chain of Glu103 (Figure 3.2). While Trp56 and Trp102 have been proposed to aid in the recruitment of the m^{7}G cap through stacking, the hydrogen bonds between m^{7}G and Glu103 stabilize the stacking contacts.[22] These interactions were persistent during the simulation where the charged purine ring (+1) of m^{7}GTP establishes cation–π–π interactions with Trp56 (occupancy = 97.8%, $\Delta G = -5.0 \pm 0.2$ kcal/mol; Figure 3.3a) and Trp102 (occupancy = 60.2%, $\Delta G = -4.9 \pm 0.6$ kcal/mol; Figure 3.3a). The results indicate a preferential stacking of m^{7}GTP to

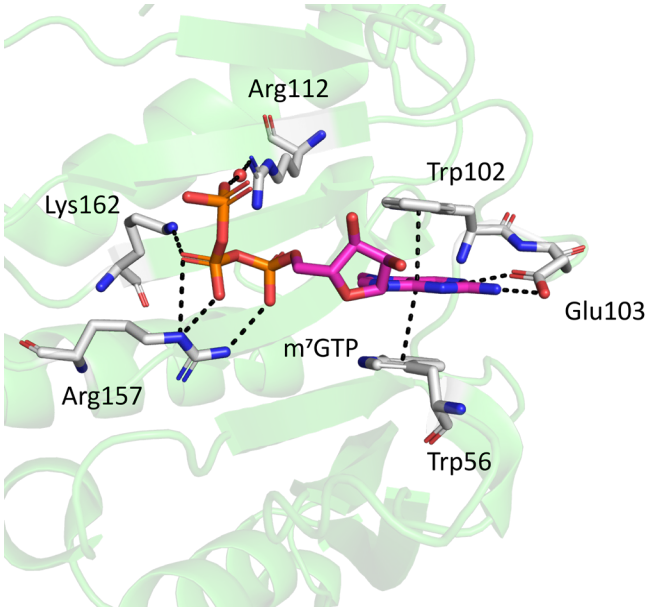

Figure 3.2 Crystal structure of the eIF4E-m^{7}GTP complex (PDB ID: 1IPC), highlighting the residues that interact with m^{7}GTP.

Trp56 over Trp102, rationalizing mutational studies that showed m^7GTP has a lower affinity when Trp56 (K_d = 40.6 μM) is mutated compared to when Trp102 is mutated (K_d = 16.8 μM).[37] Additionally, the side chain of Glu103 establishes two hydrogen bonds with the N1 (occupancy = 73.4%; Figure 3.3b) and N2 (occupancy = 66.4%; Figure 3.3b) of m^7GTP (ΔG = –1.2 ± 0.1 kcal/mol). In addition, a more persistent hydrogen bond is formed between O6 of m^7GTP and the backbone N of Trp102 (occupancy = 93.7%; Figure 3.3a), indicating the interaction of m^7GTP with Trp102 is more important than Glu103 to orient and maximize the stacking with Trp56 and Trp102. Overall, interactions between m^7GTP and residues in the cap-binding pocket facilitate the formation of a stable complex with eIF4E (RMSD = 1.7 ± 0.4 Å; Figure 3.4a, Table B.1).

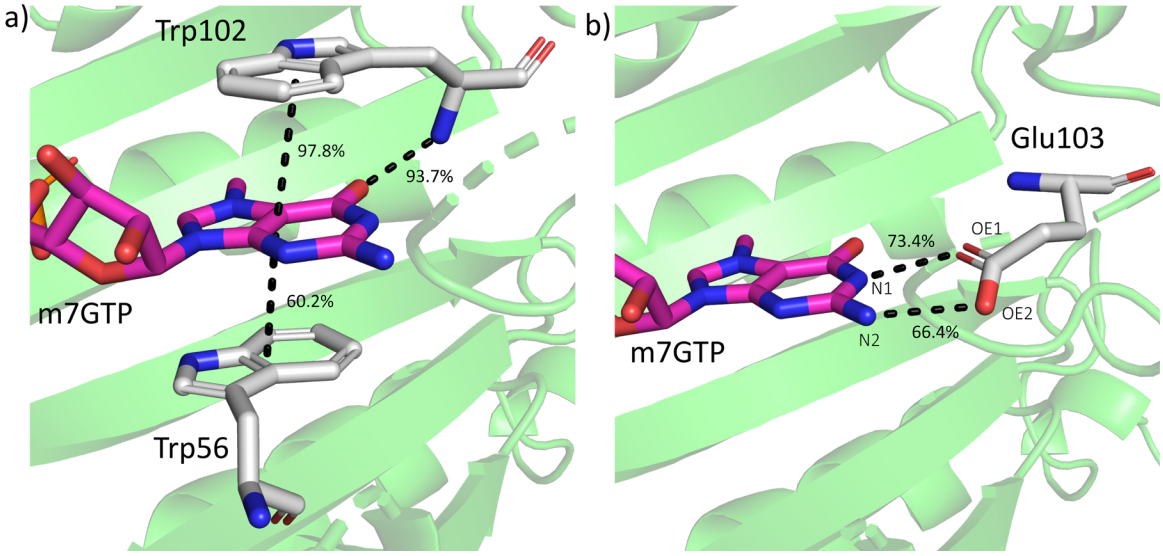

Figure 3.3 MD representative structure of the eIF4E-m^7GTP complex, highlighting a) the m^7GTP stacking interactions with Trp102 and Trp56, as well as hydrogen bonds with the backbone of Trp102, and b) the m^7GTP hydrogen bonds with the sidechain of Glu103.

The crystal structure of eIF4E-m^7GTP revealed hydrogen bonds between the triphosphate tail of m^7GTP and Arg112, Arg157, and Lys162 of eIF4E (Figure 3.2).[22, 30] However, the triphosphate tail exhibited numerous conformations in the cap-binding site

during the MD simulation, allowing m^{7}GTP to establish intermittent hydrogen bonds with Arg112 (ΔG = –6.1 ± 2.2 kcal/mol, Figure 3.5a–c, Table B.2), Arg157 (ΔG = –9.6 ± 3.3 kcal/mol, Figure 3.5c,d, Table B.2), and Lys162 (ΔG = –7.6 ± 2.2 kcal/mol, Figure 3.5b, Table B.2). However, free binding energy calculations and hydrogen bond analysis suggested that Arg157 is the major contributor to m^{7}GTP binding (Figure B.1, 3.5c,d). Thus, despite the difference in the dynamics of the triphosphate tail, consistent with crystallographic data,[22] the results from the MD simulations indicate that Arg112, Arg157, and Lys162 are the three primary residues interacting with m^{7}GTP.

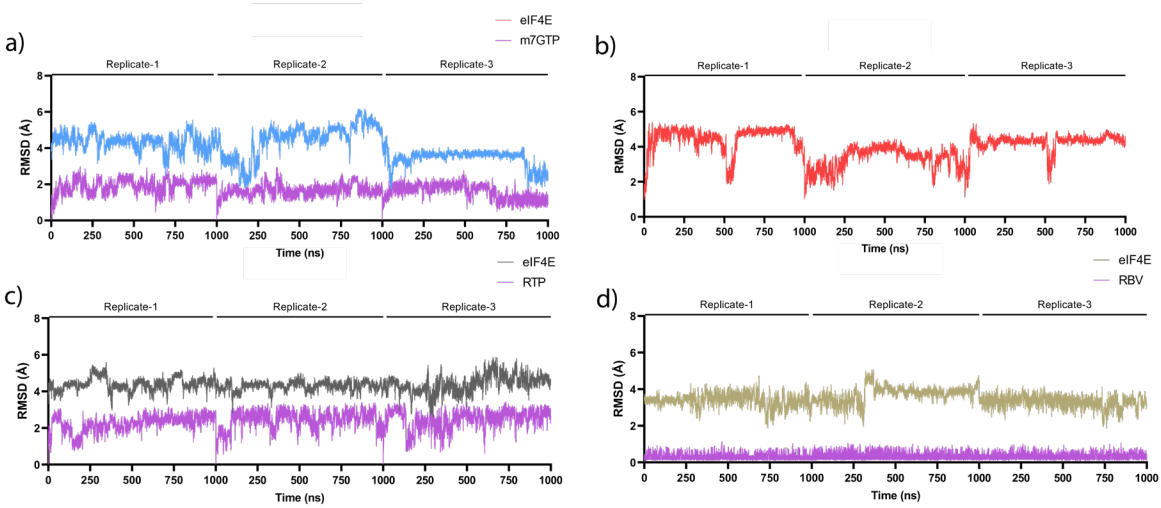

Figure 3.4 Structural deviation in the protein (backbone) or ligand (heavy atom RMSD, Å) in a) m^{7}GTP and eIF4E in the eIF4E-m^{7}GTP complex, b) apo-eIF4E, c) RTP and eIF4E in the eIF4E-RTP complex, and d) RBV and eIF4E in the eIF4E-RBV complex. RMSD was calculated with respect to the initial models (prior to minimization).

Overall, the superposition of the active site conformation in the MD representative structure and the crystal structure of the eIF4E-m^{7}GTP complex indicates no significant deviations (RMSD = 1.5 Å; Figure B.2), except for the alpha (A), beta (B), and gamma (G) phosphates of m^{7}GTP that were dynamic throughout the simulation. This conformational flexibility of m^{7}GTP was possible due to intermittent interactions with Arg112, Arg157,

and Lys162 (Figure 3.5a–d, Table B.2). Previous crystallographic studies suggested that the absence of second nucleotide adjacent to m^7GTP increases the flexibility of the eIF4E C-terminus region (203–211 residues; Figure B.3).[22, 38] Consistent with the crystallographic studies,[22] MD simulations on eIF4E-m^7GTP indicate high flexibility of the C-terminus region (Figure B.4), which impacted the overall stability of the eIF4E-m^7GTP complex (RMSD = 4.1 ± 0.8 Å; Figure 3.4a, Table B.1) and showed structural variations similar to

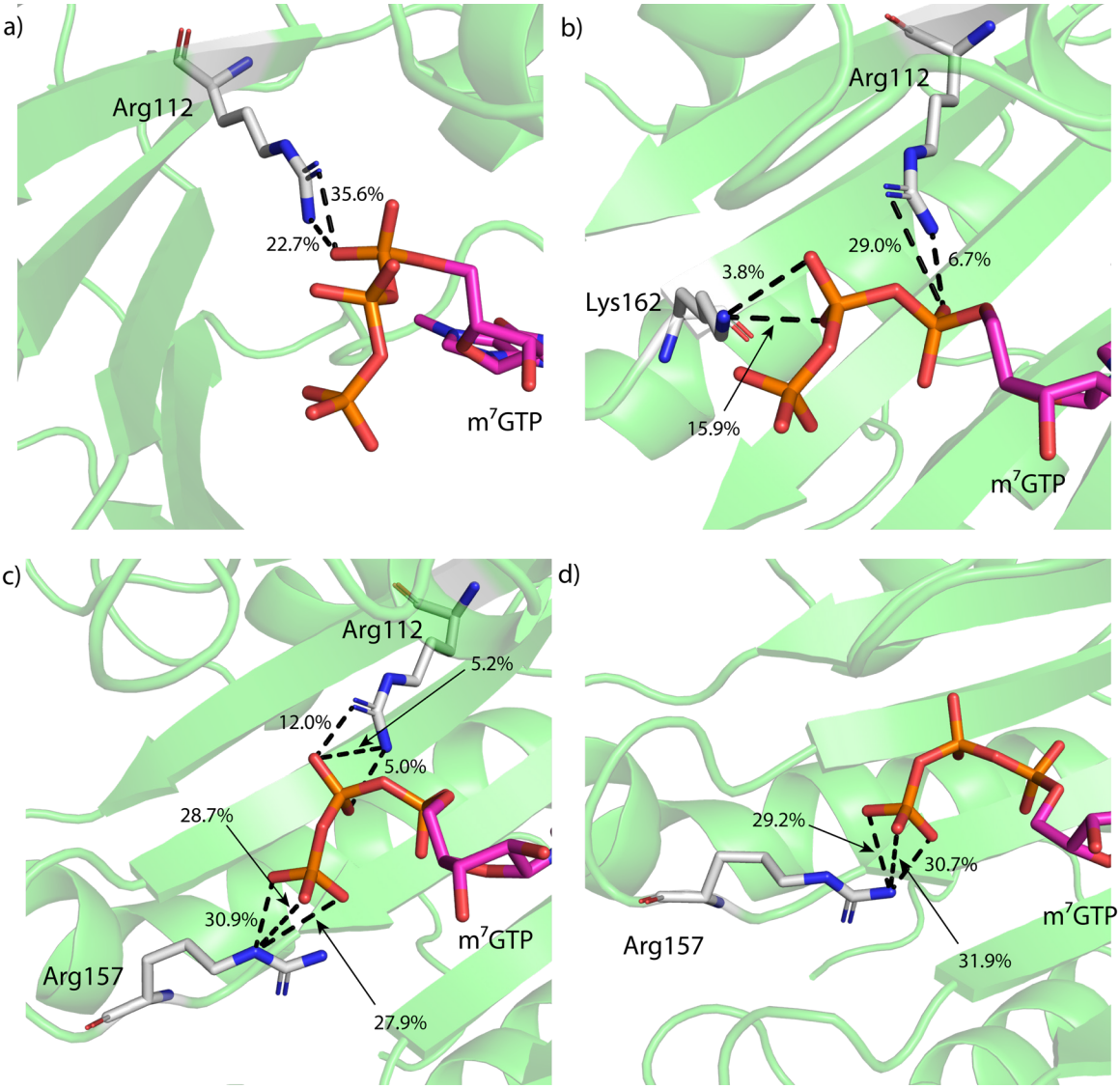

Figure 3.5 eIF4E interactions with A, B, G of m^7GTP, a) – d) showing various intermittent hydrogen bonds with the Arg112, Arg157, and Lys162 basic residues.

apo-eIF4E (RMSD = 4.1 ± 0.8 Å; Figure 3.4b, Table B.1). Interestingly, the flexibility of the C-terminus region is significantly higher in apo-eIF4E than eIF4E-m^{7}GTP (Figure B.4), indicating that the binding of m^{7}GTP reduces the flexibility of the C-terminus region to a certain extent. Similarly, compared to apo-eIF4E, the N-terminus region (28–37 residues) of eIF4E is less flexible in the presence of m^{7}GTP due to non-covalent interactions between the N-terminus and the H2, H4, and H5 α-helices (Figure 3.6, B.4). Since the N-terminus and H2 of eIF4E interacts with eIF4G,[22, 39] the presence of m^{7}GTP could affect the affinity for eIF4G.

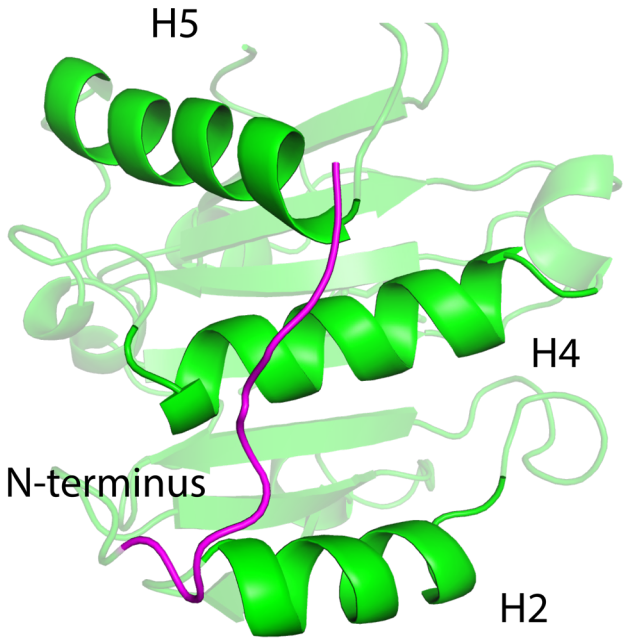

Figure 3.6 The N-terminus region (magenta) interacting with the H2, H4 and H5 α-helices (opaque green) of eIF4E when m^{7}GTP is bound.

Overall, the interactions between eIF4E and m^{7}GTP observed during the MD simulations are consistent with the crystal structure (PDB ID: 1IPC). Additionally, although the C-terminus region was not resolved in the X-ray crystal structure of the eIF4E-m^{7}GTP complex, binding of m^{7}GTP was found to reduce the flexibility of the C-terminus

to a certain extent despite the absence of the adjacent second nucleotide (Figure B.4). Apart from the flexibility of the triphosphate tail, most of the attributes of the eIF4E-m^{7}GTP complex presented here are very similar to the crystallographic and binding affinity studies. The results presented in this section validate the approach employed, which will be used to elucidate the structural dynamics of the eIF4E-RTP and eIF4E-RBV complexes in the following sections.

3.3.2. Despite a smaller ring, RTP shows similar interactions in the eIF4E cap-binding site as m^{7}GTP

Experimental binding studies indicate that m^{7}GTP and RTP compete with m^{7}G for binding in the cap-binding pocket of eIF4E.[30, 40] According to previous NMR studies, RTP binding is possible due to interactions with Trp56 and Trp102 of eIF4E.[30, 41] However, the studies also suggested that the RTP is dynamic in the binding pocket due to the smaller triazole ring (Figure 3.7a).[30] Indeed, eIF4E-RTP MD simulation data has revealed that RTP (RMSD = 2.4 ± 0.5 Å; Figure 3.4c, Table B.3) is dynamic in the binding pocket, but these variations in the ligand did not impact the overall stability of eIF4E (RMSD = 4.4 ± 0.4 Å; Figure 3.4c, Table B.3). Unlike the purine ring of m^{7}GTP, due to the small size of the triazole ring, the carboxamide N3 of RTP forms less persistent hydrogen bonds with OE1 (occupancy = 13.9%, Figure 3.7b) and OE2 (occupancy = 13.2%, figure 3.7b) of Glu103, giving rise to the dynamics of the ligand in the binding pocket (Figure 3.4c). However, the remaining contacts between RTP and eIF4E are very similar to those for m^{7}GTP. RTP and m^{7}GTP form persistent stacking with Trp56 (occupancy = 90.0%; Figure 3.7a, B.5) and Trp102 (occupancy = 70.1%; Figure 3.3a, B.5), respectively. In contrast, RTP and m^{7}GTP

relatively form less persistent stacking with Trp102 (occupancy = 70.1%; Figure 3.7a, B.5) and Trp56 (occupancy = 60.2%; Figure 3.3a, B.5), respectively.

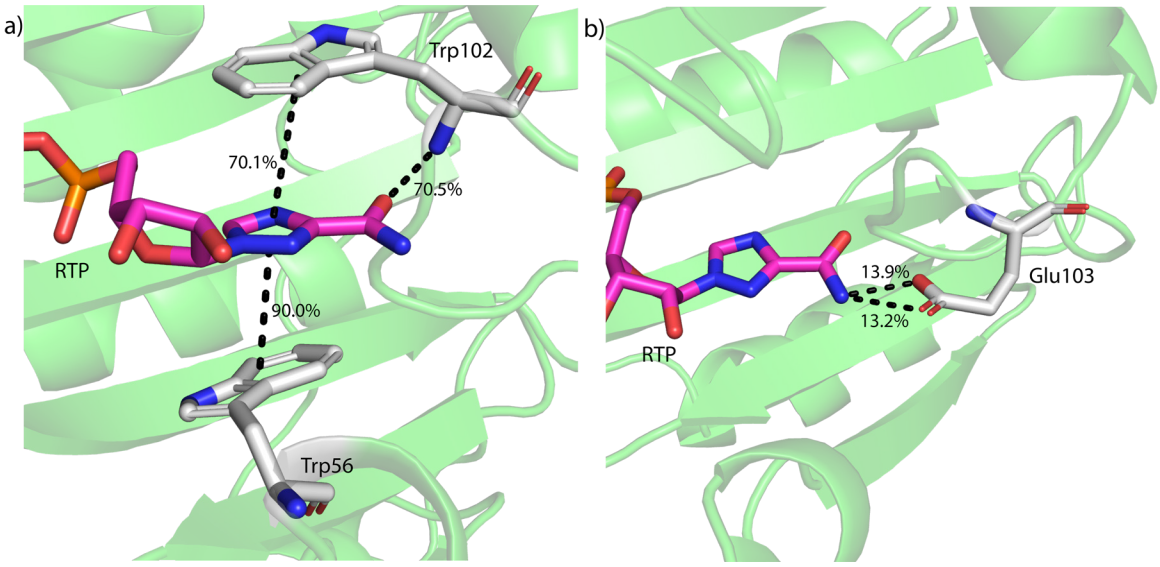

Figure 3.7 a) MD representative structure of the eIF4E-RTP complex, highlighting the RTP stacking and hydrogen bonding with the eIF4E residues in the cap-binding pocket, and b) carboxamide of RTP hydrogen bonding with the side chain of Glu103.

Moreover, a similar trend has been observed for hydrogen bonding, where the backbone N of Trp102 forms less persistent hydrogen bonds with O3 of RTP (occupancy = 70.5%; Figure 3.7a) compared to the O6 of m^7GTP (occupancy = 93.7%; Figure 3.3a). While binding of RTP reduces the flexibility of Trp56, it increases the flexibility of Trp102 compared to apo-eIF4E and eIF4E-m^7GTP (Figure 3.8). Additionally, the triphosphate tail of RTP exhibited intermittent interactions in the cap-binding pocket that are very similar to m^7GTP (Figure 3.9a–f, Table B.4). Specifically, RTP forms hydrogen bonds with Arg112 ($\Delta G = -5.3 \pm 3.8$ kcal/mol, Figure 3.9a–d), Arg157 ($\Delta G = -7.3 \pm 2.0$ kcal/mol, Figure 3.9a–c,f), and Lys162 ($\Delta G = -9.0 \pm 0.9$ kcal/mol, Figure 3.9a,b,e) of eIF4E. However, RTP displayed an additional hydrogen bond with Lys159 ($\Delta G = -6.5 \pm 0.6$ kcal/mol, Figure 3.9d,f) that was not observed in the eIF4E-m^7GTP complex. Interestingly, while m^7GTP

exhibited stronger binding to Arg157, RTP exhibited stronger binding to Lys162. Overall, despite the difference in the dynamics and per-residue free binding energy of the triphosphate

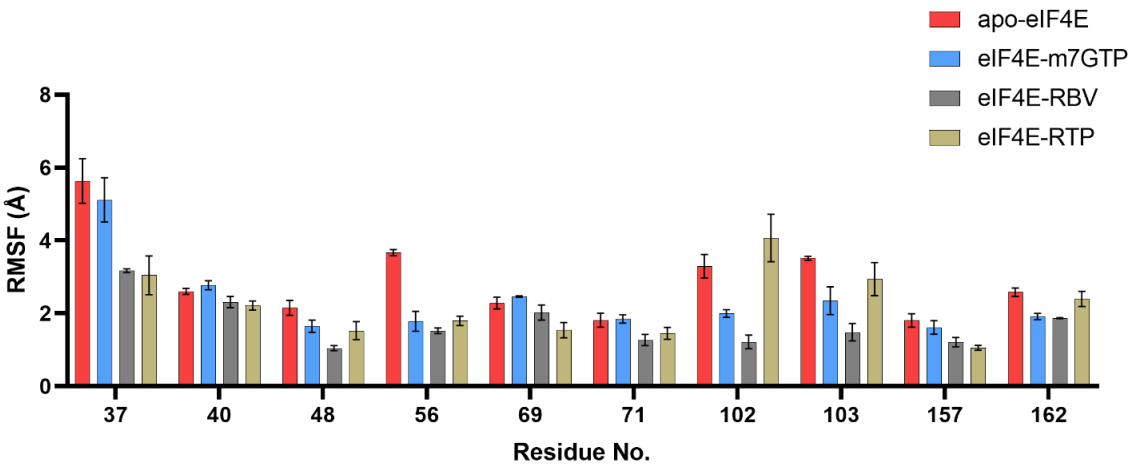

Figure 3.8 Fluctuations (RMSF, Å) in the dorsal surface and cap-binding residues of apo-eIF4E (red), as well as the eIF4E-m^{7}GTP (blue), eIF4E-RBV (grey), and eIF4E-RTP (citrine) complexes.

tail of RTP compared to m^{7}GTP, results from the MD simulations indicate that Arg112, Arg157, Lys159 and Lys162 predominantly form hydrogen bonds with RTP like m^{7}GTP.

Previous experimental affinity studies suggest that the eIF4E binding affinity for m^{7}GTP and RTP is the same. However, the calculated overall binding free energy of m^{7}GTP ($\Delta G = -30.3 \pm 3.9$ kcal/mol; Table B.5) was better than RTP ($\Delta G = -19.5 \pm 1.1$ kcal/mol; Table B.5). Previous studies have indicated that m^{7}GTP has a higher affinity for truncated eIF4E (K_d = 0.03 µM) over the full structure of eIF4E (K_d = 0.19 µM).[19, 42] However, there is no experimental evidence on how the truncated form affects the affinity

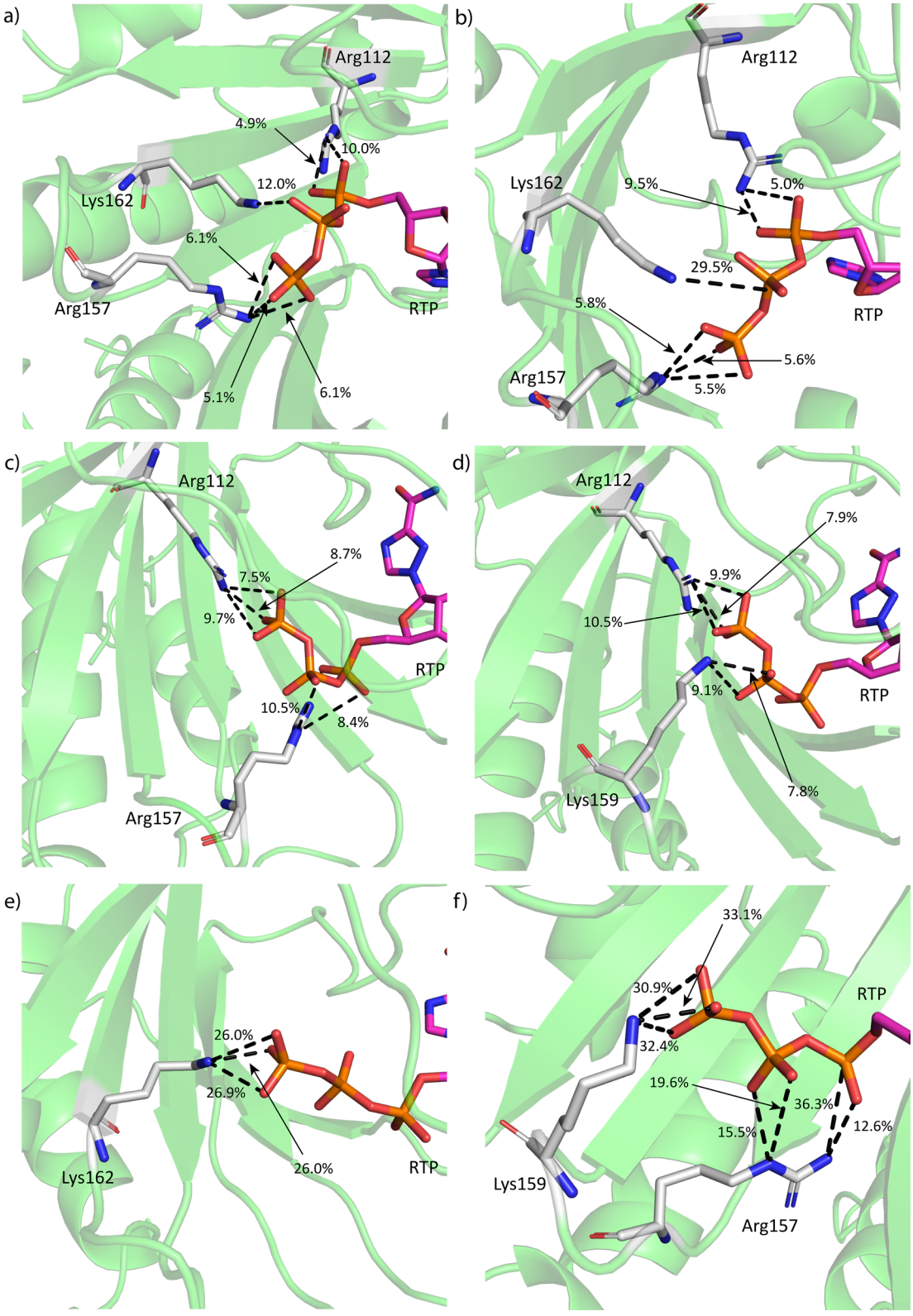

Figure 3.9 eIF4E interactions with A, B, G of RTP, a) – f) showing various intermittent hydrogen bonds with the basic residues Arg112, Arg157, Lys159, and Lys162 of eIF4E.

of RTP for eIF4E and therefore this effect could be consistent between the two ligands. Interestingly, despite the similarities between m^7GTP and RTP, a comparative NMR study suggested that binding of RTP, but not m^7GTP induces structural changes in eIF4E, which affects residues including His37, Gln40, Val69, and Asp71.[30] Indeed, when m^7GTP was bound to eIF4E, little to no change was observed in the flexibility of His37, Gln40, Val69, and Asp71, but the flexibility is reduced when RTP is bound (Figure 3.8). Despite slight differences between RTP and m^7GTP regarding the stability of His37, Gln40, Val69, and Asp71 and stacking occupancies, both ligands exhibited a similar mode of interaction in the cap-binding pocket of eIF4E.

Overall, future studies should focus improving upon the current RTP design to increase the stability and specificity. Specifically, the MD data suggests that to increase the stability of triazole ring, RTP should make more persistent contacts with the side chain oxygens of Glu103, and the backbone oxygen of Pro100, which is available to interact (both in the eIF4E-m^7GTP crystal and the eIF4E-RTP MD representative structure) in the binding pocket of eIF4E. Additionally, Lys159 and Lys162, which are important for the binding of RTP, could be further explored for lysine covalent docking. Intriguingly, preliminary studies on lysine-targeted eIF4E inhibitors have suggested that covalent binding of arylsulfonyl fluoride to Lys162 acutely inactivates eIF4E in cells,[43] and Lysine mediated inhibition has been already used to target other proteins for treating cancer.[44, 45] This chapter provides structural support for this proposal and extends this idea to the potential targeting of another lysine residue, Lys159, in the cap-binding pocket.

3.3.3. Although RBV binds to eIF4E, the mode of interaction is significantly different from m^{7}GTP, resulting in much weaker binding

The RBV cap-analogue has been shown to compete with m^{7}G to bind to eIF4E.[19] However, no information is available about the interactions that promote RBV binding, and the structural changes induced in eIF4E after binding. Similar to the purine of m^{7}GTP and the triazole of RTP, MD simulation of eIF4E-RBV show that the triazole ring of RBV stacks between Trp56 (occupancy = 94.6%, $\Delta G = -4.3 \pm 0.1$ kcal/mol; Figure 3.10) and

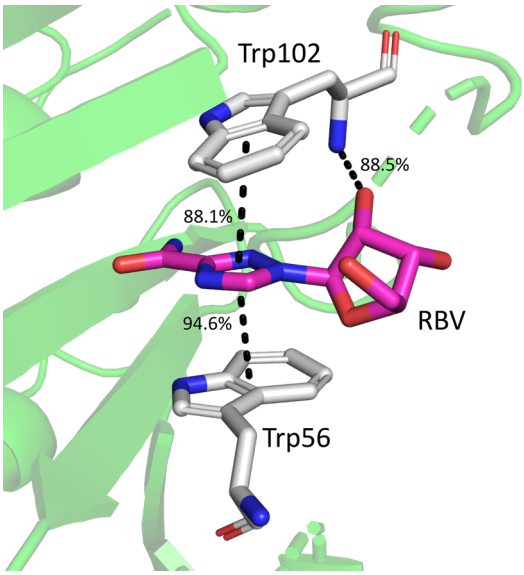

Figure 3.10 MD representative structure of the eIF4E-RBV complex, highlighting binding site residues that stack or hydrogen bond with RBV.

Trp102 (occupancy = 88.1%, $\Delta G = -4.7$ kcal/mol; Figure 3.10). Additionally, compared to apo-eIF4E, Trp56 and Trp102 exhibit reduced flexibility when RBV is bound to the cap-binding pocket (Figure 3.8), which is consistent with the conclusions from a previous NMR study.[19] Interestingly, RBV stacks with Trp56 and Trp102 of eIF4E similar to m^{7}GTP and RTP, but RBV interactions are more persistent with Trp102 than m^{7}GTP (by up to 28%,

Figure B.5) and RTP (by up to 18%, Figure B.5). While RBV:Trp56 stacking interactions are indispensable for ligand recruitment as RBV failed to compete with m^7G when Trp56 was mutated,[19] the impact of mutating Trp102 on RBV has not been investigated, which could in fact negatively affect RBV binding.

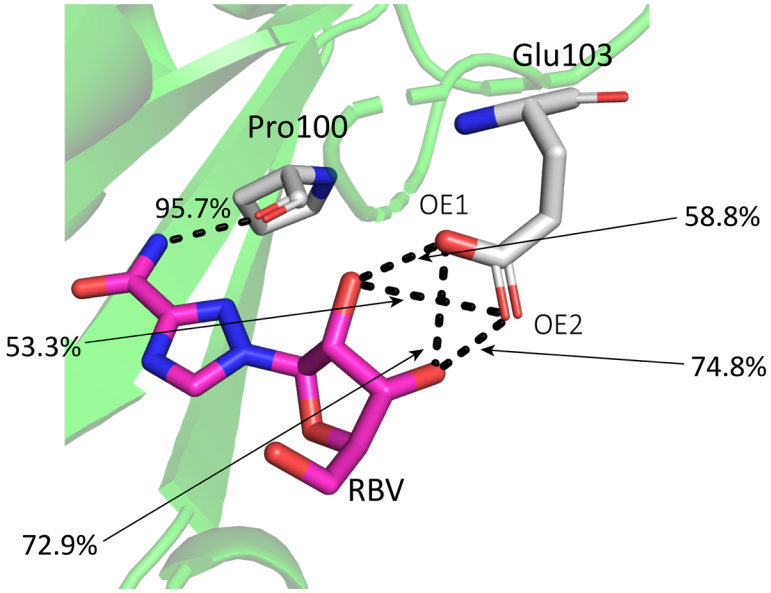

Figure 3.11 MD representative structure of the eIF4E-RBV complex, highlighting RBV hydrogen bond contacts with Pro100 and Glu103 of eIF4E.

While MD simulations revealed that the purine ring of m^7GTP hydrogen bonds with Trp102 and Glu103, the lack of the triphosphate tail facilitates the ribose group of RBV establishing hydrogen bonds with Trp102 (Figure 3.10) and Glu103 (Figure 3.11). Interestingly, the carboxamide of the RBV triazole ring forms a persistent hydrogen bond with the backbone of Pro100 (occupancy = 95.7%, $\Delta G = -1.6$ kcal/mol, Figure 3.11), which was observed neither in the eIF4E-m^7GTP nor eIF4E-RTP complexes. These distinct hydrogen bonds of the RBV carboxamide and the ribose group with Pro100, Trp102, or Glu103 in the absence of the triphosphate tail facilitates stable binding of RBV (RMSD = 0.3 ± 0.2 Å; Figure 3.4d, Table B.6) in the cap-binding site of eIF4E (RMSD = 3.5 ± 0.4

Å; Figure 3.4d, Table B.6). However, the lack of the triphosphate tail also led to a weaker overall binding free energy of RBV (ΔG = –17.7 ± 0.3 kcal/mol; Table B.5) compared to RTP (ΔG = –19.48 ± 1.09 kcal/mol; Table B.5) to eIF4E, which correlates with previous experimental data that suggested RTP has a greater binding affinity than RBV for eIF4E .[19] Similar to m^7GTP, binding of RBV decreases the flexibility of the C-terminus (204–210 residues; Figure B.4), and interestingly, the C-terminal tail (211–217 residues) of eIF4E exhibited high flexibility in the presence of RBV (Figure B.4), which was not observed for either the eIF4E-RTP or eIF4E-m^7GTP system. Additionally, the flexibility of His37, Gln40, Phe48, Val69, Asp71, and Glu103 is reduced in the presence of RBV compared to apo-eIF4E (Figure 3.8).

These results suggest that the triazole ring of RBV, similar to RTP and m^7GTP, stacks with Trp56 and Trp102 of eIF4E. However, the lack of the triphosphate, the orientation of the ligand in the binding pocket is unique, which helps RBV form distinct hydrogen bonds with Pro100, Trp102, and Glu103 compared to the other cap-analogues. Taken together, a combination of the distinct interactions elucidated for eIF4E-RBV provides the structural rationalization for the previous experimental results,[19] including lowered flexibility of cap-binding residues and weaker ligand binding compared to m^7GTP and RTP.

3.4. Conclusion

In this chapter, MD simulations were used to provide the first dynamic structural data for RTP and RBV bound to the eIF4E cap-binding pocket. Despite the dynamics of the triphosphate tail of m^7GTP, the MD data obtained for eIF4E-m^7GTP are consistent with the crystallographic data. The triphosphate tail of m^7GTP showed interactions with Arg157,

Lys159, and Lys162, but Arg157 exhibited greater binding affinity among them. MD simulations also suggested that the binding mode of m^7GTP and RTP is similar, rationalizing the NMR and mutational studies that indicated both cap-analogues compete with 5′-terminal m^7G cap in the cap-binding site.[19, 30] Additionally, RBV forms stable interactions in the binding site of eIF4E, with distinct hydrogen bonds observed that do not occur for either m^7GTP or RTP. However, the overall binding free energy of RBV is weaker than m^7GTP due to the smaller ring and lack of triphosphate tail, which explains why m^7GTP has a smaller K_d than RBV during the experimental affinity studies.[19] Based on the information generated in this chapter, amino acids including Trp56, Pro100, Trp102, Glu103, Arg112, Arg157, Lys159, and Lys162 could be great targets for obtaining high affinity inhibitors from virtual library screening.

3.5. References

1. Uttam, S.; Wong, C.; Price, T. J.; Khoutorsky, A., eIF4E-Dependent Translational Control: A Central Mechanism for Regulation of Pain Plasticity. *Frontiers in Genetics* **2018,** *9*.

2. Sonenberg, N.; Hinnebusch, A. G., Regulation of translation initiation in eukaryotes: mechanisms and biological targets. *Cell* **2009,** *136* (4), 731-745.

3. Osborne, M. J.; Borden, K. L. B., The eukaryotic translation initiation factor eIF4E in the nucleus: taking the road less traveled. *Immunological Reviews* **2015,** *263* (1), 210-223.

4. Brown, C. J.; Verma, C. S.; Walkinshaw, M. D.; Lane, D. P., Crystallization of eIF4E complexed with eIF4GI peptide and glycerol reveals distinct structural differences around the cap-binding site (vol 8, pg 1905, 2009). *Cell Cycle* **2010,** *9* (19), 4031-4031.

5. Matsuo, H.; Li, H.; McGuire, A. M.; Fletcher, C. M.; Gingras, A. C.; Sonenberg, N.; Wagner, G., Structure of translation factor eIF4E bound to m7GDP and interaction with 4E-binding protein. *Nature Structural & Molecular Biology* **1997,** *4* (9), 717-724.

6. Topisirovic, I.; Culjkovic, B.; Cohen, N.; Perez, J. M.; Skrabanek, L.; Borden, K. L., The proline-rich homeodomain protein, PRH, is a tissue-specific inhibitor of eIF4E-dependent cyclin D1 mRNA transport and growth. *EMBO Journal* **2003,** *22* (3), 689-703.

7. Cohen, N.; Sharma, M.; Kentsis, A.; Perez, J. M.; Strudwick, S.; Borden, K. L. B., PML RING suppresses oncogenic transformation by reducing the affinity of eIF4E for mRNA. *EMBO Journal* **2001,** *20* (16), 4547-4559.

8. Rousseau, D.; Kaspar, R.; Rosenwald, I.; Gehrke, L.; Sonenberg, N., Translation initiation of ornithine decarboxylase and nucleocytoplasmic transport of cyclin D1 mRNA are increased in cells overexpressing eukaryotic initiation factor 4E. *Proceedings of the National Academy of Sciences* **1996,** *93* (3), 1065-1070.

9. Iborra, F. J.; Jackson, D. A.; Cook, P. R., Coupled transcription and translation within nuclei of mammalian cells. *Science* **2001,** *293* (5532), 1139-1142.

10. Kleiner, H. E.; Krishnan, P.; Tubbs, J.; Smith, M.; Meschonat, C.; Shi, R.; Lowery-Nordberg, M.; Adegboyega, P.; Unger, M.; Cardelli, J.; Chu, Q.; Mathis, J. M.; Clifford, J.; De Benedetti, A.; Li, B. D., Tissue microarray analysis of eIF4E and its downstream effector proteins in human breast cancer. *Journal of Experimental & Clinical Cancer Research* **2009,** *28* (1), 5.

11. Batool, A.; Aashaq, S.; Andrabi, K. I., Eukaryotic initiation factor 4E (eIF4E): A recap of the cap-binding protein. *Journal of Cellular Biochemistry* **2019,** *120* (9), 14201-14212.

12. Borden, K. L., The eukaryotic translation initiation factor eIF4E wears a "cap" for many occasions. *Translation* **2016,** *4* (2), e1220899.

13. Assouline, S.; Culjkovic, B.; Cocolakis, E.; Rousseau, C.; Beslu, N.; Amri, A.; Caplan, S.; Leber, B.; Roy, D. C.; Miller, W. H.; Borden, K. L. B., Molecular targeting of the oncogene eIF4E in acute myeloid leukemia (AML): a proof-of-principle clinical trial with ribavirin. *Blood* **2009,** *114* (2), 257-260.

14. Culjkovic, B.; Borden, K. L., Understanding and Targeting the Eukaryotic Translation Initiation Factor eIF4E in Head and Neck Cancer. *Journal of oncology* **2009,** *2009*, 981679.

15. Borden, K. L. B.; Culjkovic-Kraljacic, B., Ribavirin as an anti-cancer therapy: acute myeloid leukemia and beyond? *Leukemia Lymphoma* **2010,** *51* (10), 1805-1815.

16. Mamane, Y.; Petroulakis, E.; Rong, L.; Yoshida, K.; Ler, L. W.; Sonenberg, N., eIF4E--from translation to transformation. *Oncogene* **2004,** *23* (18), 3172-3179.

17. Lu, C.; Makala, L.; Wu, D.; Cai, Y., Targeting translation: eIF4E as an emerging anticancer drug target. *Expert Reviews in Molecular Medicine* **2016,** *18*, e2.

18. Te, H. S.; Randall, G.; Jensen, D. M., Mechanism of action of ribavirin in the treatment of chronic hepatitis C. *Gastroenterology & Hepatology* **2007,** *3* (3), 218-225.

19. Kentsis, A.; Topisirovic, I.; Culjkovic, B.; Shao, L.; Borden, K. L., Ribavirin suppresses eIF4E-mediated oncogenic transformation by physical mimicry of the 7-methyl guanosine mRNA cap. *Proceedings of the National Academy of Sciences* **2004,** *101* (52), 18105-18110.

20. Willis, R. C.; Carson, D. A.; Seegmiller, J. E., Adenosine kinase initiates the major route of ribavirin activation in a cultured human cell line. *Proceedings of the National Academy of Sciences* **1978,** *75* (7), 3042-3044.

21. Ogino, A.; Sano, E.; Ochiai, Y.; Yamamuro, S.; Tashiro, S.; Yachi, K.; Ohta, T.; Fukushima, T.; Okamoto, Y.; Tsumoto, K.; Ueda, T.; Yoshino, A.; Katayama, Y., Efficacy of ribavirin against malignant glioma cell lines. *Oncology Letters* **2014,** *8* (6), 2469-2474.

22. Tomoo, K.; Shen, X.; Okabe, K.; Nozoe, Y.; Fukuhara, S.; Morino, S.; Ishida, T.; Taniguchi, T.; Hasegawa, H.; Terashima, A.; Sasaki, M.; Katsuya, Y.; Kitamura, K.; Miyoshi, H.; Ishikawa, M.; Miura, K., Crystal structures of 7-methylguanosine 5'-triphosphate (m(7)GTP)- and P(1)-7-methylguanosine-P(3)-adenosine-5',5'-triphosphate (m(7)GpppA)-bound human full-length eukaryotic initiation factor 4E: biological importance of the C-terminal flexible region. *The Biochemical Journal* **2002,** *362* (3), 539-544.

23. Tomoo, K.; Shen, X.; Okabe, K.; Nozoe, Y.; Fukuhara, S.; Morino, S.; Sasaki, M.; Taniguchi, T.; Miyagawa, H.; Kitamura, K.; Miura, K.; Ishida, T., Structural features

of human initiation factor 4E, studied by X-ray crystal analyses and molecular dynamics simulations. *Journal of Molecular Biology* **2003,** *328* (2), 365-383.

24. Scheper, G. C.; van Kollenburg, B.; Hu, J.; Luo, Y.; Goss, D. J.; Proud, C. G., Phosphorylation of eukaryotic initiation factor 4E markedly reduces its affinity for capped mRNA. *Journal of Biological Chemistry* **2002,** *277* (5), 3303-3309.

25. Gross, J. D.; Moerke, N. J.; von der Haar, T.; Lugovskoy, A. A.; Sachs, A. B.; McCarthy, J. E.; Wagner, G., Ribosome loading onto the mRNA cap is driven by conformational coupling between eIF4G and eIF4E. *Cell* **2003,** *115* (6), 739-750.

26. Hu, H.; Chen, B.; Zheng, D.; Huang, G., Revealing the selective mechanisms of inhibitors to PARP-1 and PARP-2 via multiple computational methods. *PeerJ* **2020,** *8*, e9241.

27. Michel, J., Current and emerging opportunities for molecular simulations in structure-based drug design. *Physical Chemistry Chemical Physics* **2014,** *16* (10), 4465-4477.

28. Crespo, A.; Fernández, A., Induced disorder in protein-ligand complexes as a drug-design strategy. *Molecular Pharmaceutics* **2008,** *5* (3), 430-437.

29. Di Marino, D.; D'Annessa, I.; Tancredi, H.; Bagni, C.; Gallicchio, E., A unique binding mode of the eukaryotic translation initiation factor 4E for guiding the design of novel peptide inhibitors. *Protein Science* **2015,** *24* (9), 1370-1382.

30. Volpon, L.; Osborne, M. J.; Zahreddine, H.; Romeo, A. A.; Borden, K. L., Conformational changes induced in the eukaryotic translation initiation factor eIF4E by a clinically relevant inhibitor, ribavirin triphosphate. *Biochemical and Biophysical Research Communications* **2013,** *434* (3), 614-619.

31. Zheng, J.; Li, X. Q.; Zhang, C. Y.; Zhang, Y. Q., eIF4E Overexpression Is Associated with Poor Prognoses of Ovarian Cancer. *Analytical Cellular Pathology* **2020,** *2020*, 8984526.

32. Chen, C. N.; Hsieh, F. J.; Cheng, Y. M.; Lee, P. H.; Chang, K. J., Expression of eukaryotic initiation factor 4E in gastric adenocarcinoma and its association with clinical outcome. *Journal of surgical oncology* **2004,** *86* (1), 22-27.

33. Frisch, M. J.; Trucks, G. W.; Schlegel, H. B.; Scuseria, G. E.; Robb, M. A.; Cheeseman, J. R.; Scalmani, G.; Barone, V.; Petersson, G. A.; Nakatsuji, H.; Li, X.; Caricato, M.; Marenich, A. V.; Bloino, J.; Janesko, B. G.; Gomperts, R.; Mennucci, B.; Hratchian, H. P.; Ortiz, J. V.; Izmaylov, A. F.; Sonnenberg, J. L.; Williams; Ding, F.; Lipparini, F.; Egidi, F.; Goings, J.; Peng, B.; Petrone, A.; Henderson, T.; Ranasinghe, D.; Zakrzewski, V. G.; Gao, J.; Rega, N.; Zheng, G.; Liang, W.; Hada, M.; Ehara, M.; Toyota, K.; Fukuda, R.; Hasegawa, J.; Ishida, M.; Nakajima, T.; Honda, Y.; Kitao, O.; Nakai, H.; Vreven, T.; Throssell, K.; Montgomery Jr., J. A.; Peralta, J. E.; Ogliaro, F.; Bearpark, M. J.; Heyd, J. J.; Brothers, E. N.; Kudin, K. N.; Staroverov, V. N.; Keith, T.

A.; Kobayashi, R.; Normand, J.; Raghavachari, K.; Rendell, A. P.; Burant, J. C.; Iyengar, S. S.; Tomasi, J.; Cossi, M.; Millam, J. M.; Klene, M.; Adamo, C.; Cammi, R.; Ochterski, J. W.; Martin, R. L.; Morokuma, K.; Farkas, O.; Foresman, J. B.; Fox, D. J. *Gaussian 16 Rev. C.01*, Wallingford, CT, 2016.

34. Fiser, A.; Do, R. K.; Sali, A., Modeling of loops in protein structures. *Protein Science* **2000,** *9* (9), 1753-1773.

35. Yang, Z.; Lasker, K.; Schneidman-Duhovny, D.; Webb, B.; Huang, C. C.; Pettersen, E. F.; Goddard, T. D.; Meng, E. C.; Sali, A.; Ferrin, T. E., UCSF Chimera, MODELLER, and IMP: an integrated modeling system. *Journal of Structural Biology* **2012,** *179* (3), 269-278.

36. Schrodinger, LLC, The PyMOL Molecular Graphics System, Version 1.8. 2015.

37. Osborne, M. J.; Volpon, L.; Kornblatt, J. A.; Culjkovic-Kraljacic, B.; Baguet, A.; Borden, K. L. B., eIF4E3 acts as a tumor suppressor by utilizing an atypical mode of methyl-7-guanosine cap recognition. *Proceedings of the National Academy of Sciences* **2013,** *110* (10), 3877-3882.

38. Liu, W.; Zhao, R.; McFarland, C.; Kieft, J.; Niedzwiecka, A.; Jankowska-Anyszka, M.; Stepinski, J.; Darzynkiewicz, E.; Jones, D. N. M.; Davis, R. E., Structural Insights into Parasite eIF4E Binding Specificity for m7G and m2,2,7G mRNA Caps. *Journal of Biological Chemistry* **2009,** *284* (45), 31336-31349.

39. Sonenberg, N.; Gingras, A. C., The mRNA 5' cap-binding protein eIF4E and control of cell growth. *Current opinion in cell biology* **1998,** *10* (2), 268-275.

40. Kentsis, A.; Volpon, L.; Topisirovic, I.; Soll, C. E.; Culjkovic, B.; Shao, L.; Borden, K. L. B., Further evidence that ribavirin interacts with eIF4E. *RNA* **2005,** *11* (12), 1762-1766.

41. Cohen, N.; Sharma, M.; Kentsis, A.; Perez, J. M.; Strudwick, S.; Borden, K. L., PML RING suppresses oncogenic transformation by reducing the affinity of eIF4E for mRNA. *EMBO Journal* **2001,** *20* (16), 4547-4559.

42. Liu, W.; Jankowska-Anyszka, M.; Piecyk, K.; Dickson, L.; Wallace, A.; Niedzwiecka, A.; Stepinski, J.; Stolarski, R.; Darzynkiewicz, E.; Kieft, J.; Zhao, R.; Jones, D. N.; Davis, R. E., Structural basis for nematode eIF4E binding an m(2,2,7)G-Cap and its implications for translation initiation. *Nucleic Acids Research* **2011,** *39* (20), 8820-8832.

43. Wan, X.; Yang, T.; Cuesta, A.; Pang, X.; Balius, T. E.; Irwin, J. J.; Shoichet, B. K.; Taunton, J., Discovery of Lysine-Targeted eIF4E Inhibitors through Covalent Docking. *Journal of the American Chemical Society* **2020,** *142* (11), 4960-4964.

44. Wang, S.; Cang, S.; Liu, D., Third-generation inhibitors targeting EGFR T790M mutation in advanced non-small cell lung cancer. *Journal of Hematology & Oncology* **2016,** *9* (1), 34.

45. Pettinger, J.; Jones, K.; Cheeseman, M. D., Lysine-Targeting Covalent Inhibitors. *Angewandte Chemie International Edition* **2017,** *56* (48), 15200-15209.

Chapter 4: Conclusions

4.1. Thesis Summary

Eukaryotic translation initiation factor 5B (eIF5B) prevents apoptosis in certain cancer cells by promoting the synthesis of anti-apoptotic and immune-suppressing proteins.[1, 2] Therefore, Chapter 2 investigated the interaction of eIF5B with ribavirin triphosphate (RTP) and LWW31, by combining cell viability and western blotting with protein modeling and molecular dynamics (MD) simulations. The results obtained from western blot studies helped understand the effect of ribavirin (RBV) on eIF5B and eIF5B dependent proteins in glioblastoma (GBM) cell lines. Furthermore, results from cell viability experiments suggested that late tumor necrosis factor related apoptosis-inducing ligand treatment (TRAIL; 48 hours after seeding) more efficiently inhibits BT25 and BT48 cells than early TRAIL treatment (24 hours after seeding). Quantification of the levels of eIF5B and its downstream targets using western blotting suggested that RBV does not affect the function of eIF5B. MD simulations corroborated the conclusions from western blotting, indicating that the interaction between eIF5B and RTP is unfavourable.

To study the interactions between eIF5B and small molecules (RTP and LWW31) that may show promising inhibitory activity, the first human eIF5B model (629–1220 residues) was generated using homology modeling with yeast eIF5B crystal structure (PDB ID: 1IPC) as the template.[3] Subsequent MD simulations on the human eIF5B model suggested that human eIF5B undergoes a domain release mechanism in the absence of the ribosome, leading to D4 flexibility similar to yeast eIF5B.[3] Furthermore, an equilibrated model of human eIF5B was used to identify the binding site for LWW31 in the C-terminus region (629–1220 residues) since the previously proposed N-terminus binding site (1–586

residues) does not have a known function.[4] Two binding sites for LWW31 with the same binding energy were identified using molecular docking algorithms in the C-terminus region of eIF5B. However, MD simulations and druggability predictions suggested that LWW31 in binding site-I (BS-I) in D1 of eIF5B binds with a greater binding free energy compared to binding site-II (BS-II) in the inter-domain pocket of D2 and D3. Together, these results suggest that BS-I is the possible binding site for LWW31 in the C-terminus region of eIF5B, and in future, experimental work is required to determine how LWW31 affects eIF5B function when bound to the N and C-terminus regions.

Overall, Chapter 2 highlighted how a combination of cell, molecular and computational biology can accelerate the understanding of small molecule ligand binding to eIF5B.The complementary work presented in Chapter 2 offers an interdisciplinary approach to study the structural dynamics and identify promising compounds for other proteins that lack X-ray crystal structures, especially with the advent of recent artificial intelligence-based protein model databases like AlphaFold.[5]

Like eIF5B, eukaryotic translation initiation factor 4E (eIF4E) is an eIF that is elevated in certain cancers,[6-10] and often promotes cancer cell proliferation and survival.[11, 12] Therefore, the interaction of eIF4E with previously proven inhibitors was examined in Chapter 3, including ribavirin (RBV) and its metabolite, ribavirin triphosphate (RTP). These ligands were chosen for study since there is not much information on the binding mode of inhibitors in the cap-binding site and yet such information is necessary to design improved inhibitors. Furthermore, experimental data is available for RBV and RTP, which showed that the both ligands compete with 7-methylguanosine (m^7G) nucleoside to interact with eIF4E.[13] MD simulations of 7-methylguanosine triphosphate (m^7GTP) bound to

eIF4E was also investigated, which validated the computational methodology through comparison with the crystallographic data. The same methodology was then reliably applied to study the interactions of RBV and RTP with eIF4E. The results showed that Trp56 and Trp102 of eIF4E, which have been proposed to aid in m^7G cap recruitment,[14] form persistent stacking interactions with RBV compared to m^7GTP and RTP. RBV also forms a persistent hydrogen bond with Pro100, which was not observed for either m^7GTP or RTP. Nevertheless, the triphosphate tail of m^7GTP and RTP exhibits numerous intermittent interactions in the cap-binding pocket, which was not observed in RBV. The lack of triphosphate tail in RBV led to overall weaker binding free energy to eIF4E compared to m^7GTP and RTP, rationalizing the experimental binding affinity.[13] Additionally, the MD predicted similar binding mode of m^7GTP and RTP to eIF4E rationalizes previous NMR and mutational studies that indicated both cap-analogues compete with 5′-terminal m^7G cap in the cap-binding site.[13, 15]

Based on the information presented in Chapter 3, amino acids such as Trp56, Pro100, Trp102, Glu103, Arg112, Arg157, Lys159, and Lys162 could be important targets for designing more potent inhibitors using virtual library screening. Additionally, Lys159 and Lys162, which are important for the binding of RTP, could be further explored for lysine covalent docking. Intriguingly, preliminary studies on lysine-targeted eIF4E inhibitors have suggested that covalent binding of arylsulfonyl fluoride to Lys162 acutely inactivates eIF4E in cells,[16] and Lysine mediated inhibition has been already used to target other proteins for treating cancer.[17, 18] This chapter extends the idea to target another lysine residue, Lys159, in the cap-binding pocket.

4.2. Future Directions

Since the interaction of eIF4E with the 5'-terminal m^7G cap plays an important in head and neck, prostate, ovarian, blood, and esophageal cancers and modulates interactions with proteins like eIF4G and 4E-binding proteins (4E-BPs), [8, 9, 19-22] future work could investigate how the presence of RTP and RBV affects eIF4G and 4E-BP interaction with eIF4E (Figure 4.1a). Furthermore, previous studies suggested that phosphorylation of eIF4E by MAP kinase-interacting serine/threonine-protein kinase 1 and 2 (Mnk1/2) reduces the affinity for the cap (Figure 4.1b).[23-26] Therefore, studies could be carried out to examine the affinity of RBV and RTP for phosphorylated eIF4E since the phosphorylation site of eIF4E (Ser209) is close to the cap-binding site. Such studies can be conducted using a combination of experimental and computational techniques, which could provide insights at the cellular and atomic levels, respectively.

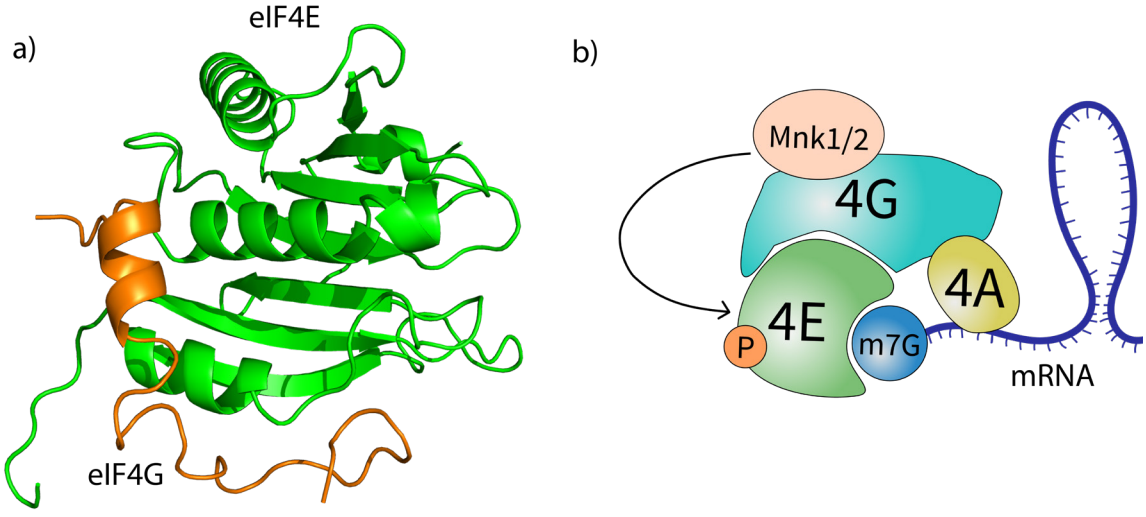

Figure 4.1 a) eIF4G (orange) interacting on the dorsal side with eIF4E (green; PDB ID: 5T46).[27] b) After binding to the C-terminus region of eIF4G, Mnk1/2 phosphorylates Ser209 of eIF4E.

On the other hand, eIF5B has implications in cancers like glioblastoma (GBM), hepatocellular carcinoma (HCC), lung adenocarcinoma (LUAD), and prostate cancer,[2, 28-30] yet only a handful of eIF5B inhibitors such as LWW31 and GTP analogues (GDPCP and GMPPNP) have been developed.[31-33] Interestingly, recent studies suggested that two eIF5B binding sites could be crucial for accomplishing function in cells.[32, 34] The first site was identified in D2 of yeast eIF5B, which interacts with ribosomal RNA when recruited on the ribosome during translation initiation (Figure 4.2a). The second site is based on a mutational study of D4 in yeast eIF5B, where mutating Arg955 prevents eIF5B interaction with initiator tRNA (Figure 4.2b).[32] These two sites could be screened against a library of compounds using docking programs, which can be used to filter molecules based on the molecular properties, including but not limited to hydrogen bond acceptors, hydrogen bond

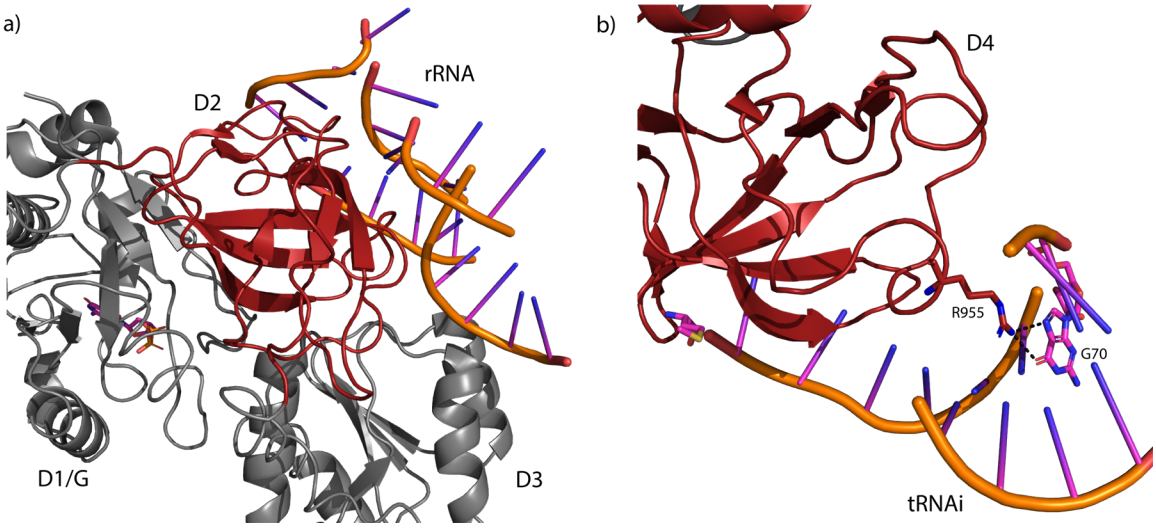

Figure 4.2 a) D2 (brick red) of eIF5B interacting with the ribosomal RNA (rRNA). b) R955 of eIF5B D4 (brick red) forming two hydrogen bonds with G70 of tRNAi (PDB ID: 6WOO).

donors, and molecular charge. However, the druggability of these pockets should be predicted before testing the compounds. Numerous studies have attempted to predict and

describe the druggable protein sites.[35] Programs like PockDrug and MetaPocket 2.0 could be used to identify the druggability of the binding sites, whereas MD simulations could be used to identify the stability and binding energy of these small molecules to human eIF5B.[36, 37] Ultimately, these molecules can then be tested in the wet lab using various cell culture and biochemical techniques such as cell viability and Annexin V apoptosis assay, which could be used to determine the half-maximal inhibitory concentration (IC_{50}) and apoptosis in cancer cells. Furthermore, the efficacy of ligands showing cytotoxicity could be improved by combining their treatment with pro-apoptotic agents. Additionally, techniques like western blotting could be crucial to determine the ligand's binding effect on the function of eIF5B by quantifying the downstream targets.[2, 30] If the identified ligand affects the activity of human eIF5B, cloning combined with fluorescence anisotropy could be used to narrow down the binding site and validate the in silico docking calculations. Ultimately, identifying inhibitors for eIF5B could prevent the initiation of non-canonical translation, which helps eIF5B promote the expression of anti-apoptotic and immune-suppressing proteins.[2, 38]

4.3. Concluding Remarks

This thesis used a combination of experimental and computational techniques to characterize the interactions of small molecule ligands (RTP and LWW31) with human eIF5B. The results suggested that RBV has no affect on eIF5B function in GBM cells. In addition, a high-quality human eIF5B model was generated using homology modeling, which facilitated in studying eIF5B-RTP interaction and identifying the binding site for LWW31 in D1. Lastly, MD simulations of cap-analogues, RBV and RTP, helped identify amino acids in the cap-binding site that could be further explored for structure-based drug

design.. The interdisciplinary research presented will pave the way to design novel effective compounds for cancers such as prostate and lung cancers, with elevated eIF5B and eIF4E levels.[29, 30, 39, 40]

4.4. References

1. Smith, R. C. L.; Kanellos, G.; Vlahov, N.; Alexandrou, C.; Willis, A. E.; Knight, J. R. P.; Sansom, O. J., Translation initiation in cancer at a glance. *Journal of Cell Science* **2021,** *134* (1).

2. Ross, J. A.; Dungen, K. V.; Bressler, K. R.; Fredriksen, M.; Khandige Sharma, D.; Balasingam, N.; Thakor, N., Eukaryotic initiation factor 5B (eIF5B) provides a critical cell survival switch to glioblastoma cells via regulation of apoptosis. *Cell Death & Disease* **2019,** *10* (2), 57.

3. Zheng, A.; Yu, J.; Yamamoto, R.; Ose, T.; Tanaka, I.; Yao, M., X-ray structures of eIF5B and the eIF5B-eIF1A complex: the conformational flexibility of eIF5B is restricted on the ribosome by interaction with eIF1A. *Acta Crystallographica Section D* **2014,** *70* (12), 3090-3098.

4. Lee, J. H.; Choi, S. K.; Roll-Mecak, A.; Burley, S. K.; Dever, T. E., Universal conservation in translation initiation revealed by human and archaeal homologs of bacterial translation initiation factor IF2. *Proceedings of the National Academy of Sciences* **1999,** *96* (8), 4342-4347.

5. Jumper, J.; Evans, R.; Pritzel, A.; Green, T.; Figurnov, M.; Ronneberger, O.; Tunyasuvunakool, K.; Bates, R.; Zidek, A.; Potapenko, A.; Bridgland, A.; Meyer, C.; Kohl, S. A. A.; Ballard, A. J.; Cowie, A.; Romera-Paredes, B.; Nikolov, S.; Jain, R.; Adler, J.; Back, T.; Petersen, S.; Reiman, D.; Clancy, E.; Zielinski, M.; Steinegger, M.; Pacholska, M.; Berghammer, T.; Bodenstein, S.; Silver, D.; Vinyals, O.; Senior, A. W.; Kavukcuoglu, K.; Kohli, P.; Hassabis, D., Highly accurate protein structure prediction with AlphaFold. *Nature* **2021,** *596* (7873), 583-589.

6. Borden, K. L., The eukaryotic translation initiation factor eIF4E wears a "cap" for many occasions. *Translation* **2016,** *4* (2), e1220899.

7. Assouline, S.; Culjkovic, B.; Cocolakis, E.; Rousseau, C.; Beslu, N.; Amri, A.; Caplan, S.; Leber, B.; Roy, D. C.; Miller, W. H.; Borden, K. L. B., Molecular targeting of the oncogene eIF4E in acute myeloid leukemia (AML): a proof-of-principle clinical trial with ribavirin. *Blood* **2009,** *114* (2), 257-260.

8. Culjkovic, B.; Borden, K. L., Understanding and Targeting the Eukaryotic Translation Initiation Factor eIF4E in Head and Neck Cancer. *Journal of oncology* **2009,** *2009*, 981679.

9. Borden, K. L. B.; Culjkovic-Kraljacic, B., Ribavirin as an anti-cancer therapy: acute myeloid leukemia and beyond? *Leukemia Lymphoma* **2010,** *51* (10), 1805-1815.

10. Mamane, Y.; Petroulakis, E.; Rong, L.; Yoshida, K.; Ler, L. W.; Sonenberg, N., eIF4E--from translation to transformation. *Oncogene* **2004,** *23* (18), 3172-3179.

11. Batool, A.; Aashaq, S.; Andrabi, K. I., Eukaryotic initiation factor 4E (eIF4E): A recap of the cap-binding protein. *Journal of Cellular Biochemistry* **2019,** *120* (9), 14201-14212.

12. Kleiner, H. E.; Krishnan, P.; Tubbs, J.; Smith, M.; Meschonat, C.; Shi, R.; Lowery-Nordberg, M.; Adegboyega, P.; Unger, M.; Cardelli, J.; Chu, Q.; Mathis, J. M.; Clifford, J.; De Benedetti, A.; Li, B. D., Tissue microarray analysis of eIF4E and its downstream effector proteins in human breast cancer. *Journal of Experimental & Clinical Cancer Research* **2009,** *28* (1), 5.

13. Kentsis, A.; Topisirovic, I.; Culjkovic, B.; Shao, L.; Borden, K. L., Ribavirin suppresses eIF4E-mediated oncogenic transformation by physical mimicry of the 7-methyl guanosine mRNA cap. *Proceedings of the National Academy of Sciences* **2004,** *101* (52), 18105-18110.

14. Tomoo, K.; Shen, X.; Okabe, K.; Nozoe, Y.; Fukuhara, S.; Morino, S.; Ishida, T.; Taniguchi, T.; Hasegawa, H.; Terashima, A.; Sasaki, M.; Katsuya, Y.; Kitamura, K.; Miyoshi, H.; Ishikawa, M.; Miura, K., Crystal structures of 7-methylguanosine 5'-triphosphate (m(7)GTP)- and P(1)-7-methylguanosine-P(3)-adenosine-5',5'-triphosphate (m(7)GpppA)-bound human full-length eukaryotic initiation factor 4E: biological importance of the C-terminal flexible region. *The Biochemical Journal* **2002,** *362* (3), 539-544.

15. Volpon, L.; Osborne, M. J.; Zahreddine, H.; Romeo, A. A.; Borden, K. L., Conformational changes induced in the eukaryotic translation initiation factor eIF4E by a clinically relevant inhibitor, ribavirin triphosphate. *Biochemical and Biophysical Research Communications* **2013,** *434* (3), 614-619.

16. Wan, X.; Yang, T.; Cuesta, A.; Pang, X.; Balius, T. E.; Irwin, J. J.; Shoichet, B. K.; Taunton, J., Discovery of Lysine-Targeted eIF4E Inhibitors through Covalent Docking. *Journal of the American Chemical Society* **2020,** *142* (11), 4960-4964.

17. Wang, S.; Cang, S.; Liu, D., Third-generation inhibitors targeting EGFR T790M mutation in advanced non-small cell lung cancer. *Journal of hematology & oncology* **2016,** *9* (1), 34.

18. Pettinger, J.; Jones, K.; Cheeseman, M. D., Lysine-Targeting Covalent Inhibitors. *Angewandte Chemie International Edition* **2017,** *56* (48), 15200-15209.

19. D'Abronzo, L. S.; Ghosh, P. M., eIF4E Phosphorylation in Prostate Cancer. *Neoplasia* **2018,** *20* (6), 563-573.

20. Zheng, J.; Li, X. Q.; Zhang, C. Y.; Zhang, Y. Q., eIF4E Overexpression Is Associated with Poor Prognoses of Ovarian Cancer. *Analytical Cellular Pathology* **2020,** *2020*, 8984526.

21. Liu, T.; Li, R.; Zhao, H.; Deng, J.; Long, Y.; Shuai, M. T.; Li, Q.; Gu, H.; Chen, Y. Q.; Leng, A. M., eIF4E promotes tumorigenesis and modulates chemosensitivity

to cisplatin in esophageal squamous cell carcinoma. *Oncotarget* **2016,** *7* (41), 66851-66864.

22. Volpon, L.; Osborne, M. J.; Topisirovic, I.; Siddiqui, N.; Borden, K. L. B., Cap-free structure of eIF4E suggests a basis for conformational regulation by its ligands. *Embo Journal* **2006,** *25* (21), 5138-5149.

23. Scheper, G. C.; Proud, C. G., Does phosphorylation of the cap-binding protein eIF4E play a role in translation initiation? *European Journal of Biochemistry* **2002,** *269* (22), 5350-5359.

24. Zuberek, J.; Wyslouch-Cieszynska, A.; Niedzwiecka, A.; Dadlez, M.; Stepinski, J.; Augustyniak, W.; Gingras, A. C.; Zhang, Z.; Burley, S. K.; Sonenberg, N.; Stolarski, R.; Darzynkiewicz, E., Phosphorylation of eIF4E attenuates its interaction with mRNA 5' cap analogs by electrostatic repulsion: intein-mediated protein ligation strategy to obtain phosphorylated protein. *RNA* **2003,** *9* (1), 52-61.

25. Zuberek, J.; Jemielity, J.; Jablonowska, A.; Stepinski, J.; Dadlez, M.; Stolarski, R.; Darzynkiewicz, E., Influence of electric charge variation at residues 209 and 159 on the interaction of eIF4E with the mRNA 5' terminus. *Biochemistry* **2004,** *43* (18), 5370-5379.

26. Leroux, L.-P.; Chaparro, V.; Jaramillo, M., Infection by the Protozoan Parasite Toxoplasma gondii Inhibits Host MNK1/2-eIF4E Axis to Promote Its Survival. *Frontiers in Cellular and Infection Microbiology* **2020,** *10*.

27. Gruner, S.; Peter, D.; Weber, R.; Wohlbold, L.; Chung, M. Y.; Weichenrieder, O.; Valkov, E.; Igreja, C.; Izaurralde, E., The Structures of eIF4E-eIF4G Complexes Reveal an Extended Interface to Regulate Translation Initiation. *Molecular Cell* **2016,** *64* (3), 467-479.

28. Wang, Z. G.; Zheng, H.; Gao, W.; Han, J.; Cao, J. Z.; Yang, Y.; Li, S.; Gao, R.; Liu, H.; Pan, Z. Y.; Fu, S. Y.; Gu, F. M.; Xing, H.; Ni, J. S.; Yan, H. L.; Ren, H.; Zhou, W. P., eIF5B increases ASAP1 expression to promote HCC proliferation and invasion. *Oncotarget* **2016,** *7* (38), 62327-62339.

29. Suresh, S.; Chen, B.; Zhu, J.; Golden, R. J.; Lu, C.; Evers, B. M.; Novaresi, N.; Smith, B.; Zhan, X.; Schmid, V.; Jun, S.; Karacz, C. M.; Peyton, M.; Zhong, L.; Wen, Z.; Sathe, A. A.; Xing, C.; Behrens, C.; Wistuba, I. I.; Xiao, G.; Xie, Y.; Fu, Y.-X.; Minna, J. D.; Mendell, J. T.; O'Donnell, K. A., eIF5B drives integrated stress response-dependent translation of PD-L1 in lung cancer. *Nature Cancer* **2020,** *1* (5), 533-545.

30. Li, Q.; Xiao, M.; Shi, Y.; Hu, J.; Bi, T.; Wang, C.; Yan, L.; Li, X., eIF5B regulates the expression of PD-L1 in prostate cancer cells by interacting with Wig1. *BMC Cancer* **2021,** *21* (1), 1022.

31. Wu, C. Y.; Wang, D. H.; Wang, X.; Dixon, S. M.; Meng, L.; Ahadi, S.; Enter, D. H.; Chen, C. Y.; Kato, J.; Leon, L. J.; Ramirez, L. M.; Maeda, Y.; Reis, C. F.;

Ribeiro, B.; Weems, B.; Kung, H. J.; Lam, K. S., Rapid Discovery of Functional Small Molecule Ligands against Proteomic Targets through Library-Against-Library Screening. *ACS Combinatorial Science* **2016,** *18* (6), 320-329.

32. Wang, J.; Wang, J.; Shin, B. S.; Kim, J. R.; Dever, T. E.; Puglisi, J. D.; Fernandez, I. S., Structural basis for the transition from translation initiation to elongation by an 80S-eIF5B complex. *Nature Communications* **2020,** *11* (1), 5003.

33. Pestova, T. V.; Lomakin, I. B.; Lee, J. H.; Choi, S. K.; Dever, T. E.; Hellen, C. U., The joining of ribosomal subunits in eukaryotes requires eIF5B. *Nature* **2000,** *403* (6767), 332-5.

34. Wang, J.; Wang, J.; Shin, B.-S.; Kim, J.-R.; Dever, T. E.; Puglisi, J. D.; Fernández, I. S., Structural basis for the transition from translation initiation to elongation by an 80S-eIF5B complex. *Nature Communications* **2020,** *11* (1), 5003.

35. Zheng, X.; Gan, L.; Wang, E.; Wang, J., Pocket-based drug design: exploring pocket space. *The AAPS Journal* **2013,** *15* (1), 228-241.

36. Borrel, A.; Regad, L.; Xhaard, H.; Petitjean, M.; Camproux, A.-C., PockDrug: A Model for Predicting Pocket Druggability That Overcomes Pocket Estimation Uncertainties. *Journal of Chemical Information and Modeling* **2015,** *55* (4), 882-895.

37. Zhang, Z.; Li, Y.; Lin, B.; Schroeder, M.; Huang, B., Identification of cavities on protein surface using multiple computational approaches for drug binding site prediction. *Bioinformatics* **2011,** *27* (15), 2083-8.

38. Thakor, N.; Holcik, M., IRES-mediated translation of cellular messenger RNA operates in eIF2alpha- independent manner during stress. *Nucleic Acids Research* **2012,** *40* (2), 541-552.

39. Furic, L.; Rong, L. W.; Larsson, O.; Koumakpayi, I. H.; Yoshida, K.; Brueschke, A.; Petroulakis, E.; Robichaud, N.; Pollak, M.; Gaboury, L. A.; Pandolfi, P. P.; Saad, F.; Sonenberg, N., eIF4E phosphorylation promotes tumorigenesis and is associated with prostate cancer progression. *Proceedings of the National Academy of Sciences* **2010,** *107* (32), 14134-14139.

40. Yoshizawa, A.; Fukuoka, J.; Shimizu, S.; Shilo, K.; Franks, T. J.; Hewitt, S. M.; Fujii, T.; Cordon-Cardo, C.; Jen, J.; Travis, W. D., Overexpression of Phospho-eIF4E Is Associated with Survival through AKT Pathway in Non-Small Cell Lung Cancer. *Clinical Cancer Research* **2010,** *16* (1), 240-248.

Appendix A: Supplementary information for Chapter 2:

Interactions of Eukaryotic Translation Initiator Factor 5B (eIF5B) with RTP and LWW31: A Combined in cellulo and in silico Investigation

Figures A.1 – A.13 and Tables A.1 – A.8

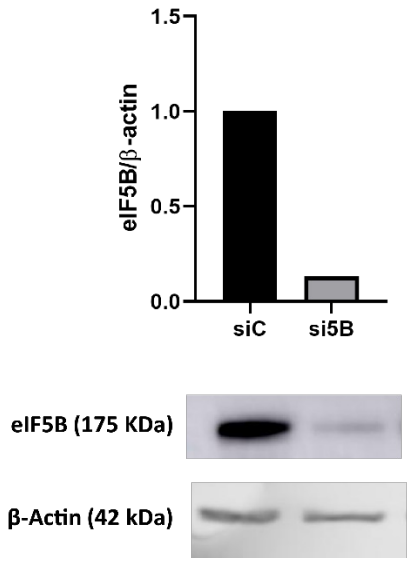

Figure A.1 Levels of eIF5B in siC and si5B treated U343 cells. siC and si5B were normalized over β-actin.

```
IF2P_HUMAN       594 DSDDDRTKEERAYDKAKRRIEKRRLEHSKNVNTEKLRAPIICVLGHVDTG    643
                                                 |.:.|.:.||:||.|:|||||||
IF2P_YEAST       395 --------------------------SASPNKKDLRSPICCILGHVDTG    417

IF2P_HUMAN       644 KTKILDKLRHTHVQDGEAGGITQQIGATNVPLEAINEQTKMIKNFDRENV    693
                     |||:|||:|.|:||.||||||||||||..|::||..:||::..::::..
IF2P_YEAST       418 KTKLLDKIRQTNVQGGEAGGITQQIGATYFPIDAIKAKTKVMAEYEKQTF    467

IF2P_HUMAN       694 RIPGMLIIDTPGHESFSNLRNRGSSLCDIAILVVDIMHGLEPQTIESINL    743
                     .:||:|:|||||||||||||:||||||:||||||.|||||||.|||||.|
IF2P_YEAST       468 DVPGLLVIDTPGHESFSNLRSRGSSLCNIAILVIDIMHGLEQQTIESIKL    517

IF2P_HUMAN       744 LKSKKCPFIVALNKIDRLYDWKKSPDSDVAATLKKQKKNTKDEFEERAKA    793
                     |:.:|.||:|||||||||||||..|::....:..||.:..::||:.|...
IF2P_YEAST       518 LRDRKAPFVVALNKIDRLYDWKAIPNNSFRDSFAKQSRAVQEEFQSRYSK    567

IF2P_HUMAN       794 IIVEFAQQGLNAALFYENKDPRTFVSLVPTSAHTGDGMGSLIYLLVELTQ    843
                     |.:|.|:||||:.|:::||:...:||:|||||.||:|:..|::||:||||
IF2P_YEAST       568 IQLELAEQGLNSELYFQNKNMSKYVSIVPTSAVTGEGVPDLLWLLLELTQ    617

IF2P_HUMAN       844 TMLSKRLAHCEELRAQVMEVKALPGMGTTIDVILINGRLKEGDTIIVPGV    893
                     ..:||:|.:...:.|.::|||.:.|.|||||||.||.|:|||.|::.|:
IF2P_YEAST       618 KRMSKQLMYLSHVEATILEVKVVEGFGTTIDVILSNGYLREGDRIVLCGM    667

IF2P_HUMAN       894 EGPIVTQIRGLLLPPPMKELRVKNQYEKHKEVEAAQGVKILGKDLEKTLA    943
                     .|||||.||.||.|.|::|||:|::|..||||:||.||||...||||.::
IF2P_YEAST       668 NGPIVTNIRALLTPQPLRELRLKSEYVHHKEVKAALGVKIAANDLEKAVS    717

IF2P_HUMAN       944 GLPLLVAYKEDEIPVLKDELIHELKQTLNAIKLEEKGVYVQASTLGSLEA    993
                     |..|||...||:...|.|:::.:|...|:::....|||.||||||||||
IF2P_YEAST       718 GSRLLVVGPEDDEDELMDDVMDDLTGLLDSVDTTGKGVVVQASTLGSLEA    767

IF2P_HUMAN       994 LLEFLKTSEVPYAGINIGPVHKKDVMKASVMLEHDPQYAVILAFDVRIER   1043
                     ||:|||..::|...|.:|||:|:||||||.|||..|:|||:|.|||:::
IF2P_YEAST       768 LLDFLKDMKIPVMSIGLGPVYKRDVMKASTMLEKAPEYAVMLCFDVKVDK    817

IF2P_HUMAN      1044 DAQEMADSLGVRIFSAEIIYHLFDAFTKYRQDYKKQKQEEFKHIAVFPCK   1093
                     :|::.|:..|::||:|::|||||||:||.|::...:::::::|...|:|||.
IF2P_YEAST       818 EAEQYAEQEGIKIFNADVIYHLFDSFTAYQEKLLEERRKDFLDYAIFPCV    867

IF2P_HUMAN      1094 IKILPQYIFNSRDPIVMGVTVEAGQVKQGTPMC-------VPSKNFVDIG   1136
                     ::.|  .|.|.|.|:::||.|..|.::.|||:|       ...:..:.:|
IF2P_YEAST       868 LQTL--QIINKRGPMIIGVDVLEGTLRVGTPICAVKTDPTTKERQTLILG    915

IF2P_HUMAN      1137 IVTSIEINHKQVDVAKKGQE---VCVKIEPIPGESPKMFGRHFEATDILV   1183
                     .|.|:||||:.|...||||.   |.|::|...|:.| ::|||.:..|.|.
IF2P_YEAST       916 KVISLEINHQPVQEVKKGQTAAGVAVRLEDPSGQQP-IWGRHVDENDTLY    964

IF2P_HUMAN      1184 SKISRQSIDALKD-WFRDEMQKSDWQLIVELKKVFEII   1220
                     |.:||:|||.||| .|||::.:|||.|:.:||.||.|.
IF2P_YEAST       965 SLVSRRSIDTLKDKAFRDQVARSDWLLLKKLKVVFGIE   1002
```

Figure A.2 Pairwise alignment of human and yeast eIF5B using BLOSUM62 matrix. The quality of alignment is represented as a vertical "|", ":" and ".". "|" indicates fully conserved residue, ":" indicates strong similarity in properties, and "." indicates lower similar properties, and gaps are regions of no similarities.

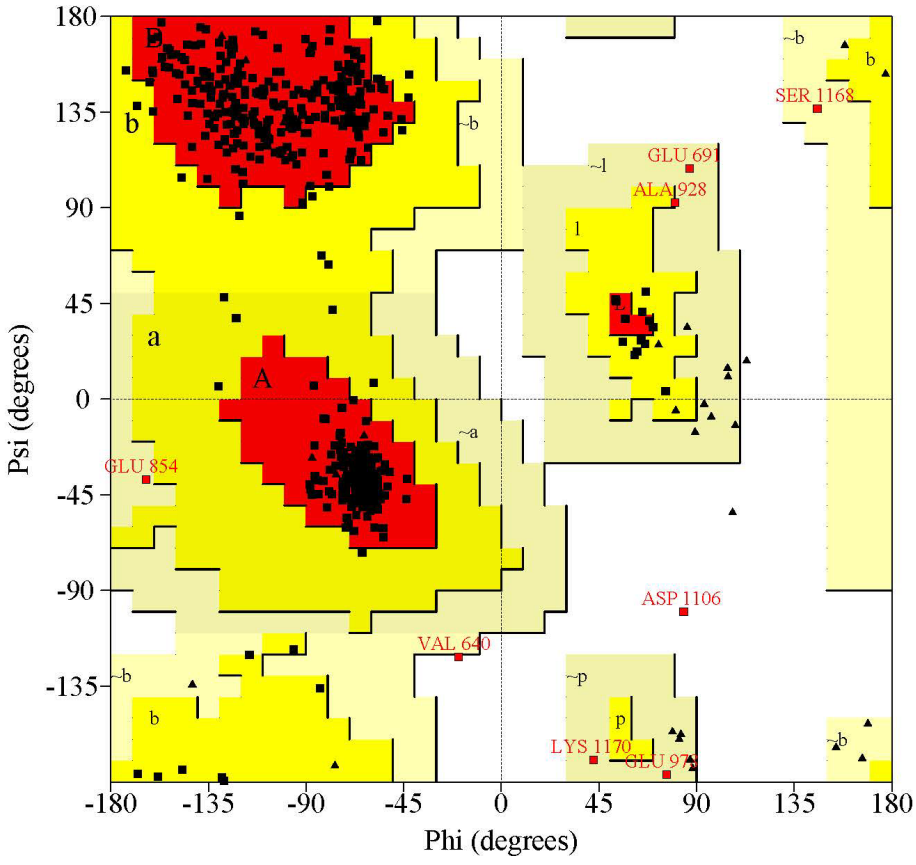

Plot statistics

Residues in most favoured regions [A,B,L]	481	91.4%
Residues in additional allowed regions [a,b,l,p]	37	7.0%
Residues in generously allowed regions [~a,~b,~l,~p]	6	1.1%
Residues in disallowed regions	2	0.4%
Number of non-glycine and non-proline residues	526	100.0%
Number of end-residues (excl. Gly and Pro)	2	
Number of glycine residues (shown as triangles)	36	
Number of proline residues	28	
Total number of residues	592	

Based on an analysis of 118 structures of resolution of at least 2.0 Angstroms and R-factor no greater than 20%, a good quality model would be expected to have over 90% in the most favoured regions.

Figure A.3 Ramachandran plot of human eIF5B model before refinement and loop remodeling.

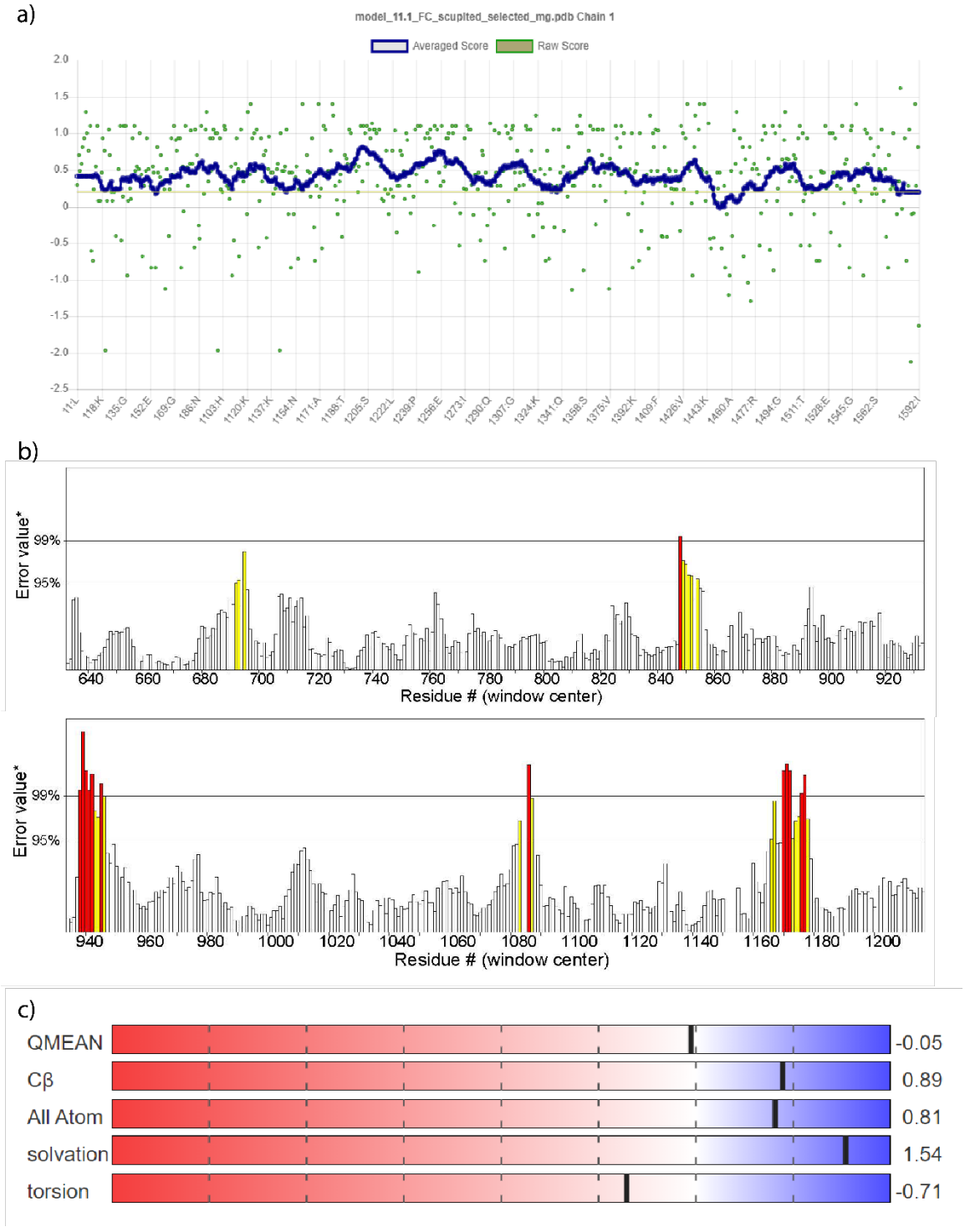

Figure A.4 a) Verify3D results show 95.95% of residues have average 3D-1D score ≥0.2, with structures requiring at least 80% within the range specified to pass. b) ERRAT analysis gave the model 94.43%. c) Quality estimate for the model generated gives values from negative to positive, with 0 being a native-like structure, a positive value being better than the experimentally derived structure, and any value below –4 considered to be a bad structure.

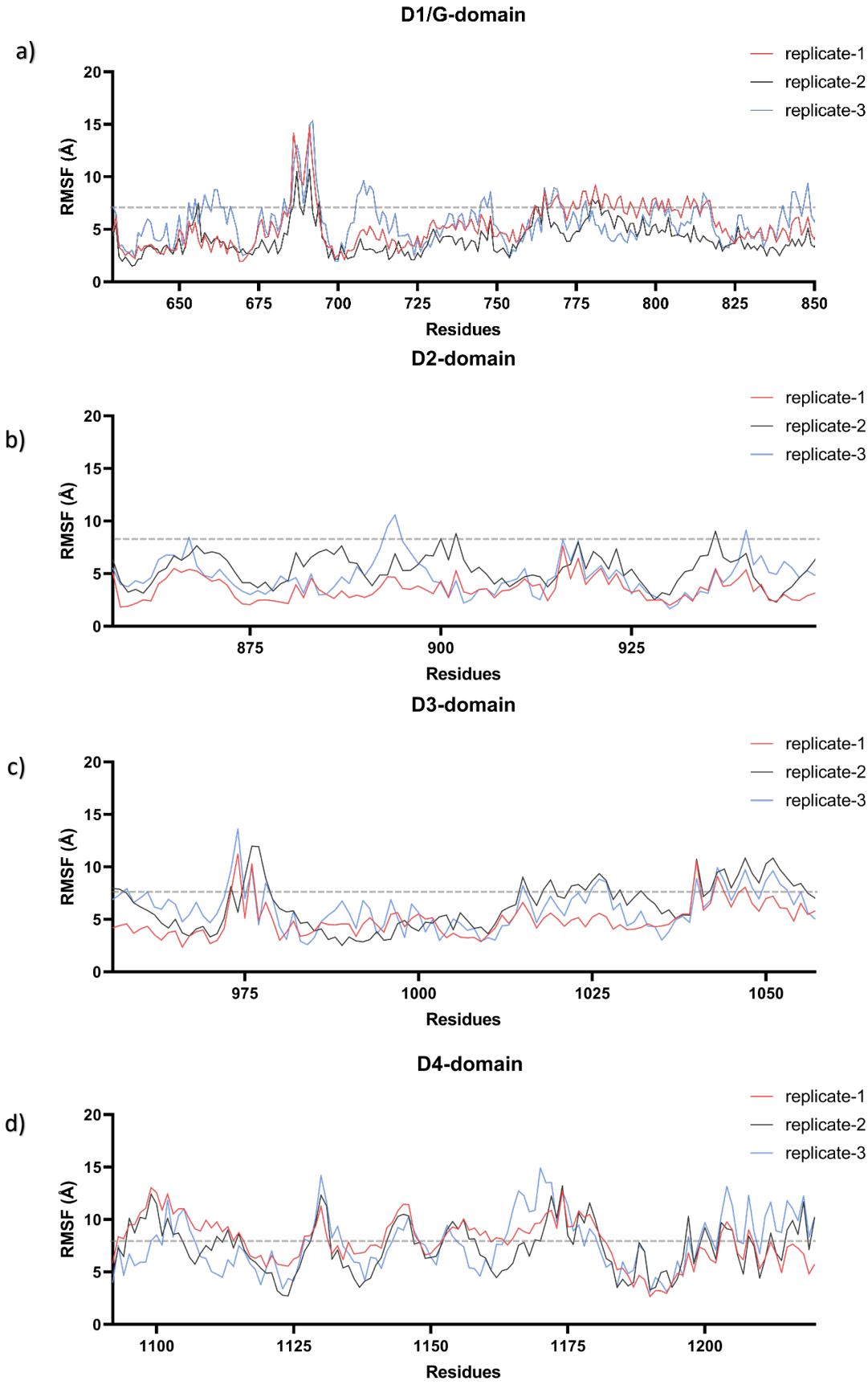
a)
D1/G-domain
replicate-1
replicate-2
replicate-3
RMSF (Å)
Residues
b)
D2-domain
c)
D3-domain
d)
D4-domain

Figure A.5 Per-residue RMSF for a) D1, b) D2, c) D3, and d) D4 of eIF5B.

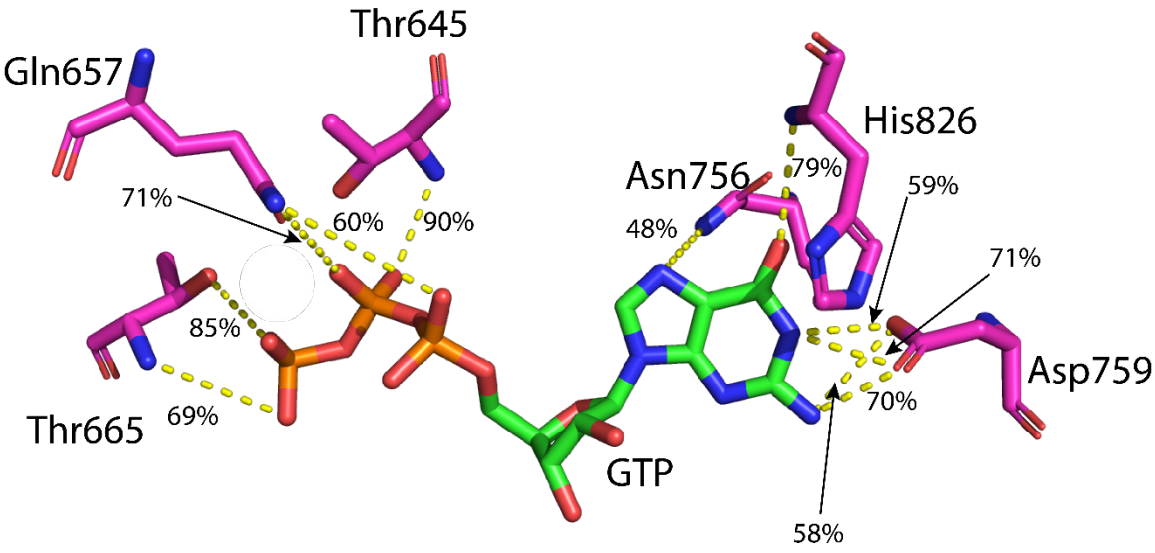

Figure A.6 Percentage occupancy of hydrogen bonds between eIF5B and GTP.

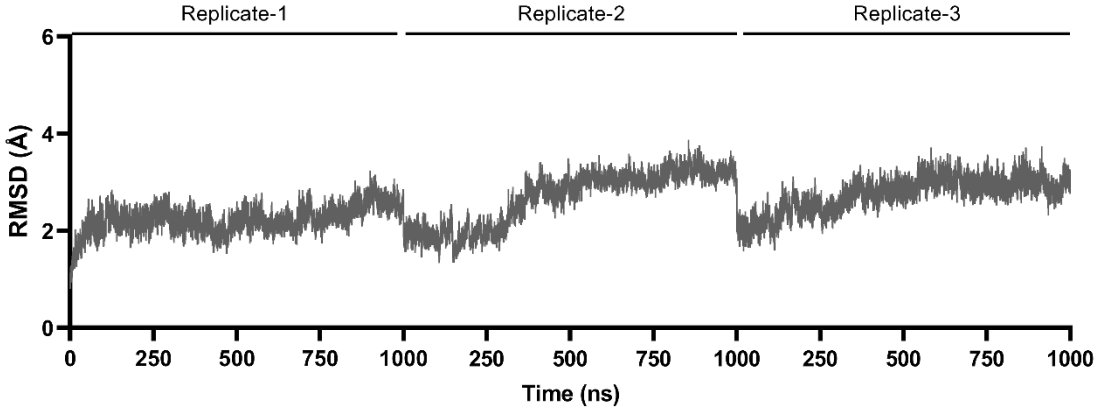

Figure A.7 Backbone RMSD of the apo-eIF5B G-domain with respect to the initial model (prior to minimization) in the absence of GTP.

Figure A.8 Superimposition of yeast eFI5B (grey) bound to the ribosome and the initial AF eIF5B-GTP model (prior to minimization; brick red).

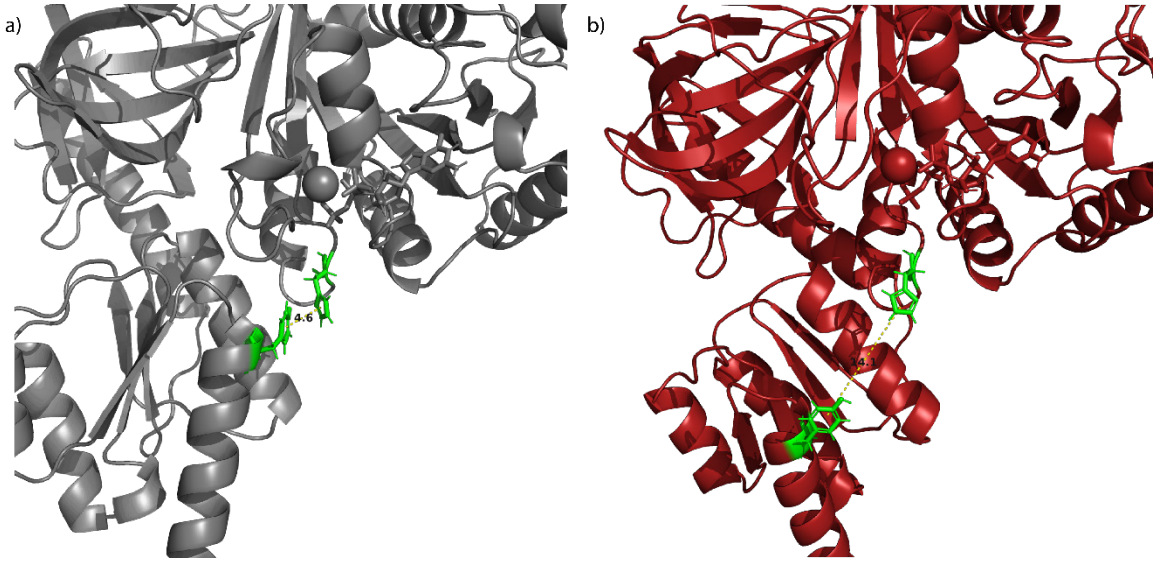

Figure A.9 Different conformations of AF eIF5B-GTP, a) showing distance between His706 and Tyr1063 (green) in the initial model (prior to minimization), and b) the final structure post MD simulation.

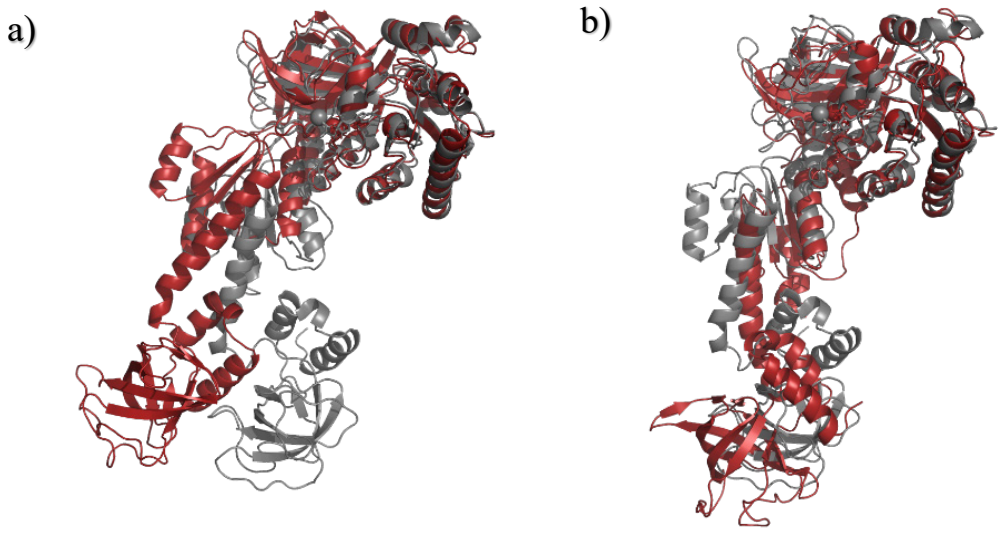

Figure A.10 Superimposition of AF eIF5B-GTP model (red) with representative structure of MOD eIF5B-GTP (grey), a) prior to minimization, and b) after MD simulation.

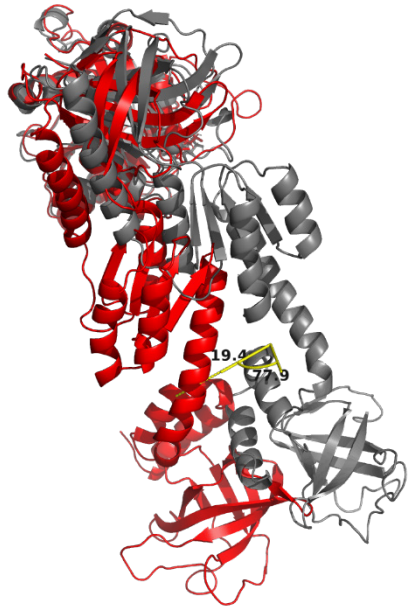

Figure A.11 Initial (grey) and final (brick red) structures of the AF eIF5B-GTP model aligned through D1. D3 and D4 rotated by ~78° upon simulation, showing a displacement of ~19 Å.

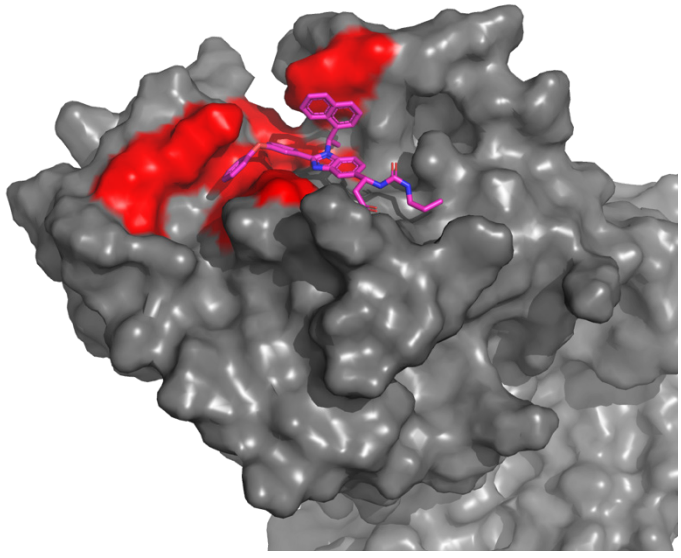

Figure A.12 Surface of eIF5B with LWW31 bound, showing the Pockdrug predicted pocket (surface colored in red).

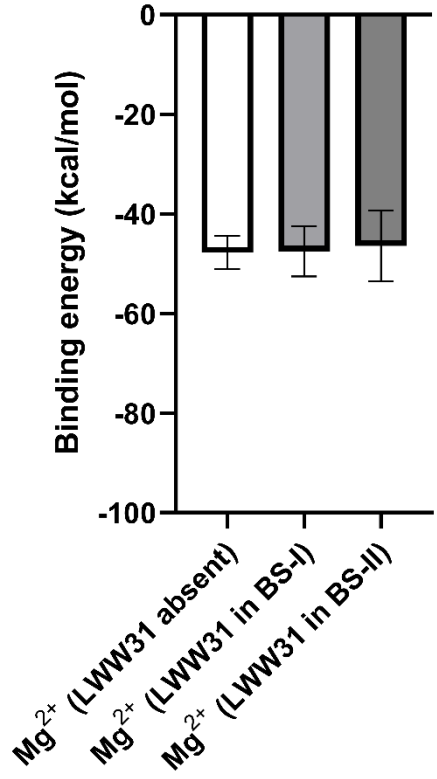

Figure A.13 Binding free energy of GTP to Mg2+ when LWW31 is absent, or present in BS-I or BS-II of eIF5B.

Table A.1 List of antibodies used for western blotting.

Company Antibody	Target	Catalogue number
Abcam	Secondary: Goat anti-rabbit-HRP conjugate	ab97051
Cell Signalling Tech.	Bcl-xL	2762
Bio-Rad	β-actin (hFAB Rhodamine)	12004163
Abcam	cIAP1	ab108361
	cIAP2	ab137393
	eIF1A	ab177939
	Nrf2	ab71890
ProteinTech	eIF5B	13527-1-AP

Table A.2 Average RMSD and associated standard deviation (SD) for individual replicates and across all replicates with respect to initial refined MOD eIF5B-GTP model.

	eIF5B		GTP	
	Mean (Å)	**SD**	**Mean (Å)**	**SD**
Replicate-1	7.6	1.2	0.8	0.6
Replicate-2	10.3	1.4	0.7	0.3
Replicate-3	9.2	1.2	0.4	0.1
All replicates	9.0	1.7	0.6	0.4

Table A.3 Average distance between Mg^{2+} and phosphate oxygens of GTP for individual replicates and across all replicates.

	Mg^{2+}–O1B distance[a]		Mg^{2+}–O1G distance[b]	
	Mean (Å)	**SD**	**Mean (Å)**	**SD**
Replicate-1	1.91	0.05	1.89	0.04
Replicate-2	1.91	0.04	1.88	0.04
Replicate-3	1.92	0.05	1.88	0.04
All replicates	1.91	0.05	1.88	0.04

[a]Average distance between β-phosphate oxygen O1B and Mg^{2+} throughout the simulation.
[b]Average distance ϒ-phosphate oxygen O1G and Mg^{2+}.

Table A.4 Different non-covalent interactions of LWW31 with eIF5B in BS-I.

	Hydrophobic Interactions		
Index	Residue Name	Residue No.	Distance (Å)
1	Ile	685	3.9
2	Phe	688	3.4

3	Phe	688	3.4
4	Asp	689	3.7
5	Ala	774	4.0
6	Tyr	809	4.0
7	Pro	814	3.8
8	Tyr	836	3.9
9	Glu	840	3.4
	Hydrogen Bonding		
Index	Residue Name	Residue No.	Distance (Å)
1	Glu	810	3.0
2	Lys	812	3.7

Table A.5 Different non-covalent interactions of LWW31 with eIF5B in BS-II.

	Hydrophobic Interactions		
Index	Residue Name	Residue No.	Distance (Å)
1	Arg	849	3.6
2	Glu	962	3.7
	Hydrogen Bonding		
Index	Residue Name	Residue No.	Distance (Å)
1	Ala	858	3.6
2	Ala	858	3.1

Table A.6 RTP atom types and partial charges.

Atom Name	Atom Type	Charge
P1	P5	1.13861
P2	P5	1.405929
P3	P5	1.204083
C1	C3	0.022289
O1	OS	-0.43272
C2	C3	0.047778
O2	OS	-0.27228
C3	C3	0.180382
O3	OH	-0.64476
C4	C3	0.054354
O4	OH	-0.58593
C5	C3	0.002211
O5	O	-0.77469
O6	O	-0.87143

O7	O	-0.93099
O8	O	-0.77469
O9	O	-0.87143
O10	O	-0.93099
O11	OS	-0.57885
O12	OS	-0.56863
O13	O	-0.93099
N1	NA	0.292979
C6	CC	0.293015
H1	H5	0.176919
C7	CC	0.263295
H2	HN	0.383589
N2	ND	-0.51458
N3	NA	-0.31562
C8	C	0.712123
O14	O	-0.57132
N4	N	-0.86608
H3	HN	0.401963
H4	HN	0.401963
H5	H2	0.182404
H6	H1	0.071375
H7	HO	0.415879
H8	HO	0.409942
H9	H1	0.082266
H10	H1	0.171485
H11	H1	0.060563
H12	H1	0.060563

Table A.7 GTP atom type and partial charges

O1G	O3	-0.9526
PG	P	1.2650
O2G	O3	-0.9526
O3G	O3	-0.9526
O3B	OS	-0.5322
PB	P	1.3852
O1B	O2	-0.8894
O2B	O2	-0.8894
O3A	OS	-0.5689
PA	P	1.2532

O1A	O2	-0.8799
O2A	O2	-0.8799
O5'	OS	-0.5987
C5'	CT	0.0558
H06	H1	0.0679
H04	H1	0.0679
C4'	CT	0.1065
H4'	H1	0.1174
O4'	OS	-0.3548
C1'	CT	0.0191
H1'	H2	0.2006
N9	N*	0.0492
C8	CK	0.1374
H8	H5	0.1640
N7	NB	-0.5709
C5	CB	0.1744
C6	C	0.4770
O6	O	-0.5597
N1	NA	-0.4787
H1	H	0.3424
C2	CA	0.7657
N2	N2	-0.9672
H21	H	0.4364
H22	H	0.4364
N3	NC	-0.6323
C4	CB	0.1222
C3'	CT	0.2022
O3'	OH	-0.6541
H3T	HO	0.4376
H3'	H1	0.0615
C2'	CT	0.0670
H05	H1	0.0972
O2'	OH	-0.6139
H07	HO	0.4186

Table A.8 LWW31 atom types and partial charges.

Atom Name	Atom Type	Charge
C1	CA	0.40476
C2	CA	-0.075

C3	CA	-0.1977
C4	CA	-0.2061
C5	CA	-0.0808
C6	CA	-0.1963
H1	HA	0.17166
H2	HA	0.15043
H3	HA	0.10776
N1	NA	-0.0235
N2	NC	-0.5931
C7	CA	-0.0157
C8	CA	-0.105
C9	CA	-0.0444
C10	CA	-0.2355
H4	HA	0.14461
C11	CA	0.10573
H5	HA	0.14286
C12	CA	-0.091
H6	HA	0.16879
C13	CD	0.25738
C14	CA	0.15234
C15	CA	-0.0922
C16	CA	-0.0922
C17	CA	-0.1964
H7	HA	0.12668
C18	CA	-0.1964
H8	HA	0.12668
C19	CA	-0.1258
H9	HA	0.15846
H10	HA	0.15846
H11	HA	0.14049
O1	OS	-0.2719
C20	C3	0.06525
H12	H1	0.10005
C21	C3	-0.0681
H13	HC	0.03128
H14	HC	0.03128
C22	C	0.67868
N3	N	-0.0661
H15	HN	0.20714
C23	C	0.43259

O2	O	-0.5833
N4	N	-0.6282
H16	HN	0.38527
C24	C3	0.12389
H17	H1	0.02347
H18	H1	0.02347
C25	C3	0.0715
H19	HC	-0.014
H20	HC	-0.014
C26	C3	-0.0499
H21	HC	0.00979
H22	HC	0.00979
H23	HC	0.00979
O3	O	-0.5681
N5	N	-0.9277
H24	HN	0.3975
H25	HN	0.3975
C27	C3	0.02124
H26	H1	0.09317
C28	CA	-0.0109
C29	CA	0.03578
C30	CA	-0.1061
C31	CA	-0.085
C32	CA	0.07072
C33	CA	-0.2242
H27	HA	0.14046
C34	CA	-0.1489
H28	HA	0.06287
C35	CA	-0.1675
C36	CA	-0.1554
H29	HA	0.16259
C37	CA	-0.1663
H30	HA	0.14918
H31	HA	0.13971
H32	HA	0.14659
H33	HA	0.15297
C38	C3	-0.215
H34	HC	0.06868
H35	HC	0.06868
H36	HC	0.06868

H37	HA	0.14109

Appendix B: Supplementary information for Chapter 3:

The Interactions of Eukaryotic Translation Initiation Factor 4E (eIF4E) with m^7GTP, RBV, and RTP: A MD Study

Figures B.1 – B.5 and Tables B.1 – B.9

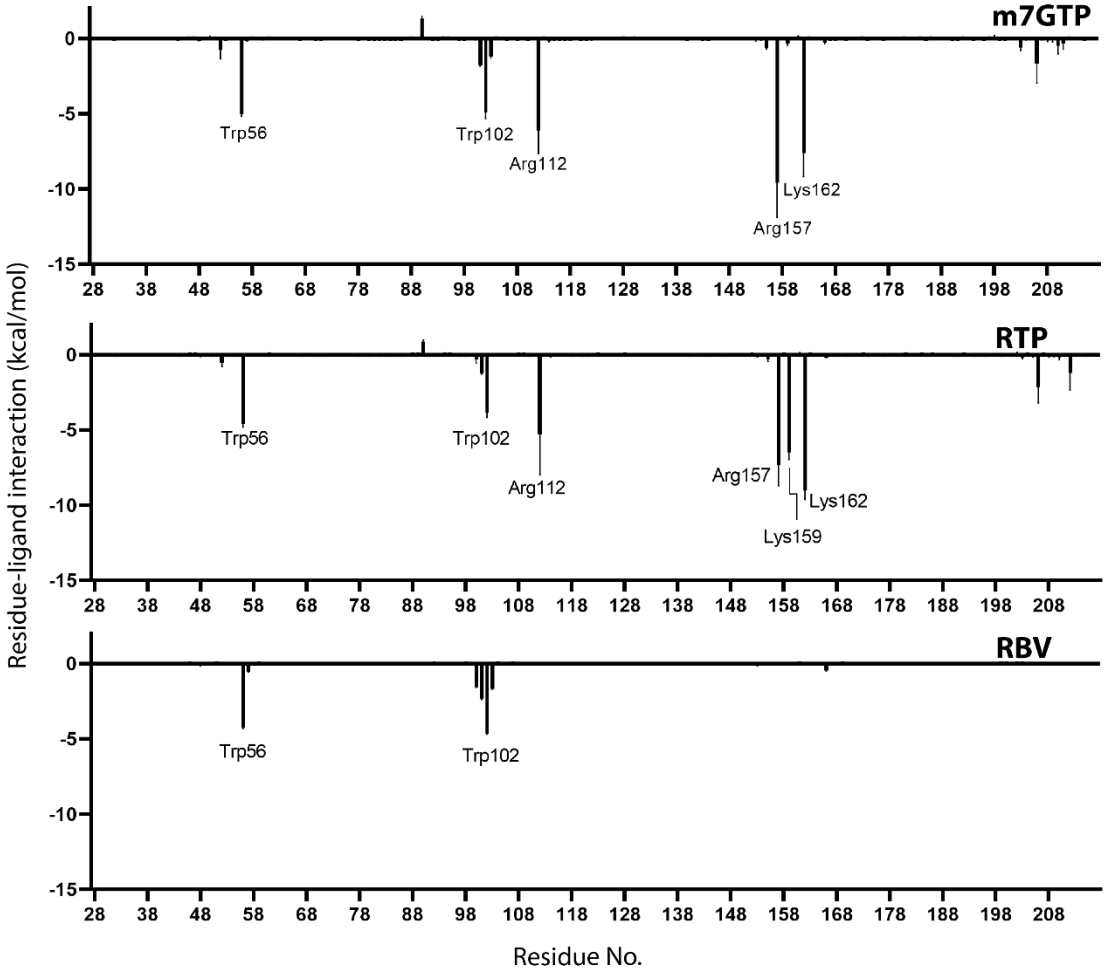

Figure B.1 Per-residue decomposition of the binding free energies for the eIF4E-m^{7}GTP, eIF4E-RTP, and eIF4E-RBV complexes.

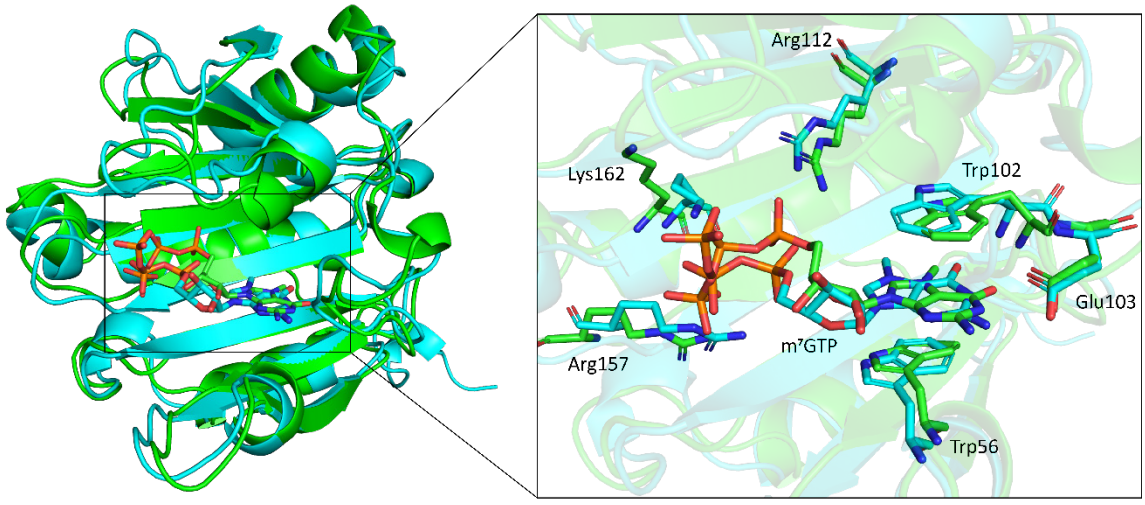

Figure B.2 Overlay of the eIF4E cap-binding site heavy atoms in the crystallographic (PDB ID: 1IPC; blue) and MD representative (green) structures.

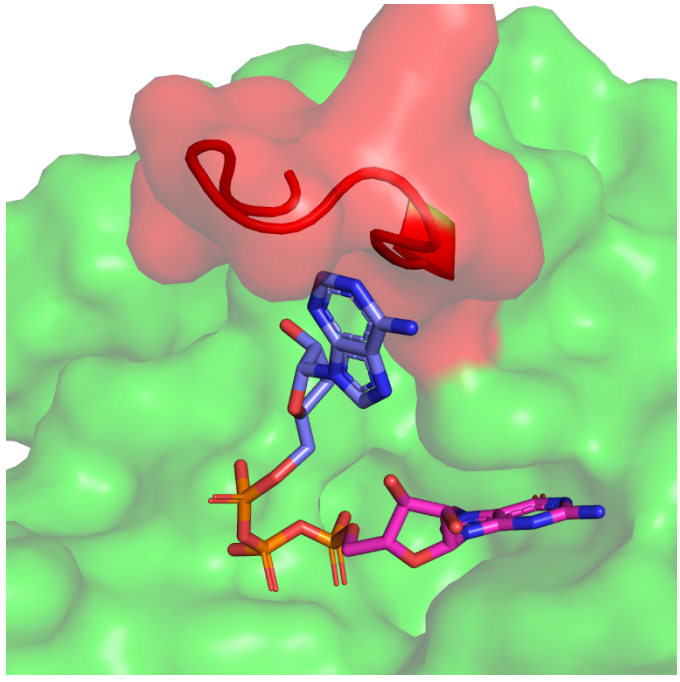

Figure B.3 X-ray crystal structure of the eIF4E-m^{7}GpppA complex (PDB ID: 1IPB), highlighting adenosine (violet) of m^{7}GpppA interacting with the C-terminus region (red) of eIF4E.

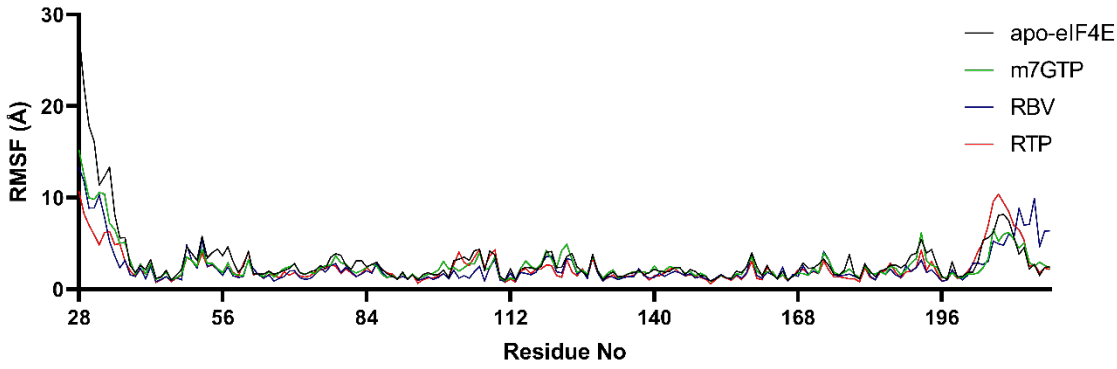

Figure B.4 Per-residue RMSF analysis of eIF4E in the apo form and in complex with m^7GTP, RBV, or RTP.

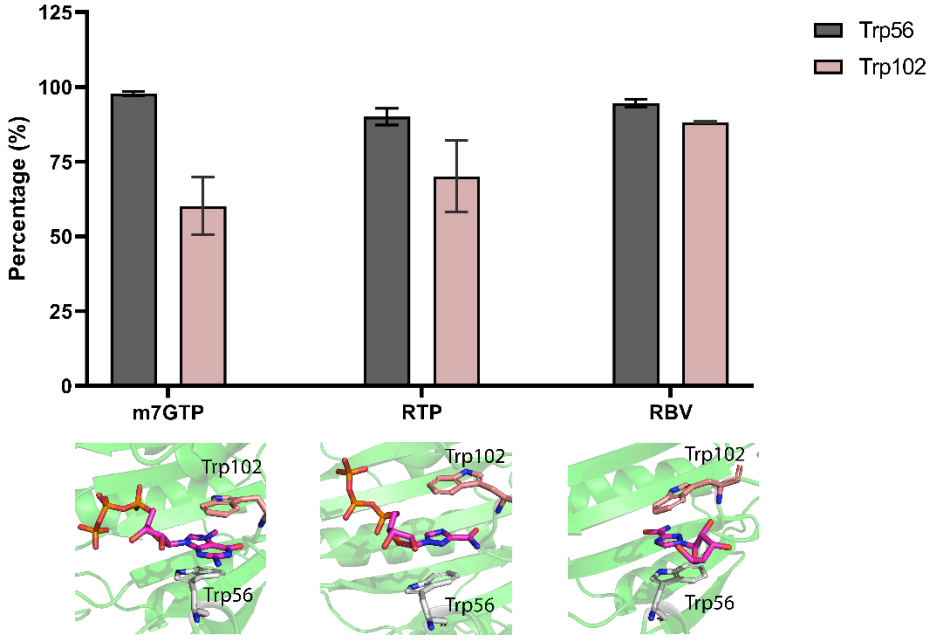

Figure B.5 Stacking occupancies between Trp56 (grey) or Trp102 (pastel pink) of eIF4E and m^7GTP, RTP or RBV.

Table B.1 Average RMSD (Å) and associated standard deviation (SD) for individual and across all replicates of the apo-eIF4E and eIF4E-m^{7}GTP systems.

			eIF4E-m^{7}GTP complex			
	Apo-eIF4E[a]		eIF4E[a]		m^{7}GTP[b]	
	Mean (Å)	SD	Mean (Å)	SD	Mean (Å)	SD
Replicate-1	4.5	0.7	4.3	0.4	1.9	0.4
Replicate-2	3.3	0.6	4.5	0.9	1.6	0.3
Replicate-3	4.3	0.5	3.4	0.5	1.6	0.4
All replicates	4.0	0.8	4.1	0.8	1.7	0.4

[a]RMSD of the eIF4E backbone is calculated with respect to the eIF4E-m^{7}GTP crystal structure (PDB: 1IPC). [b]RMSD of the GTP heavy atoms is calculated with respect eIF4E-m^{7}GTP crystal structure (PDB: 1IPC).

Table B.2 Summary of the hydrogen bonds between the polyphosphate tail (A, B, and G) of m^{7}GTP and Arg112, Arg157, or Lys162.

Atom Name	A[a,b]		B[a,b]		G[a,b]		
	O1A	O2A	O1B	O2B	O1G	O2G	O3G
Arg112(NH1)	22.7	29.0	12.0	5.0	0.0	0.0	0.0
Arg112(NH2)	35.6	6.7	5.2	2.2	0.0	0.0	0.0
Arg157(NE)	1.9	0.9	3.0	3.4	30.9	28.7	27.9
Arg157(NH2)	2.1	1.8	3.5	3.2	30.7	29.2	31.9
Lys162(NZ)	12.8	1.4	15.9	3.8	4.8	2.5	4.2

[a]Percentage occupancy of hydrogen bonds, evaluated using a distance and angle cut off of 3.4 Å and 120^o, respectively. [b]Refer to the Figure 3.5 in the main text for hydrogen bond details.

Table B.3 Average RMSD (Å) and associated standard deviation (SD) for individual and across all replicates with respect to the initial eIF4E-RTP model (prior to minimization).

	eIF4E[a]		RTP[b]	
	Mean (Å)	SD	Mean (Å)	SD
Replicate-1	4.4	0.3	2.3	0.4
Replicate-2	4.3	0.2	2.4	0.5
Replicate-3	4.4	0.5	2.5	0.5
All replicates	4.4	0.4	2.4	0.5

[a]RMSD is calculated for the backbone and heavy atoms of eIF4E and RTP, respectively.

Table B.4 Percentage occupancies of hydrogen bonds formed between the polyphosphate tail (A, B, and G) of RTP and Arg112, Arg157, Lys159, or Lys162 of eIF4E.

Atom Name	A[a,b]		B[a,b]		G[a,b]		
	O1A	O2A	O1B	O2B	O1G	O2G	O3G
Arg112(NH1)	4.9	10.0	2.2	3.3	9.9	7.9	10.5
Arg112(NH2)	9.5	5.0	2.6	1.5	7.5	8.7	9.7
Arg157(NE)	8.4	10.5	19.6	15.5	5.6	5.8	5.5
Arg157(NH2)	12.6	36.3	3.4	7.9	6.1	6.1	5.1
Lys159(NZ)	1.3	0.5	7.8	9.1	30.9	33.1	32.4
Lys162(NZ)	2.9	5.1	12.0	29.5	26.0	26.0	26.9

[a]Percentage occupancy of hydrogen bonds, evaluated using a distance and angle cut off of 3.4 Å and 120°, respectively. [b]Refer to Figure 3.9 in the main text for hydrogen bond details.

Table B.5 Individual energy terms and the total binding free energy (kcal/mol) for m^7GTP, RTP and RBV binding in the cap-binding site of eIF4E.

Protein	**eIF4E**		
Ligand	**m^7GTP**	**RTP**	**RBV**
ΔE_{vdW}	–30.65 ± 0.52	–21.38 ± 1.08	–19.39 ± 0.25
ΔE_{elec}	–669.54 ± 37.41	–810.06 ± 5.08	–47.86 ± 1.73
ΔG_{GB}	674.15 ± 34.44	816.03 ± 6.63	52.54 ± 1.70
ΔG_{SA}	–4.25 ± 0.16	–4.08 ± 0.06	–3.00 ± 0.03
ΔE_{nonpol}	–700.20 ± 37.85	–831.44 ± 5.53	–67.26 ± 1.67
ΔE_{polar}	669.91 ± 34.30	811.95 ± 6.62	49.54 ± 1.70
ΔG_{bind}	–30.29 ± 3.89	–19.48 ± 1.09	–17.72 ± 0.27

Table B.6 Average RMSD (Å) and associated standard deviation (SD) for individual replicates and across all replicates with respect to the initial eIF4E-RBV model (prior to minimization).

	eIF4E[a]		RBV[a]	
	Mean (Å)	SD	Mean (Å)	SD
Replicate-1	3.4	0.3	0.3	0.1
Replicate-2	3.7	0.4	0.3	0.2
Replicate-3	3.3	0.3	0.3	0.1
All replicates	3.5	0.4	0.3	0.2

[a]RMSD is calculated for the backbone and heavy atoms of eIF4E and RBV, respectively.

Table B.7 m^7GTP atom types and partial charges.

Atom Name	Atom Type	Charge
C1	C3	-0.0222
P1	P5	1.0053
P2	P5	1.1822
P3	P5	1.1713
C2	C3	0.0711
O1	OS	-0.3796
C3	C3	0.1239
O2	OS	-0.4873
C4	C3	0.2113
O3	OH	-0.6801
C5	C3	0.1497
O4	OH	-0.7121
C6	C3	0.2803
N1	N	-0.3948
O5	O	-0.7743
O6	O	-0.8357
O7	O	-0.8729
C7	CC	0.6906
N2	NH	-0.9756
O8	O	-0.7743
O9	O	-0.8357
O10	O	-0.8729
N3	ND	-0.5409
O11	OS	-0.4370
O12	OS	-0.4960
O13	O	-0.8729

C8	CD	0.1721
C9	CC	-0.0234
C10	C	0.4588
O14	O	-0.5692
N4	NA	-0.0309
C11	CC	0.0754
N5	NA	0.0044
H1	H5	0.2555
H2	HN	0.3110
H3	H1	0.0800
H4	H1	0.0800
H5	H1	0.0800
H6	H1	0.0794
H7	H1	0.0794
H8	H1	0.0787
H9	H1	0.0681
H10	HO	0.4290
H11	H1	0.0421
H12	HO	0.4476
H13	H2	0.0847
H14	HN	0.4379
H15	HN	0.4379

Table B.8 RTP atom types and partial charges.

Atom Name	Atom Type	Charge
P1	P5	1.1386
P2	P5	1.4059
P3	P5	1.2041
C1	C3	0.0223
O1	OS	-0.4327
C2	C3	0.0478
O2	OS	-0.2723
C3	C3	0.1804
O3	OH	-0.6448
C4	C3	0.0544
O4	OH	-0.5859
C5	C3	0.0022
O5	O	-0.7747
O6	O	-0.8714

O7	O	-0.9310
O8	O	-0.7747
O9	O	-0.8714
O10	O	-0.9310
O11	OS	-0.5789
O12	OS	-0.5686
O13	O	-0.9310
N1	NA	0.2930
C6	CC	0.2930
H1	H5	0.1769
C7	CC	0.2633
H2	HN	0.3836
N2	ND	-0.5146
N3	NA	-0.3156
C8	C	0.7121
O14	O	-0.5713
N4	N	-0.8661
H3	HN	0.4020
H4	HN	0.4020
H5	H2	0.1824
H6	H1	0.0714
H7	HO	0.4159
H8	HO	0.4099
H9	H1	0.0823
H10	H1	0.1715
H11	H1	0.0606
H12	H1	0.0606

Table B.9 RBV atom types and partial charges.

Atom Name	Atom Type	Charge
C1	C3	0.0535
C2	C3	0.0982
O1	OS	-0.3965
C3	C3	0.2922
O2	OH	-0.6744
C4	C3	0.0710
O3	OH	-0.5890
C5	C3	0.0815

N1	NA	0.2632
N2	NC	-0.4629
C6	CD	0.3283
N3	N	-0.8623
O4	O	-0.5357
N4	NA	-0.2823
C7	CC	0.1175
C8	C	0.6758
H1	H5	0.2428
H2	HN	0.3663
H3	H1	0.0950
H4	H1	0.0950
H5	H1	0.1443
H6	H1	0.0218
H7	HO	0.4586
H8	H1	0.0908
H9	HO	0.4393
H10	H2	0.2126
H11	HN	0.4314
H12	HN	0.4314
O5	OH	-0.6651
H13	HO	0.4579